Information processing in the cortex: The relevance of coherent oscillations for neuronal communication

Andres Buehlmann

Tesi Doctoral UPF / 2010

Supervised by
Prof. Gustavo Deco
Department of Information and Communication Technologies

Barcelona, May 2010

Dipòsit Legal:
ISBN:

The text was typeset with LaTeX using the `memoir` class hacking on `vim`, all running under Gentoo GNU/Linux.

Acknowledgments

I am indebted to a lot of people, both within and outside the university, whose help proved invaluable during this PhD. I'd thus like to thank

- Gustavo, for supervising my thesis and giving me the opportunity to work in his group.
- Anders, Albert, Ralph, and Rita, for their comments and discussions, helping me substantially with my work.
- Andrea, Cristian, Daniel, Étienne, Joana, Johan, Larissa, Laura, Marina, Mario, Pedro, Tim, and Yota, for all the good times and cheerful moments, and especially for keeping me entertained with their challenging and less challenging computer problems, which provided me with welcome excuses for not working on my thesis.
- Dani, for his hospitality, patience in teaching me Catalan, and being such an uncomplicated officemate and friend.
- Pedro, compadre, for suffering together with me through the more difficult moments of this PhD and for the skiing excursions to Andorra.
- Ernest, for the always interesting discussions and insights into local politics.
- Marco, for avoiding my starvation by constant provision of cookies.
- Larissa, for baking a cake for my birthday.
- Andreas, for all the relaxed Thursday lunches.
- Gloria, Laura, Enric, Mar, Arantxa, Johan, and Yota, for bearing with my grumbling personality in the office.

- Ivan, Fran, and Ronald, for letting me mess with the cluster and helping me out when I got in trouble.

On occasions, there was even room for a little spare time. I'd thus like to thank

- The excursion team (Adrian, Andrej, Anders, Enric, Gabriele, Gloria, Juan, Laura, Leticia, Miguel, Oscar, Pablo, Ping, Vicenç, ...), for strenuous walks, dangerous expeditions and excellent calçotades.

- The members of the Orquestra de la Universitat de Barcelona (Sara, Isabel, Jens, Laia, Geno, Alicia, Blanca, Vicent, Lali, Josep Maria, Masha, Gemma, Giselle, Emili, Juanjo, Sheila, Joan, Celia, Neus, ...), for letting me have a glimpse of Catalan culture and for all the after-rehearsal beers.

- Ralph, for motivating me to cycle up Turó de l'Home yet another time.

- Aina, Victor, Nacho, Oscar, Jordi, and all the others, for unforgettable climbing far from daily routines.

I'd finally like to thank

- Jérôme, for moral support both up in the mountains and on lower grounds.

- Jens, for his help in the quest for meaning of life.

- Iva, for the wonderful time we have been having together, for proofreading all my texts, and for being my sunshine.

- My sisters and brother Esther, Ursula and Gregor, for all their motivating visits to Barcelona.

- My parents, for all their loving support and patience, without which this thesis would never have been possible.

Abstract

Oscillatory neuronal activity is an omnipresent phenomenon in the cerebral cortex. However, the actual function of these oscillations remains unclear. Are they just an epiphenomenon of elevated firing rates or do they represent a fundamental process on their own? Based on experimental work, we apply computational modeling to address this question. We first study the role of oscillations in attentional processes and then in a more general, information theoretical context. Our results support the idea that oscillations represent an independent mechanism. In particular, we show that attention modulates gamma oscillations independently of rates and that the flow of information between brain areas depends both on the phase and on the spectral power of oscillations. Moreover, we show that the speed of information exchange increases as a function of spectral power in specific frequency bands. Taken together, these results suggest that oscillations are a mechanism employed by the brain to control actual interactions between brain areas and thus likely have a link to behavior.

Resum

Les oscil·lacions d'activitat neuronal són un fenomen omnipresent a l'escorça cerebral. La funció d'aquestes oscil·lacions, però, no està clara. ¿Són només un epifenomen de les elevades taxes de descàrrega de potencials d'acció, o representen un procés fonamental? Per tal d'aclarir aquesta qüestió, en aquest treball hem aplicat models computacionals basats en xarxes neurobiològicament plausibles per tal d'investigar alguns dels resultats experimentals recents més rellevants. Primerament, estudiem la rellevància de les oscil·lacions en processos d'atenció i després en un context més general de teoria d'informació. Els resultats donen suport a la idea que les oscil·lacions representen un mecanisme independent. Demostrem que l'atenció modula les oscil·lacions gamma de manera independent de la taxa de descàrrega de potencials d'acció. També es mostra que la transmissió d'informació entre àrees corticals depèn tant de la fase com de la potència espectral de les oscil·lacions. A més, la velocitat amb què es produeix aquesta transmissió d'informació augmenta en funció de la potència espectral en bandes de freqüències específiques. Aquests resultats suggereixen que les oscil·lacions representen un mecanisme biològicament plausible per mitjançar les interaccions entre àrees cerebrals i, per tant, per establir un vincle entre activitat neuronal i comportament.

Contents

1 Introduction

Temporally correlated activity is a phenomenon widely observed in the brain. Gamma band oscillations were found in anesthetized cats and monkeys (Eckhorn et al., 1988; Gray et al., 1989; Gray & Singer, 1989; Engel et al., 1991a,b,c) using moving gratings or stationary squares as stimuli (Rols et al., 2001). Gamma band oscillations were also found in awake cats and monkeys (Frien et al., 1994; Kreiter & Singer, 1996; Gray & Prisco, 1997; Fries et al., 1997; Friedman-Hill et al., 2000; Maldonado et al., 2000; Fries et al., 2001, 2002, 2008; Bichot et al., 2005; Taylor et al., 2005; Womelsdorf et al., 2006, 2007), and subsequently in other species, such as rats and mice (Bragin et al., 1995; Buhl et al., 2003; Csicsvari et al., 2003; Montgomery & Buzsaki, 2007) and invertebrates (Wehr & Laurent, 1996; Stopfer et al., 1997; Laurent, 2002). Such oscillations were also found in other neocortical areas, such as the monkey auditory cortex (Brosch et al., 2002) and the monkey lateral intraparietal area (Pesaran et al., 2002), and even outside the neocortex, e.g., in the hippocampus of rats (Bragin et al., 1995; Csicsvari et al., 2003; Montgomery & Buzsaki, 2007; Montgomery et al., 2008) or the olfactory system of invertebrates (Wehr & Laurent, 1996; Stopfer et al., 1997; Laurent, 2002).

This omnipresence of rhythmic activity raises the question of whether oscillations are just an epiphenomenon, present whenever neurons are firing at elevated rates, or whether they have a function of their own. This will be the underlying question of this thesis. To get to the possible functions of oscillations, we will first have to understand how oscillations are generated. We will therefore first outline the basic mechanisms involved in oscillation generation in a network (1.1) and then briefly review existing literature on the function of oscillations (1.2). Many studies on the function of oscillations were done in the context of attention. We will thus review existing literature on attention (1.3) and then summarize our own work (1.4). In chapters 2 and 3 we will present our results in detail and finally discuss these results in chapter 4.

1.1 Mechanisms of oscillation generation in computational modeling

How are oscillations generated? Different mechanisms can give rise to oscillatory activity in models of recurrent networks of spiking neurons, like mutual inhibitory interactions (Wang & Buzsaki, 1996; Bartos et al., 2007) or feedback loop between excitatory and inhibitory neurons (Jefferys et al., 1996; Mann et al., 2005).

Wang & Buzsaki (1996) systematically examined the conditions under which gamma oscillations were generated in interneuron networks. They parted from the hypothesis that rhythmic activity could emerge in a random network of interconnected GAGAergic fast-spiking interneurons and showed that this was true under specific conditions. First, the amplitude of the spike afterhyperpolarization had to be above the $GABA_A$ synaptic reversal potential, because then the effect of synaptic input was always hyperpolarizing during the time course of an active potential and its repolarization. Second, the ratio between the synaptic decay time constant (τ_{syn}) and the oscillation period had to be sufficiently large, because with small τ_{syn} the network synchronization decreased due to synaptic effects. Third, the network had to present few heterogeneities as network coherence deteriorated rapidly if applied currents varied. In their study, Wang & Buzsaki (1996), made the assumption that inhibition is slow, weak and hyperpolarizing. Under these circumstances, inhibitory interneuron networks can generate coherent oscillation in the gamma frequency range if neurons are exposed to tonic excitatory drive. This synchronization is sensitive to changes in kinetics of synaptic conductance, connectivity and reversal potential. But the requirement for minimal heterogeneity is inconsistent with experimental data (van Hooft et al., 2000; Fisahn et al., 2004). Robustness against heterogeneity can be improved by incorporating fast and strong rather than slow and weak inhibitory synapses (Neltner et al., 2000). However, under these conditions, large excitatory drive is needed to counterbalance increased inhibition. More robustness to oscillation in inhibitory networks can be achieved by adding delays (Bartos et al., 2001, 2002). In the presence of short delays, fast inhibition consistently supports synchronization independently of whether delays are assumed to be constant (Bartos et al., 2001) or distance-dependent (Bartos et al., 2002). A rapid inhibitory synaptic event generated after a short delay is a maximally synchronizing signal. It precisely defines an early time interval with strong inhibition. Accordingly, temporal windows of firing and suppression follow in an alternating manner.

Another factor: How does addition of fast glutamatergic synapses affect synchronization in interneuron network models? It certainly implies several additional parameters. In a simple two-population network, there are now four types of chemical synapses (I-I, E-I, I-E, E-E, where E stands for excitatory neurons and I for inhibitory ones). Several different (and sometimes reduced) cases of this type of network have been studied.

Eeckman & Freeman (1990) developed a model for induced rhythms in olfactory structures, in which synchronous oscillation was generated by a feedback loop between excitatory and inhibitory neurons. They proposed that some mutual connectivity was also required within the pools of both excitatory and inhibitory neurons to stabilize the oscillations. Similar models were made for the piriform cortex (Wilson & Bower, 1992) and the primary visual cortex (Wilson & Bower, 1991). The geometric structure of these models differed, but the essential idea in both was that the amplitude and the frequency of coherent 30-60 Hz oscillation were determined by a fast-feedback inhibitory loop. Essentially, if the stimulus was appropriate (not too strong), enough activity in the recurrent excitatory connections between pyramidal cells persisted after each recurrent inhibition wave in order to re-excite the pyramidal cell population. They showed that the time constant of inhibition tuned the frequency of the gamma rhythm, so that longer time spent open for the chloride channels resulted in slower rhythms. In both the visual cortex and the piriform cortex versions of the model, gamma rhythms arose from interactions between networks of excitatory neurons, could depend on the conduction velocities of intrinsic cortical connections and were tuned by the time constants of excitatory and inhibitory synapses.

Traub et al. (1997) studied a network of hippocampal pyramidal cells and interneurons. They showed that pools of synaptically interconnected inhibitory cells were sufficient to produce gamma frequency rhythms, but the network behavior could be modified by participation of pyramidal cells as follows: Tonic excitation of the principal neurons caused them to fire repetitively. This firing induced both slow and fast excitation of interneurons. The slow excitation triggered interneuron network gamma oscillations (Whittington et al., 1995). The synchronized IPSPs interacted with the repetitive firing of pyramidal cells, and with the intrinsic oscillatory properties of pyramidal cells, to shape a coherent pyramidal cell network oscillation. When this happened, the fast excitation of interneurons appeared as brief, large EPSP following the interneuronal network spike.

Mann et al. (2005) showed in vitro that an AMPA receptor-specific antagonist blocked both the field oscillations and rhythmic inhibitory cur-

rents on pyramidal neurons, suggesting that interneuronal synchronization was mediated by fast recurrent excitation. Therefore, cholinergically induced fast network oscillations in the hippocampus appeared to be generated by a synaptic feedback circuit between pyramidal cells and perisomatic-targeting interneurons, consistent with the model originally suggested for the piriform cortex by Freeman (1968).

Several studies showed that single cell discharge rates are typically much lower than local field potential (LFP) oscillation frequency (Csicsvari et al., 1998, 1999; Hajos et al., 2004). This was taken into account in a modeling study with integrate-and-fire neurons by Brunel & Wang (2003). These authors studied several different types of networks: (i) networks consisting exclusively of interneurons (I-I), (ii) networks with pyramidal-interneuron feedback loop (E-I, I-E) and (iii) networks with both types of connections. Networks consisting only of inhibitory neurons needed a strong external input to be activated. Once activated, the neurons exhibited strong inhibitory firing. Consequently, every neuron in the network got a massive inhibitory input. Due to this inhibitory current, the activity went down and there was a trough in global activity. Subsequently, the inhibitory synaptic currents decayed away, after which the total input became high again due to strong external input, which caused another surge of activity, the cycle thus starting over again. In a network with both excitatory and inhibitory neurons that had a pyramidal-interneuron feedback loop (i.e., E-I, I-E), pyramidal neurons excited interneurons. Activity in the interneurons went up and consequently, the interneurons sent inhibition back on pyramidal cells and hence decreased their activity. Once the excitatory activity was inhibited, the inhibitory activity also decayed. The population frequency was determined by the sum of excitatory and inhibitory lags. This frequency was therefore lower than the population frequency of a purely inhibitory network. Adding recurrent inhibitory connections (I-I) lead to a mixture of the two types of network and lead to a frequency that lay in-between the two types of network mentioned above. Adding pyramidal to pyramidal connections with all other types of connection tended to decrease the oscillation frequency of the network. This was because these connections tended to prolong the positive phase of each cycle. The recurrent excitatory connections helped keeping the activity of the pyramidal neurons up and, in turn, it took the inhibitory neurons longer to shut this activity down.

In the model of Brunel & Wang (2003), the population frequency of a network depended on the interplay between excitatory and inhibitory neurons. Therefore, the oscillation frequency depended on the balance between AMPA and GABA currents, as both E-I and E-E connections

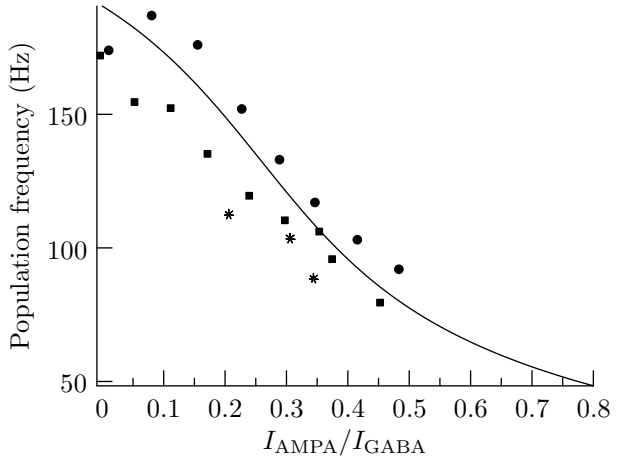

Figure 1.1: Population oscillation frequency decreases with the recurrent excitation/inhibition balance. The ratio $I_{\mathrm{AMPA}}/I_{\mathrm{GABA}}$ is the same for both pyramidal cells and interneurons and is changed by varying the AMPA conductance on both pyramidal cells and interneurons. Solid line: analytical prediction. Symbols: network simulation data (circles, 12 kHz external inputs; squares, 6 kHz external inputs; stars, 4 kHz external inputs). Adapted from Brunel & Wang (2003).

decreased the population frequency (Fig. 1.1). Different values of synaptic temporal parameters could favor one of the two competing oscillation instabilities. If the AMPA decay time (τ_{AMPA}) was sufficiently shorter than the GABA decay time (τ_{GABA}), the network exhibited oscillations of the E-I loop type. On the other hand, if τ_{GABA} was sufficiently shorter than τ_{AMPA}, a purely inhibitory loop (I-I) established itself. If the two decay constants were too similar, no stable oscillatory activity built up (Fig. 1.2a). In other words, if τ_{GABA} was kept fix, a short τ_{AMPA} implied a slow E-I type oscillation frequency, while a long τ_{AMPA} implied a high oscillation frequency of the I-I type (Fig. 1.2b).

The question of whether oscillations are generated mostly by interneurons or by an inhibitory-excitatory feedback loop has still not been answered conclusively. Tiesinga & Sejnowski (2009), after comparing modeling and experimental studies, concluded that both these sources of evidence were consistent with the pyramidal-interneuron gamma (PING) mechanism in the cortex but were not strong enough to rule out the interneuron gamma (ING) mechanism.

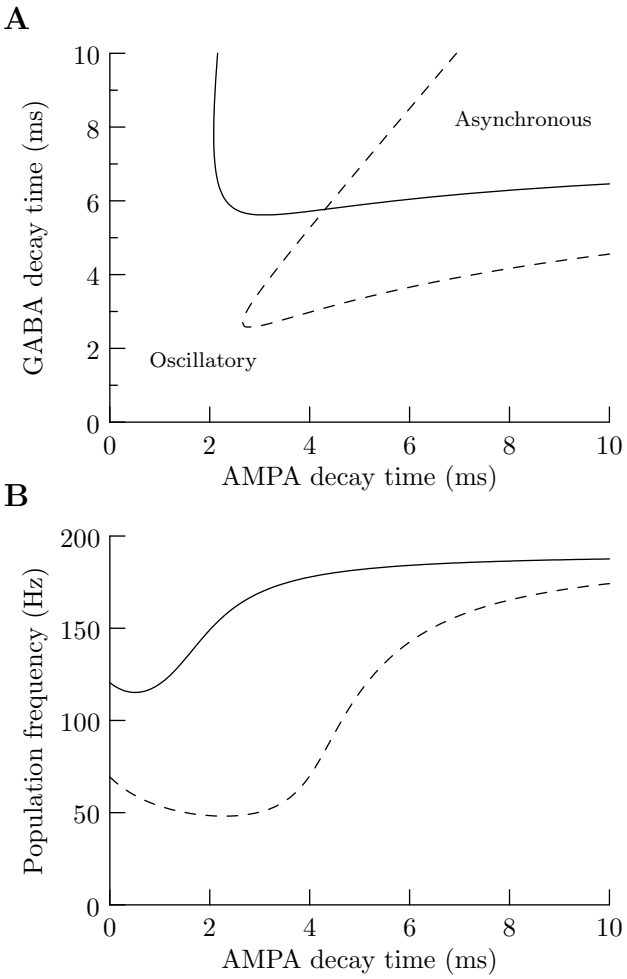

Figure 1.2: Dependence of coherent fast oscillations on the relative time constants and balance of synaptic excitation and inhibition. The balance between the AMPA and GABA currents ($I_{\mathrm{AMPA}}/I_{\mathrm{GABA}}$) is 0.2 (solid line) and 0.8 (dashed line). **(a)** Network dynamical behavior on the parameter plane of τ_{AMPA} and τ_{GABA}. There are two kinds of coherent oscillations. For a fixed τ_{GABA}, oscillations develop through delayed negative feedback when τ_{AMPA} is much smaller than τ_{GABA}. On the other hand, when τ_{AMPA} is sufficiently large, the interneuronal network by itself generates synchronous oscillations. **(b)** Population frequency as a function of the excitatory synaptic delay time constant τ_{AMPA} with a fixed τ_{GABA} of 5 ms. Adapted from Brunel & Wang (2003).

1.2 Functional role of oscillations

Correlations in neuronal signals are very abundant. But correlations are likely not very important per se, as they could be due to common input or receptive field (RF) overlay. However, things look differently when change in correlation structure reflects changes in functional connectivity. To measure such change, several things have to be taken into account. Recordings should be from multiple sites and across multiple conditions, and neuronal activity, apart from correlations, should change as little as possible across conditions. In the following, we will look at several particularly interesting experiments. Note that synchronization between neuronal signals takes place at different levels, it can be very local or across distant brain areas. The first recordings of neuronal synchrony were thus examples of local synchrony, where neurons acted mostly as coincidence detectors and the correlations were stimulus-dependent. These experiments led to the hypothesis of binding-by-synchronization. Later, synchronization was also detected across different brain areas, where they acted more as neuronal gain modulator. Synchronization was found to be stimulus independent, controlling the flow of information. These experiments have led to the hypothesis of communication through coherence, as described below. Synchronization as a local phenomenon is treated in section 1.2.1 and synchronization as a large scale phenomenon is treated in section 1.2.2.

1.2.1 Local synchronization

Several authors have provided evidence supporting synchronization as a mechanism for the integration of signals in the brain. This mechanism has been explored most intensively in relation to the so called binding problem, which reflects the task of binding together representations of different properties of an object. One proposed solution is that the different features of an object are integrated by cell assemblies that fire synchronously (Gray et al., 1989; for a review see Roskies, 1999). This integration takes place on a local scale, within neighboring cortical areas, specialized in the same modality. Here, local integration refers to a network distributed over an area of maximally 1 cm with conduction delays of about 4–6 ms (Girard et al., 2001). On a scale of 2 mm and below, clusters of excitatory and inhibitory neurons tend to synchronize (Gray, 1999). Cortical columns in the primary visual cortex, slightly further apart (2–7 mm) are prone to synchronize if their neurons share similar feature properties (Gray, 1999). Traub et al. (1999) observed similar synchronizations over distances of several millimeters in hippocampal slices. Destexhe et al. (1999) observed

oscillatory activity in the cat visual cortex between electrodes separated by up to 5 mm. The correlations decreased as a function of distance.

An example from the primary auditory cortex showed that, following a stimulus, neurons responded by changing both their firing rates and their correlations. In many cases, the changes in correlation were more persistent than the changes in rates. This implied that the stimulus could be represented even in the absence of firing rate changes (deCharms & Merzenich, 1996).

In an example from the visual cortex, the RF of neurons was stimulated by either one or two objects, in a way that the evoked firing rates were practically identical for both conditions. However, whether one or two stimuli were shown was reflected in the synchronization between pairs of neurons (Kreiter & Singer, 1996).

In sum, as the summation of postsynaptic neurons is only effective when postsynaptic potentials are within a few milliseconds, local synchronization can act as a feedforward coincidence detector; postsynaptic impact is greater if spikes are focused in time. Neuronal codes are therefore more efficient if correlations are taken into account (Salinas & Sejnowski, 2000). But all these correlations happen within reciprocal connections between areas at the same level of the network (Phillips & Singer, 1997). Also, the correlations are driven by a stimulus: they either represent features of the stimulus or group several stimulus features together.

1.2.2 Large scale integration

Correlations can also change as a function of internal events rather than being driven by a stimulus, and such correlations have been observed over large distances in the brain, between different areas, linking different levels of the network. We will refer to this as *large scale synchronization.* Large scale means synchronization between neuronal clusters separated by more than 1 cm, which implies transmission delays greater than 8–10 ms (Girard et al., 2001). Evidence for large-scale synchronization has been presented by several authors.

Roelfsema et al. (1997) recorded from several electrodes implanted in the cortex of cats. Cats had to detect a change in the orientation of a grating. Electrodes were placed in visual, association, somatosensory and motor areas. Correlations between area 17 (the primary visual cortex) and area 7 of the parietal cortex, as well as correlations between area 4 of the motor cortex and the medial subdivision of area 5 of the parietal cortex increased until the task was completed (see Fig. 1.3). Significant correlations occurred also between the areas of the parietal cortex (5mc,

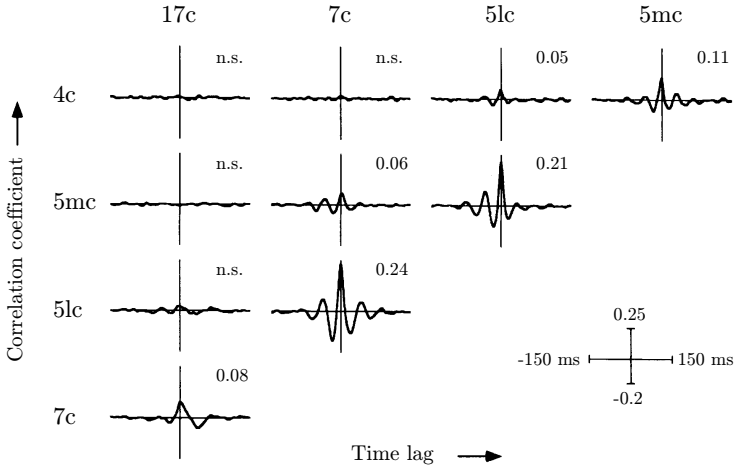

Figure 1.3: Pattern of interactions among areas of the visual (17c), parietal (5lc, 5mc, 7c) and motor (4c) cortex. Shown are the correlation functions of one cat averaged over trials. c indicates that recordings were made in the hemisphere contralateral to the paw that the animal used for pressing the lever, l stands for lateral and m for medial. Adapted from Roelfsema et al. (1997).

5lc, 7c). The correlations disappeared after the task was completed.

Bressler et al. (1993) recorded from the cortex of monkeys during a preparation and discrimination task. Broadband frequency coherence was observed between widely spaced cortical areas and changed dynamically during task performance. Frequency coherence between striate and motor cortex was elevated at the time of response. Frequency coherence between striate and parietal cortex was elevated between 100 and 200 ms after stimulus onset.

Vaadia et al. (1995) showed changes in synchronization independent of variations in the firing rates. Their recording supports the idea that neurons might change its coupling to other groups of neurons (both locally and over larger distances) and can participate in different neuronal ensembles.

Several studies have shown that correlations can vary independently of firing rates. Riehle et al. (1997) trained monkeys to perform a delayed-response task in which two cues were presented. The first cue indicated the target position, the second cue gave the go signal for the requested hand movement. The second cue could appear after 600, 900, 1200 or 1500 ms.

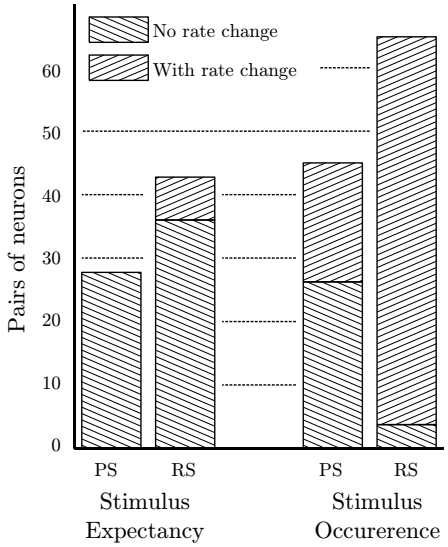

Figure 1.4: Numbers of pairs of neurons with coincident spike constellations that occurred significantly more often than expected by chance when the stimulus was either expected (left) or when it actually appeared (right). Increase in synchrony was only accompanied by increase in rate when the stimulus actually appeared. Adapted from Riehle et al. (1997).

Neurons in primary motor cortex showed increased synchrony both when the stimulus appeared and when the monkey expected the signal but the stimulus did not appear. When the stimulus actually appeared, the increase in synchrony was accompanied by an increase in firing rate, but if the stimulus did not appear, there was no such accompanying rise in firing rate. In other words, in the first case, which was like a sensory evoked response, the rates changed, but in the second case, which depended entirely on the internal state of the brain, they did not change (Fig. 1.4).

Steinmetz et al. (2000) trained monkeys to do two tasks, a tactile and a visual one. In the tactile task, the monkey had to indicate whether a stimulus presented to the fingertip matched a visual pattern. In the visual task, the same stimulus was applied to the finger, but the monkey had to ignore it and instead detect a dimming of the target spot on the monitor. During both tasks, these authors measured from somatosensory cortex (S2). That way, they obtained data from the same neurons under two conditions, once with attention directed to the tactile stimulus, once

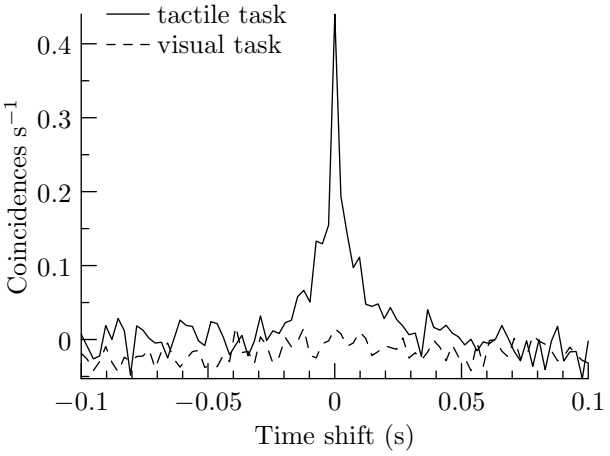

Figure 1.5: Crosscorrelogram for a pair of neurons. Crosscorrelograms are shown for the tactile (solid line) and the visual (dashed line) task. Adapted from Steinmetz et al. (2000).

not. These authors observed an increase in synchrony when attention was directed to the fingertips (Fig. 1.5).

Fries et al. (2001) studied how correlations between neurons in visual area V4 change with attention. Monkeys had to detect a color change in one of two stimuli presented at the same time while fixating a central spot, at the same time ignoring color changes in the other stimulus. One of the two stimuli was inside the RF of a recorded neuron, while the other was outside. At the same time, the LFP was recorded. They found that if attention was directed to the stimulus inside the RF, power in the gamma band increased while power in the low frequency band decreased, i.e., neuronal activity was more synchronized in the gamma band under attention (Fig. 1.6).

Pesaran et al. (2002) trained monkeys to do a memory saccade task. The monkey had to fixate a central spot and was then cued to one of four possible locations. He had to keep the location in memory for 1000 ms and then do the corresponding saccade. These authors found that, during the delay period, spikes and LFP measured from the lateral intraparietal area showed increased synchronization in the gamma band. They also showed that the direction of an upcoming saccade could be decoded from the LFP spectrum in the range of 30–100 Hz. This is a further example that gamma band synchronization is not restricted to cortical areas driven by sensory stimuli.

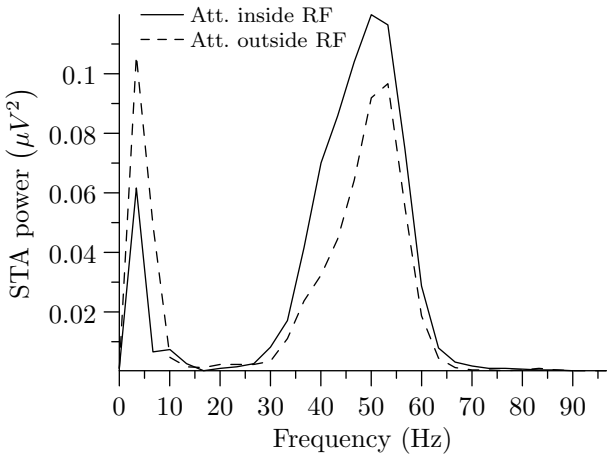

Figure 1.6: Power spectra of the STA during the stimulus presentation. Dashed curve: attention outside the RF; solid curve: attention inside the RF. Adapted from Fries et al. (2001).

Bichot et al. (2005) tested for parallel and serial attentional mechanisms in area V4 in monkeys performing a search task with free gaze. They recorded neuronal responses and LFP, and studied the synchronization between the two. Monkeys were cued to either shape or color and had to find a matching target among several distractors. The neurons showed feature-selective firing. The recorded data was divided into four sets: (i) both the stimulus in the RF and the cue had the neuron's preferred feature; (ii) the stimulus had the preferred feature but the cue had the neuron's non-preferred feature; (iii) the RF stimulus had the non-preferred feature but the cue had the preferred feature; (iv) both the RF and the cue had the non-preferred feature. Bichot et al. (2005) found that the coherence between spikes and LFP (spike-field-coherence, SFC) in the gamma band was greater when the RF stimulus had the preferred feature compared to when it had a non-preferred feature (comparison of conditions (i) and (iii), solid and dash-dotted line in Fig. 1.7). But more importantly, the coherence for the preferred feature in the RF was enhanced when the RF contained the target feature that the animal was searching for but had not yet found (comparison of conditions (i) and (ii), solid and dashed line in Fig. 1.7). While the former is an example of stimulus-driven rhythmic activity, the latter is independent of the stimulus in the RF.

Similarly, Taylor et al. (2005) measured from visual area V4 in monkeys performing a shape-tracking task. They found that attention strongly

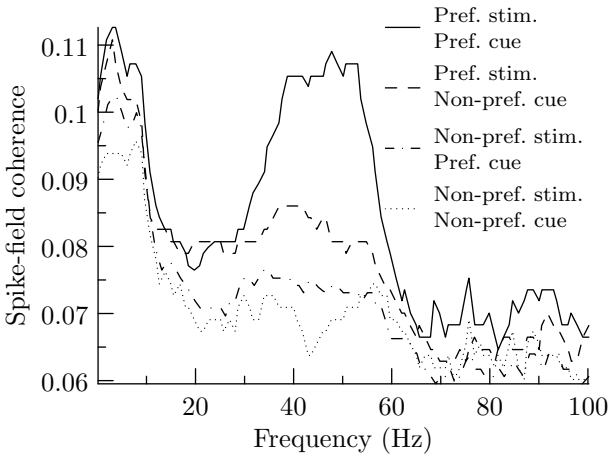

Figure 1.7: SFC for the color task. The SFC is higher for the preferred stimulus (solid line) than for the non-preferred stimulus (dashed line). The SFC is also higher in the condition where the stimulus is the preferred one and the animal has to look for this preferred stimulus (solid line) as compared to when the stimulus is the preferred one but the animal is cued to look for the non-preferred stimulus (dash-dotted line). Adapted from Bichot et al. (2005).

increases oscillatory currents in the local field potential in the gamma frequency range.

A direct link between neuronal synchrony and behavior was shown in Womelsdorf et al. (2006). They analyzed the data from Fries et al. (2001), where the monkey had to detect a change in one stimulus while ignoring the other. They showed that the behavioral response times to the stimulus change could be predicted by the degree of gamma band synchronization among those neurons in monkey visual area V4 that were activated by the cued stimulus. SFC was calculated separately for the 25% trials with the slowest behavioral reaction and the 25% trials with the fastest reactions. Trials leading to fast reactions times contained more gamma band power and had a higher gamma band SFC before and after the stimulus change (Fig. 1.8).

All these experiments show evidence of large scale synchronization and changes of synchronization independent of changes in the firing rate. Many of these experiments are related to attention and rivalry, which represent internal states of the brain. They point to a role for synchronization that is independent of stimulus representation. In particular, synchronization

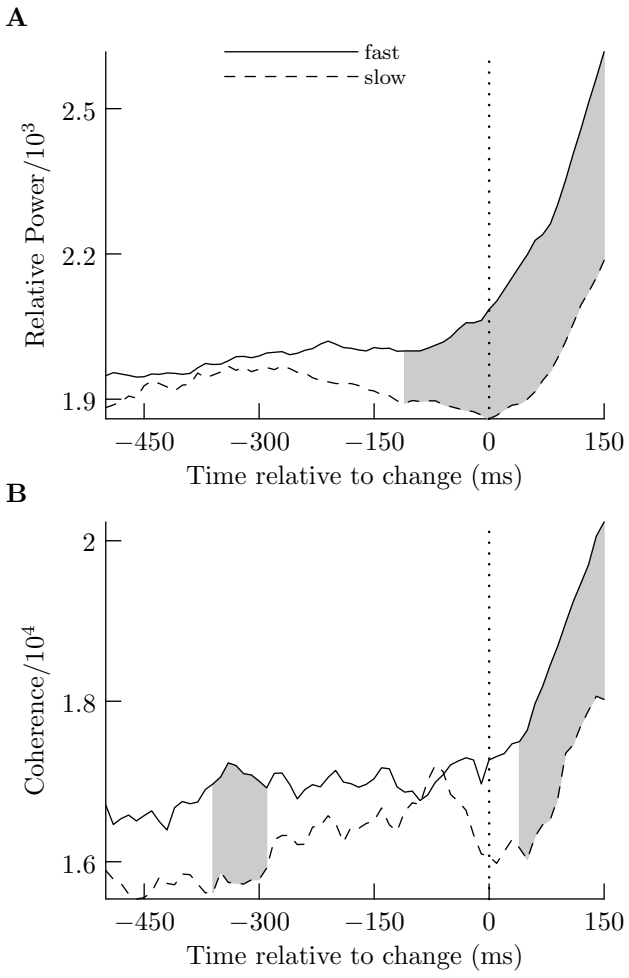

Figure 1.8: Neuronal activity parameters in trials with fast (solid line) and slow (dashed line) change detection. **(a)** Relative power in the gamma band. **(b)** SFC in the gamma band. Both power and SFC are higher in the trials with fast change detection. Grey shading indicates significance. Adapted from Womelsdorf et al. (2006).

adjusts the flow of information by a mechanism of gain modulation, and it controls the strength of a signal rather than representing the signal itself. If correlations can control the flow of information, they can also be used to control which neuronal clusters connect and interact with each other. Synchronization could generate effective networks on the basis of existing anatomical networks (Salinas & Sejnowski, 2001; Varela et al., 2001). This hypothesis has been named communication-through-coherence (Fries, 2005). If rhythmical activity really has an influence on the correlations between neuronal clusters, the correlations between them have to depend on the phase relation between the groups of neurons. This idea was explored in Womelsdorf et al. (2007).

More specifically, Womelsdorf et al. (2007) explored the mutual influence of two groups of neurons as a function of their phase shift. These authors quantified the mutual influence of the multi unit activity (MUA) in the two groups as the Spearman rank correlation coefficient of the two MUA's 60 Hz power. They showed evidence that the correlation between the two groups of neurons varied as a function of the phase shift of the oscillations at 60 Hz. There was a specific phase shift at which the correlation between the two groups was highest. Womelsdorf et al. (2007) concluded that the effective connectivity in a network could thus be maximized or minimized through synchronization of a specific phase relation, resulting in an effective interaction pattern.

1.3 Attention

Over 100 years ago William James wrote in his *Principles of Psychology*:

> Millions of items [...] are present to my senses which never properly enter my experience. Why? Because they have no interest for me. My experience is what I agree to attend to. [...] Everyone knows what attention is. It is the taking possession by the mind, in clear and vivid form, of one out of what seem several simultaneously possible objects or trains of thought. Focalization, concentration, of consciousness are of its essence. It implies withdrawal from some things in order to deal effectively with others [...]

Attention should be distinguished from arousal. Arousal can be defined as the state of physiological reactivity (Broadbent, 1971), ranging from sleep at one end to excitement or panic at the other. Robbins (1984)

has discussed experimental evidence suggesting that arousal may be modulated by dopaminergic and noradrenergic mechanisms. So while arousal describes the general activation of mind, attention would be the focused activation of mind. Attention can be subdivided into (a) attentional orientation (the direction of attention to a particular stimulus); (b) selective attention (giving attentional priority to one stimulus in favor of another); and (c) divided attention (dividing attention between two or more different stimuli; Coull, 1998).

1.3.1 Biased competition model

Attention has been studied most thoroughly in the visual system. Given that not all of the many different visual inputs received by the retina can be fully processed, attention is needed as a mechanism to filter these inputs and separate relevant from non-relevant stimuli. An early model of attention was the *spotlight of attention*, where attention enhances the responses of neurons representing stimuli at a single behaviorally relevant location in the visual field. But attention can both increase and decrease neuronal activity, as was shown, e.g., by Moran & Desimone (1985). This lead to the biased competition hypothesis (Desimone & Duncan, 1995). According to Desimone (1998), there are five main principles in the biased competition model: (i) objects in the visual field compete for the responses of cells in the visual cortex; (ii) competitive interactions are strongest in a given cortical area when competing stimuli activate cells in the same local region of the cortex; (iii) these competitive interactions can be biased in favor of one stimulus by virtue of different mechanisms which include both bottom-up (stimulus-driven) and top-down (feedback) mechanisms; (iv) the bias is not purely spatial: processing can be biased in favor of relevant features such as color, shape, texture, and so on; (v) a main source of top-down biasing derives from structures involved in working memory.

Experimental results that demonstrated many of these points were presented in Reynolds et al. (1999). They started with two basic assumptions: (a) When multiple stimuli appeared together, they activated populations of neurons that automatically competed with one another; (b) Attending to a stimulus biased this competition in favor of neurons that responded to the attended stimulus. They ran two experiments. First, these authors measured neuronal responses to the probe (preferred stimulus) and the reference (non-preferred stimulus) which both fell within the RF, while the monkey was not required to attend to either of them. The stimuli were presented one at a time and also together as a pair. Reynolds et al. (1999) found that the neuronal response to the paired stimuli was in-between the

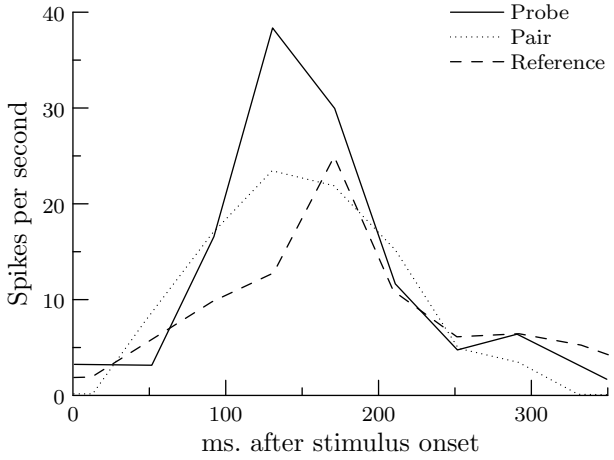

Figure 1.9: The response of a single V4 neuron to the reference, a probe and the corresponding pair. The solid line represents the response to the probe (a 45° green bar), the dashed line the response to the reference (a vertical green bar), and the dotted line the pair response. Figure adapted from Reynolds et al. (1999).

responses to each of the stimuli presented alone (Fig. 1.9). In the second experiment, they measured the response to the pair of stimuli while the monkey attended to each individual stimulus. They found that attending to only one element of the pair drove the neuronal response toward the response elicited when the attended stimulus appeared alone (Fig. 1.10).

1.3.2 Multiplicative gain modulation

McAdams & Maunsell (1999) studied the effects of attention on orientation tuning curves. They found that the effects of attention were consistent with a multiplicative scaling of the driven response.

In a similar study, Treue & Martínez Trujillo (1999) presented data studying tuning curves of neurons while placing two stimuli side-by-side inside the RF. In any given trial, either one of the patterns was designated as the target. They found that attention to one of the two stimuli either enhanced or decreased the neuronal response, depending on whether the target was the preferred or the non-preferred stimulus (Fig. 1.11). As the stimuli in this experiment were moving random dots, the monkey did not have to shift attention spatially. Therefore, these results indicate non-spatial, feature-based modulation of sensory responses. The results from

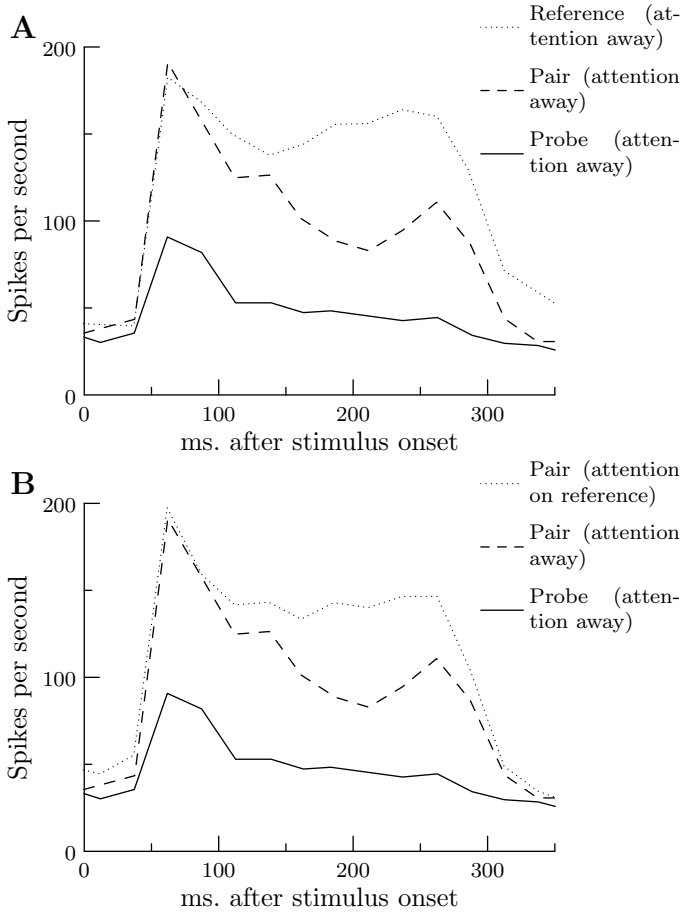

Figure 1.10: Attention filtering out the effects of a suppressive probe in V2. **(a)** The dotted line shows the response to the reference stimulus. The solid line shows the response elicited by the probe. The response to the pair (dashed line) was suppressed by the addition of the probe. **(b)** The upper dotted line shows the pair response when attention was directed to the reference stimulus. The responses to the unattended probe (solid line) and pair (dashed line), taken from (a), are repeated for comparison. Attention to the reference stimulus caused the cell's response to move upward, toward the response that was elicited by the unattended reference stimulus presented alone (dotted line in (a)). Figure adapted from Reynolds et al. (1999).

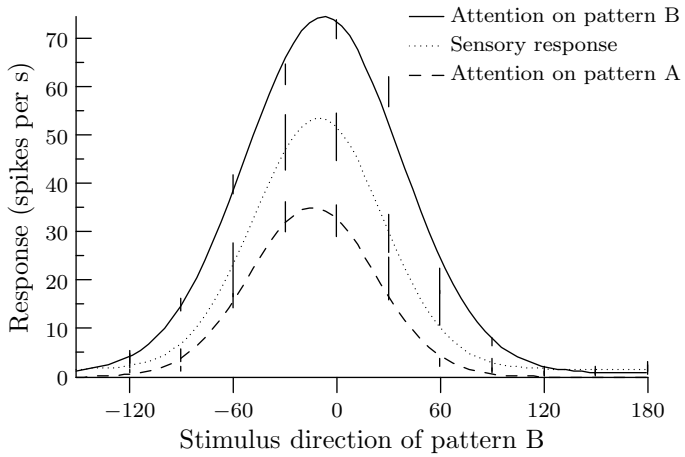

Figure 1.11: Effect of directing attention to one of two stimuli inside the RFs. Tuning curves when pattern B was the target (upper curve), when pattern A was the target (lower curve) and when neither pattern was behaviorally relevant (central curve), because the animal was instructed to respond to a luminance change at the fixation point. Figure adapted from Treue & Martínez Trujillo (1999).

both experiments are compatible with the biased competition hypothesis.

1.3.3 Attention and oscillations

The question remains of how the response enhancement caused by attention (as described in sec. 1.3) is achieved. One possible mechanism is an increase in response synchronization (Salinas & Sejnowski, 2001). And starting with Steinmetz et al. (2000) and Fries et al. (2001), many experiments have linked attention and neuronal oscillations, as described in the previous chapter.

1.4 Short summary of PhD work

Given all this experimental evidence, the main goal of this thesis is to complement these results using computational modeling, and study the role of oscillations in attentional processes as well as in information transmission. We start by presenting the network model we used for the simulations and then summarize the main results.

1.4.1 Neuronal network

Our neural network simulations are based on the recurrent network model developed for working memory properties of the prefrontal cortex (Brunel & Wang, 2001). Each IF unit charges up to its stationary value as long as its membrane potential stays below a threshold. The membrane potential $V(t)$ is given by:

$$C_m \frac{dV(t)}{dt} = -g_m(V(t) - V_L) - I_{\text{syn}}(t). \tag{1.1}$$

C_m is a membrane capacitance, g_m, a membrane leak conductance, V_L, a resting potential and I_{syn}, the total synaptic current flowing into the cell. When the membrane potential reaches the threshold potential, it sends out a spike to all connected neurons and resets its membrane potential to the reset potential. The circuit remains shunted for a refractory period. Synaptic currents are mediated by excitatory (AMPA and NMDA) and inhibitory (GABA) receptors. The total synaptic current is given by

$$I_{\text{syn}}(t) = I_{\text{AMPA,ext}} + I_{\text{AMPA,rec}} + I_{\text{NMDA}} + I_{\text{GABA}}. \tag{1.2}$$

Each current is of the form $I = gV$. AMPA has a very short decay time (2 ms) while NMDA has a long one (100 ms) and the GABA decay time lies in-between (10 ms). The rise times of AMPA and GABA currents are neglected, as they are typically very short ($<$ 1 ms). The equations are integrated using a fourth order Runge-Kutta method with a time step of 0.02 ms. The network is organized in pools (Fig. 1.12).

Pools are created because different parts of the network get different exposure to stimuli. Neurons in one pool are defined by increased mutual connection strength and by the input they receive. The synaptic efficacies are kept fixed through the simulation. They are set consistent with a Hebbian rule: the synapse between two cells is strong if they were active in a correlated manner in the past. Therefore, cells within one pool have strong recurrent connections while the connections between pools are weak. All our different network models consisted of 80% excitatory neurons and 20% inhibitory interneurons. These are the proportions observed in the cerebral cortex. The networks are fully connected. A network typically consists of several pools of excitatory neurons that are selective to input. These pools are connected to a pool of inhibitory neurons, accounting for global inhibition. Both excitatory and inhibitory neurons are exposed to an external firing rate of 2.4 kHz, mimicking the spontaneous activity of the surrounding cortex. The random fluctuations in this external input make the whole system behave stochastically. Inputs to the neuronal pools are

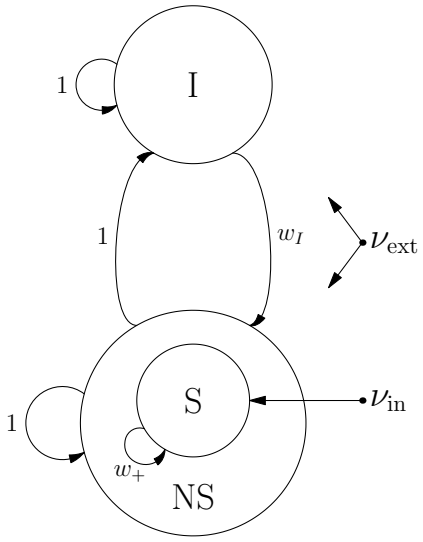

Figure 1.12: Schematic representation of a generic network module. The network module consists of excitatory and inhibitory neurons. The excitatory neurons are organized in a pool of selective neurons (S) and a pool of nonspecific neurons (NS). The selective neurons receive the input encoding the stimulus (ν_{in}). All the neurons get an input (ν_{ext}) that simulates the spontaneous activity in the surrounding cerebral cortex. The connection weight of the recurrent connections is w_+ for the selective pool and 1 for the nonspecific and inhibitory neurons. The inhibitory pool connects to the excitatory pools with a connection weight of w_I and the excitatory pools connect with the inhibitory pool with a connection weight of 1.

modeled as Poisson spike trains. Detailed mathematical descriptions and all parameter values for the studies are given in the Appendix.

Different variants of this basic model are presented in chapters 2 and 3. In the following, we briefly summarize this work.

1.4.2 The neuronal basis of attention: Rate vs. synchronization modulation

In this part, we study the role of oscillations in attentional processes. The starting point was the article by Fries et al. (2001). They found that neurons activated by the attended stimulus showed increased gamma-frequency synchronization compared with neurons activated by the distractor (see Fig. 1.6). A computational model for biased competition has

been proposed by Deco & Rolls (2005). They have shown that competition between pools of neurons combined with top-down biasing of this competition gives rise to a process that can be identified as attentional processing. However, they limit their analysis to studying rate effects. Effects on gamma synchronization are not addressed. This leaves open questions: Does attention modulate both rates and gamma synchronization? Are both types of modulation mutually exclusive or are they concomitant effects?

In our work (see also chapter 2), we address these questions by modeling one layer of the visual cortex with a network of integrate-and-fire (IF) neurons. Attention is modeled as an additional Poisson input to the neurons encoding the attended stimulus. First we show that our model can reproduce several of the experimental findings. There are two dominant frequency bands in the power spectrum, one at low frequencies and one in the gamma frequency range (40–60 Hz). The peak in the gamma frequency band is only present during the stimulus period. The height of the peak in the gamma band can be controlled by adjusting the AMPA (g_{AMPA}) and NMDA (g_{NMDA}) conductances. Increasing g_{AMPA} and decreasing g_{NMDA} increases the gamma oscillations. We then study the attentional modulations as a function of the power in the gamma band. The rate modulation shows a constant decrease. The gamma-frequency modulation in turn increases until a $g_{\mathrm{AMPA}}/g_{\mathrm{NMDA}}$ modification ratio of about 0.12 is reached and then decreases. In sum, rate and gamma frequency modulations do not covary (Fig. 1.13). In addition, we studied the effects of gamma synchronization on the efficiency of stimulus representation. There is a latency from presenting a stimulus to the network until this stimulus has an effect on the firing rates. We find that this latency is shortest in the same range of gamma power as modulation is highest (Fig. 1.14). Thus, our results suggest that gamma modulations make the system more efficient, which implies that gamma modulation has behavioral relevance. In a next step, we extended our model to two layers. This permitted us to study the variation of attentional modulation along the visual pathway. We show that the modulatory effects in both layers are qualitatively similar, but more pronounced in the upper layer. These modeling results are compatible with an increase of gamma modulation along the visual pathway.

1.4.3 Optimal information transfer in the cortex through synchronization

In the previous section we presented work studying the link between synchronization and attention. But as described in section 1.2.2, temporally

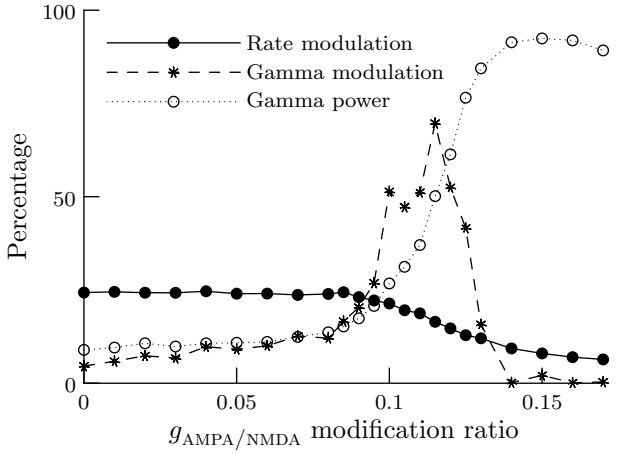

Figure 1.13: Rate modulation (solid curve) and gamma modulation (dashed curve) as a function of $g_{\mathrm{AMPA}}/g_{\mathrm{NMDA}}$ modification ratio. Increasing the $g_{\mathrm{AMPA}}/g_{\mathrm{NMDA}}$ modification ratio has the effect of increasing the oscillations in the gamma band (dotted curve). Rate modulation decreases monotonically while gamma modulation has a peak at a $g_{\mathrm{AMPA}}/g_{\mathrm{NMDA}}$ modification ratio of about 0.12. Either of the two modulations can be dominant, depending on the strength of the oscillations. Results obtained in chapter 2.

correlated neuronal activity could also have a role independent of attention, i.e., adjusting the flow of information in the brain as a whole. Womelsdorf et al. (2007) studied the correlation between neuronal areas as a function of phase shifts in the gamma frequency band. They show evidence that there is a specific phase shift at which the correlation is highest. The correlations are lower the further away the phase shift is from this optimal phase shift. These authors conclude that the effective connectivity in a network can thus be maximized or minimized through synchronization of a specific phase. While this result is compatible with the CTC hypothesis, it leaves open questions. Correlations do not tell us anything about functional dependences. If phase shifts shape effective network connections, there must be a measurable effect on information throughput. Other questions are whether this dependency is restricted to the gamma band or it can be generalized to other frequencies, and what the influence of the gamma power is in the signal.

We address these questions using a detailed biophysical model net-

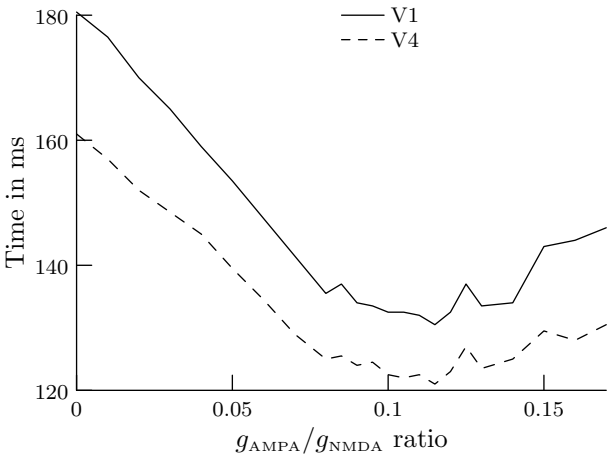

Figure 1.14: Average time to reach the mean firing rate after stimulus presentation to the selective pools. There is an optimal $g_{\mathrm{AMPA}}/g_{\mathrm{NMDA}}$ modification ratio at which these reaction time is shortest. This ratio coincides with the one at which attentional gamma modulation is strongest (compare Fig. 1.13). The latencies in the upper layer (dashed line) are generally shorter than the latencies in the lower layer (solid line). Results obtained in chapter 2.

work (see also chapter 3). Using a modeling approach for this purpose has several advantages. First, we are able to generate more data then in an experiment, which enables us to use a better statistical measure for the mutual interaction than just rank correlation. We opted to use transfer entropy (TE), introduced by Schreiber (2000). TE is an information theoretical measure that quantifies the statistical coherence between systems. It has the advantage that it does not only measure the coherence between two signals, but is able to distinguish between driving and responding elements and therefore between shared and transported information. We measure the TE between the MUA of two neuronal clusters, allowing us to study the interdependence of the spiking activity in each of them and not just the correlation of the spectral power in a specific frequency band, as was done in the experimental work. Second, the modeling approach enables us to vary network parameters systematically and therefore to explore the dynamical range of the network. Our model network consists of IF neurons. Two pools of excitatory neurons are connected to each other by feedforward and feedback connections. An input is applied to one of the pools, which is then passed on to the second pool. TE is used to mea-

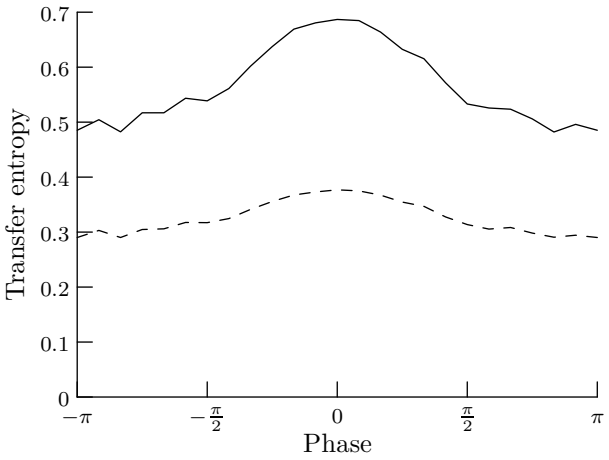

Figure 1.15: TE as a function of phase shifts. The phases are aligned relative to the mean phase, i.e., a phase shift of zero represents mean phase shift. TE is highest for the mean phase shift. The solid line represents TE from the first neuronal pool to the second (forward), the dashed line from the second pool to the first (backward). Results obtained in chapter 3.

sure the information exchange between the two pools. Each excitatory pool is connected to an inhibitory pool, which generates oscillations in the gamma frequency band through a pyramidal-interneuron feedback loop.

In support of the experimental results, we show that the correlation between the neuronal activity in the two pools depends on the phase in the gamma frequency band. After applying TE to measure the information exchange between the two pools, we find that TE very similarly depends on the phase shift, i.e., there is an optimal phase relation where the information exchange between the two neuronal clusters is maximal (Fig. 1.15). In addition, if the network is modified to oscillations in the beta band, we find a dependence of TE on the power in the beta band. We then sort the trials according to the power in the gamma band. We find that TE increases as a function of the gamma band power (Fig. 1.16). Finally, we show that the information exchange is not only stronger but also fast, if gamma oscillations are present (Fig. 1.17).

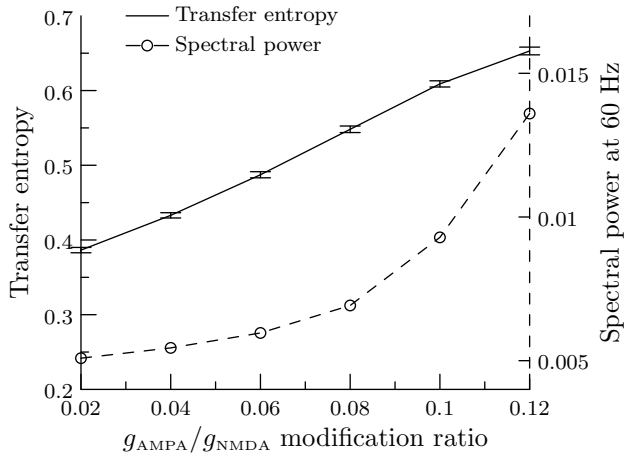

Figure 1.16: TE as a function of gamma frequency power. TE is shown for six different values of the $g_{\mathrm{AMPA}}/g_{\mathrm{NMDA}}$ modification ratio (solid line). A higher $g_{\mathrm{AMPA}}/g_{\mathrm{NMDA}}$ modification ratio causes the network to oscillate in the gamma frequency range and thus increases the power in this frequency band (dashed line). Results obtained in chapter 3.

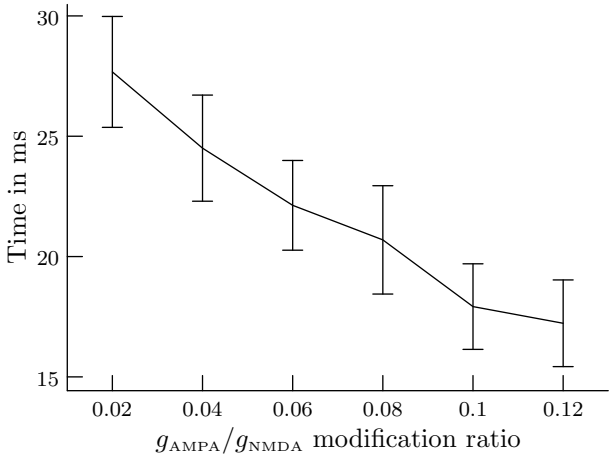

Figure 1.17: Average latency to reach 50% of the average TE as a function of the $g_{\mathrm{AMPA}}/g_{\mathrm{NMDA}}$ modification ratio. The higher the $g_{\mathrm{AMPA}}/g_{\mathrm{NMDA}}$ modification ratio, the shorter the latencies, and therefore the stronger the oscillations. Results obtained in chapter 3.

1.5 Conclusions

Oscillations in both single cortical neurons and in neuronal clusters have been reported for years. However, it has remained unclear how these oscillations link to behavior. Here, we approach this question by means of computational modeling. Our results indicate that attention modulates gamma synchronization independently of firing rates, which suggests that the two mechanisms are independent of each other. In addition, we show that input to the part of the network that encodes the attended stimulus is passed on faster the stronger the oscillations in the gamma band are. This signal transmission can be interpreted in terms of reaction time and provides a link to behavior.

We also present results showing that information transfer between two neuronal areas depends on the relative phase in the dominant frequency band. There is an optimal phase relation ship between the two signals. If the phase shift deviates from this optimal phase shift, the exchanged information decreases. Therefore, shifting the phases in the oscillations provides a mechanism to control the actual connectivity between different brain areas. These results clearly support the CTC hypothesis which proposes that neuronal synchronization can control effective network connections. We show that this result is not restricted to the gamma band, suggesting that this could be a more general mechanism for controlling brain signals.

Furthermore, we show that both the amount and the speed of the information exchange depend on the strength of the oscillations, which again provides a link between oscillations and behavior. As neuronal oscillations improve the signal transmission in a network, they could have direct behavioral relevance.

In the following, we proceed to present the results comprising this dissertation in detail.

2 The neuronal basis of attention: Rate vs. synchronization modulation

The work presented in this chapter is published in the Journal of Neuroscience[1] *and in* New Mathematics and Natural Computation[2].

2.1 Introduction

In this chapter, we focus on the role of oscillations in attentional processing. Experimental work has shown evidence of two neuronal correlates of attention, namely modulation of firing rates and modulation of neuronal synchronization. Biased competition has been suggested as a mechanism to account for the modulation of firing rates (Moran & Desimone, 1985; Chelazzi et al., 1993; Desimone & Duncan, 1995; Chelazzi, 1999), while modulation of synchronization has been reported in several recent studies (Gruber et al., 1999; Steinmetz et al., 2000; Fries et al., 2001). A computational model for biased competition has been proposed by Deco & Rolls (2005). They have shown that competition between pools of neurons combined with top-down biasing of this competition gives rise to a process that can be identified as attentional processing (see appendix 2.A.1 on p. 46). However, they limit their analysis to studying rate effects. The effects on gamma synchronization are not addressed. This leaves some open questions: Is attention modulated by both rates and gamma synchronization? Are they both mutually exclusive or are they concomitant effects? We

[1] Buehlmann, A. & Deco, G. (2008). The neuronal basis of attention: Rate versus synchronization modulation. *Journal of Neuroscience*, 28:7679–7686.

[2] Buehlmann, A. & Deco, G. (2009). Rate and gamma modulation in attentional tasks. *New Mathematics and Natural Computation*, 5(1).

address these questions by modeling one layer of the visual cortex with a network of integrate-and-fire neurons.

Our main results are the following:

- The effect of the attentional bias can be both an increase in the rates or an increase in the gamma synchronization. Depending on the dynamical working regime, one of the two effects is dominant.
- Gamma modulation can be altered without affecting the present rate modulation.
- The mean rate in the pools encoding the stimulus is reached fastest in the working regime where gamma modulation is strongest.
- Altogether, gamma modulation and rate modulation are not concomitant effects. However, if both are present, information is processed advantageously.

2.2 Methods

2.2.1 Experimental paradigm

We propose a model to account for the results from the attentional visual task used by Fries et al. (2001). In this task, the monkey had to fixate a central spot. After 1500 to 2000 ms, two stimuli, consisting of black and white luminance grating, appeared. We will call the attended stimulus target and the one that is unattended distractor. A cue indicated where to locate attention. The cue was either the color of the fixation spot or a line next to the fixation spot, pointing to the location of the target. After 500 to 5000 ms one of the two stimuli changed its color to yellow. This change was close to the monkey's detection threshold. If the color change occurred in the target, the monkey had to respond by releasing a bar. If it occurred in the distractor, the monkey had to ignore it. The monkey was only rewarded if it released a bar upon change in the target. The monkeys performed about 85% correctly.

All recordings were done in the extrastriate cortical area V4 of the visual cortex. From the two presented stimuli, one was inside the recorded receptive field (RF), one outside. The condition where the monkey was attending to the stimulus inside the RF is referred to as "with attention", and the condition with attention outside the RF as "without attention". To measure the synchronization between spikes and the local field potential

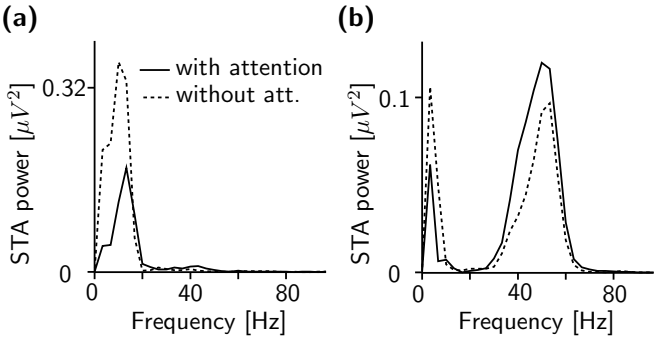

Figure 2.1: STA power spectra. Dashed curve: attention outside the RF; solid curve: attention into the RF. Adapted from Fries et al. (2001). **(a)** Power spectrum of the delay period STAs. The delay period was the 1 s interval before stimulus onset. **(b)** Power spectrum of the stimulus-period STAs. The stimulus period lasted from 300 ms after stimulus onset until one of the stimuli changed its color.

(LFP), the spike triggered average (STA) and its power spectrum are used (see below).

Fries et al. (2001) found that there are two dominating frequency bands in the STA during the stimulus period: One below 10 Hz and another between 35 to 50 Hz. During the delay period, in the "with attention" condition, there was a reduction in the low frequency synchronization (Fig. 2.1a). During the stimulus period, in the "with attention" condition, there was a reduction in the low frequency synchronization and an increase in the gamma frequency synchronization (Fig. 2.1b). Simultaneously, the median of the firing rates was enhanced by 16% during the state of attention.

2.2.2 Theoretical framework

As a description at the neural level, we use models of neurons with leaky integrate-and-fire (IF) dynamics. We follow the model of Brunel & Wang (2001). Synaptic currents are mediated by the excitatory receptors AMPA and NMDA and the inhibitory receptor $GABA_A$. There are two types of excitatory synapses, AMPA and NMDA, that have different time constants. AMPA decays very fast (2 ms) while NMDA decays slowly (100 ms). The decay constant of GABA (10 ms) lies in between the two. The network is organized in pools. Cells within one pool have strong recurrent

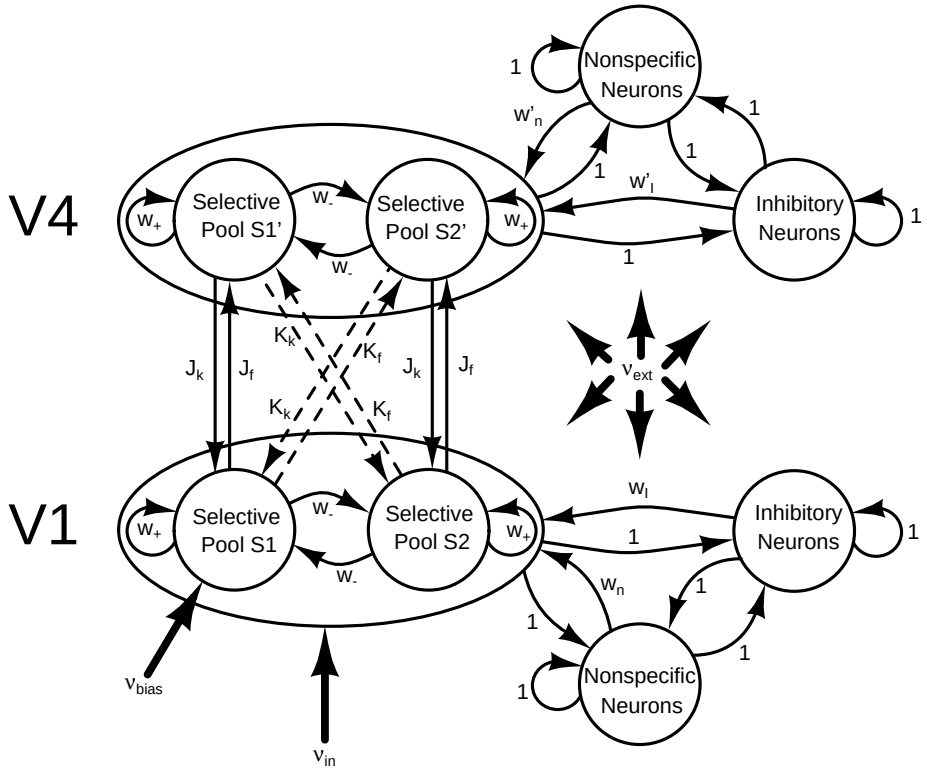

Figure 2.2: Schematic representation of the network. The network consists of inhibitory and excitatory neurons. The excitatory neurons are organized in three pools per layer: the nonspecific neurons and the two selective pools (S1, S2 or S1', S2') that receive the input encoding the stimulus ν_{in}. One of the two selective pools gets an additional bias ν_{bias}. All neurons in the network get an input ν_{ext} that simulates the spontaneous activity in the cerebral cortex. The selective pools of the two layers are connected. There are strong (J_f) and weak (K_f) feedforward connections and strong (J_k) and weak (K_k) feedback connections. Recurrent connections are denoted as w_+, between-pool connection as w_-. w_I, w'_I are the connection weights from the inhibitory to the excitatory pools and w_n, w'_n the connection weights from the nonspecific to the selective pools.

connections while the connections between pools are weak. Our model, shown in Fig. 2.2, consists of two layers (corresponding to V1 and V4). Each layer consists of 800 pyramidal neurons and 200 interneurons. The network is fully connected. Each layer is subdivided into four pools. There are three pools of excitatory neurons (the two selective pools and the non-specific neurons) that are all connected to one pool of inhibitory neurons. The selective pools are the ones that receive the input, either externally (as in V1) or from the lower layer (as in V4). The nonspecific pool emulates the spontaneous activity in surrounding brain areas. The selective pools (S1, S2, S1', S2') of the two layers are connected to each other. Between the layers, we take into account that a stimulus that is a preferred one for S1 (S2) also provokes a strong stimulation of S1' (S2'). Therefore, the J connections are stronger than the K connections. The two selective pools in layer V1 (S1, S2) encode two non-overlapping RF. The RFs in layer V4 are larger, each covering the two selective pools in V1. By having overlapping RFs, the competition in V4 is stronger than in V1. This is taken into account by setting the inhibitions in V4 to be stronger than in V1. In our model of attention, we assume that the stimulus is passed on to the modeled brain area V1 as a Poisson spike train. The attentional bias is modeled as an additional Poisson spike train, received only by the attended pool S1. In addition to the recurrent connection, the network is exposed to an external current, modeling the spontaneous activity observed in the cerebral cortex. In our network, oscillations are generated by adjusting the conductances g_{AMPA} and g_{NMDA}. An increase of g_{AMPA} and a decrease of g_{NMDA} is equivalent to an increase in the excitation/inhibition ratio and will increase the power of oscillations (Brunel & Wang, 2003).

Full details of the network and a table with the default values for all the parameters can be found in appendices A.1, A.2 and A.3, respectively, on p. 79 and following.

2.2.3 Analysis

Local Field Potential

In their experiment, Fries et al. (2001) use separate extracellular electrodes to record spikes and local field potential (LFP) activity. The spikes measured from one electrode belong to 2 to 10 neurons. They state that the LFP reflects the average transmembrane currents of neurons in a volume of a few hundred micrometers' radius around the electrode tip.

In our simulations, we have access to all the spikes of all the neurons in one pool and therefore we calculate the LFP as an average over all neurons

in one pool. The LFP is thought to be a weighted average of the input signals of a neural population; see Logothetis (2003) for a revision. As it is not exactly clear what measure in a simulation corresponds to this, we used three different ways of calculating the LFP. The first method was to average the spike rates of all neurons in one pool. The second one was to average the membrane potentials of all neurons in one pool. The third one was to average the incoming synaptic currents to a neuron over all neurons. We found that in our case these three measurements were highly correlated and that the qualitative results did not depend on the way we computed the LFP. The results reported here are obtained using method one. From the similarity of the three measurements one could deduce that looking at spike-spike correlations instead of spike-LFP correlations might suffice. However, to be able to compare our results with the experimental results, we still need to calculate the LFP.

Spike Triggered Average

To measure the synchronization between spikes and the LFP, we used the spike triggered average (STA). We used the same method as Fries et al. (2001) in order to be able to compare our modeling results with the experimental ones. An explanatory figure of the way the STA is calculated is plotted in Fig. 2.3. Around each spike time, a window of predefined size (typically $\pm$100 ms) is cut out of the LFP. These time windows are plotted as shaded areas. The average over all these windows is called the STA. In order to characterize the STA, we calculate its power spectrum, using a fast Fourier transformation. The resulting power spectrum is then normalized by dividing it by the total power in the spectrum. The idea behind the STA is that, if spike times have a reliable temporal relation to the local neuronal activity as measured by the LFP, these fluctuations add up during the averaging process. Otherwise, if there is no temporal relation between spike times and the activity of surrounding neurons, fluctuations in the LFP average out during averaging. We define the low frequency range as 0–20 Hz and the gamma frequency range as 35–65 Hz.

Attentional Modulation

We denote the stationary values of the averaged firing rate in the attended state with ν^{att} and in the unattended state with ν^{noatt}. The firing rate is averaged over the period from 200 ms after the stimulus onset until the end of the stimulus presentation. Similarly, we calculate the STA with all the spikes occurring in the period from 200 ms after the stimulus onset

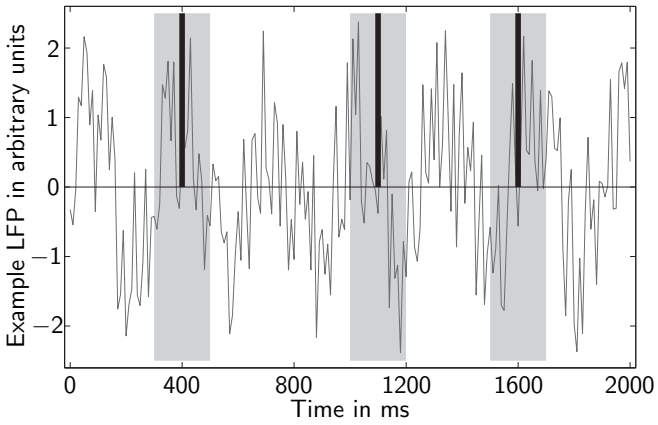

Figure 2.3: Calculation of the STA: The figure shows an example LFP (gray curve) in arbitrary units and three spikes depicted as black bars. Around each spike, a window of ±100 ms (shaded area) is cut out of the LFP. The average over these LFP segments is called the STA.

until the end of the stimulus presentation, once for the pool of neurons encoding the attended stimulus (STA^{att}) and once for the pool encoding the unattended stimulus (STA^{noatt}). The power spectrum of these two STAs we denote as $pSTA^{att}$ and $pSTA^{noatt}$, respectively. The attentional modulation in the selective pools is then given by

$$M_\xi = \frac{\xi^{att} - \xi^{noatt}}{\xi^{noatt} + \xi^{att}},$$

ξ being one of ν or $pSTA$.

2.3 Results

The aim of this study is to show the relationship between attentional rate modulation and attentional gamma modulation. First, we show how oscillations are generated in the network and that there are only oscillations in the gamma band if a stimulus is present. Then, we study the parameters that influence attentional modulation, in particular the attentional bias, inhibition and the synchronization in the network. We show that rate modulation and gamma modulation are not concomitant, but that it is advantageous if both are present. This suggests behavioral relevance for gamma modulation. Finally we study attentional modulation in different

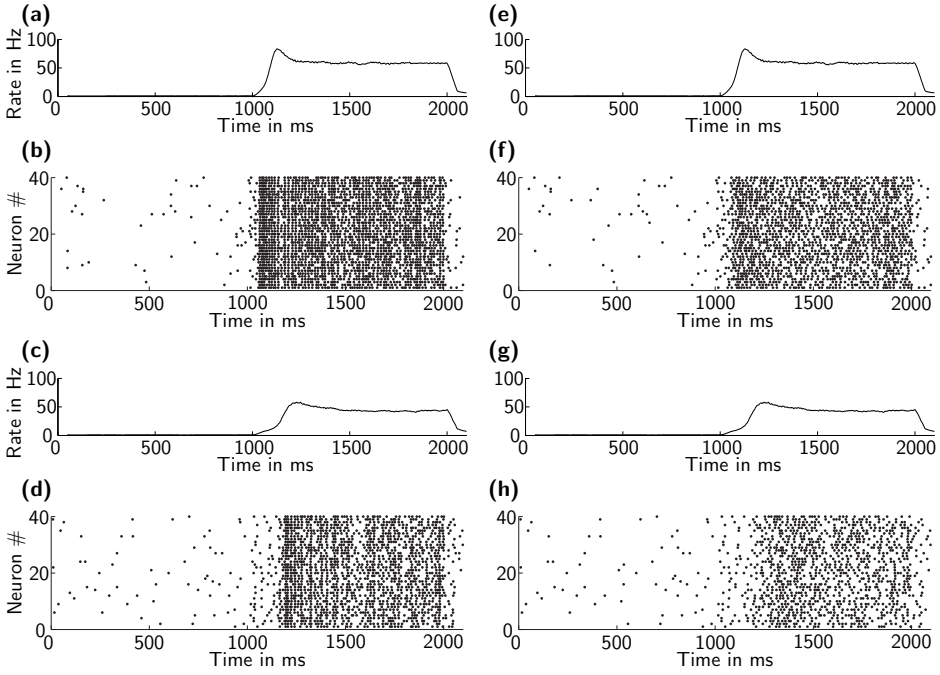

Figure 2.4: Raster plot of 40 neurons from the selective pools in V1. Stimulus onset is at 1000 ms and stimulus offset at 2000 ms. **(a)**–**(d)**: Neurons in the oscillatory regime ($g_{\mathrm{AMPA}}/g_{\mathrm{NMDA}}$ modification ratio=0.12). **(a)** Average rate with attention, **(b)** Spikes with attention, **(c)** Average rate without attention, **(d)** Spikes without attention. **(e)**–**(h)**: Neurons outside the oscillatory regime ($g_{\mathrm{AMPA}}/g_{\mathrm{NMDA}}$ modification ratio=0.0).

layers and show that both gamma and rate modulation are stronger in the upper layer. This is compatible with an increase of attentional modulation along the visual pathway. Fig. 2.4 shows a raster plot of a typical trial with neurons synchronizing after the stimulus onset at 1000 ms.

2.3.1 Oscillation generation

As explained in the Methods section, the crucial parameter to generate oscillations in the network is the relative contribution of the slow NMDA and the fast AMPA receptors to the total synaptic currents.

Fig. 2.5 shows the power spectrum of the STA during the stimulus period for selected values of the $g_{\mathrm{AMPA}}/g_{\mathrm{NMDA}}$ modification ratio. For low contributions of g_{AMPA} (e.g., solid curve), there is little power in the gamma

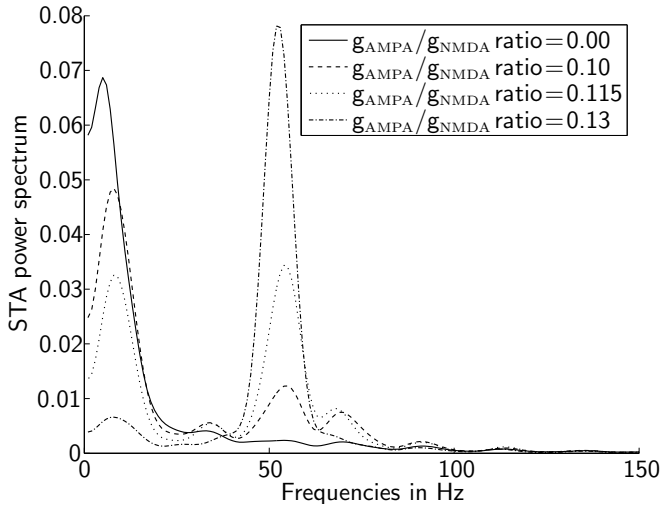

Figure 2.5: Changes in the STA power spectrum depending on the $g_{\text{AMPA}}/g_{\text{NMDA}}$ modification ratio. For a selection of $g_{\text{AMPA}}/g_{\text{NMDA}}$ modification ratios (indicated in the figure legend) we plot the power spectrum of the corresponding STAs. Averaged over 20 trials.

frequency band and for a high contribution of g_{AMPA} (e.g., dash dotted curve), there is a lot of power in the gamma frequency band.

The effects on the low frequency and the gamma frequency band are shown separately in Fig. 2.6. We plot the percentage of power in the STA for the low frequency (dashed curve) and the gamma frequency band (solid curve) against different values of the $g_{\text{AMPA}}/g_{\text{NMDA}}$ modification ratio. The more g_{AMPA} is increased, the stronger the oscillations in the gamma frequency band and the weaker the oscillations in the low frequency band. In the experiment by Fries et al. (2001), the peak values in the power spectrum of the STA were about equal for the low frequency and the gamma frequency band. Therefore, in the range of $g_{\text{AMPA}}/g_{\text{NMDA}}$ from 0.11 to 0.13, the network exhibits the same power distribution as found in the experiment by Fries et al. (2001).

Stimulus Presentation

In the experimental findings by Fries et al. (2001), the peak in the gamma band of the power spectrum of the STA is only observed during the stimulus presentation. Our model has the same property (illustrated in Fig. 2.7). We plot the power spectrum of the STA on the y-axis against the frequen-

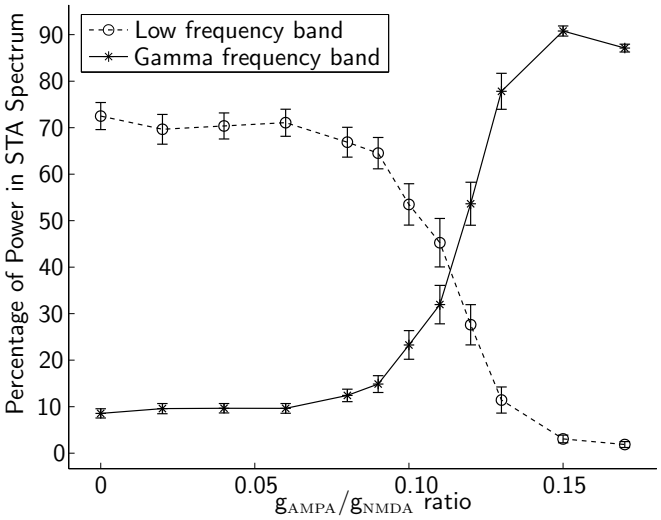

Figure 2.6: Power in the low frequency (0–20 Hz) and gamma frequency band (35–65 Hz) of the STA depending on the $g_{\mathrm{AMPA}}/g_{\mathrm{NMDA}}$ modification ratio. For each value of the $g_{\mathrm{AMPA}}/g_{\mathrm{NMDA}}$ modification ratio we plot the percentage of power in the low frequency band (dashed curve) and in the gamma frequency band (solid curve). The error bars indicate the 95% confidence intervals. Averaged over 20 trials.

cies on the x-axis. It demonstrates clearly the desired behavior, namely that almost all the power is in the low frequency band during the delay (spontaneous) period before stimulus onset (dashed curve). During the stimulus presentation (solid curve), the percentages of power in the low frequency band and in the gamma frequency band are equilibrated.

2.3.2 Parameters that modify attentional modulation

What parameters does the attentional modulation of the rates and gamma frequency synchronization depend on?

Bias

The most obvious parameter that influences attentional modulation is the applied bias (ν_{bias}). The modulation of the rates and the gamma frequency synchronization both correlate positively with the bias (see Fig. 2.8a). Additionally, we observe that also the total gamma power in the STA

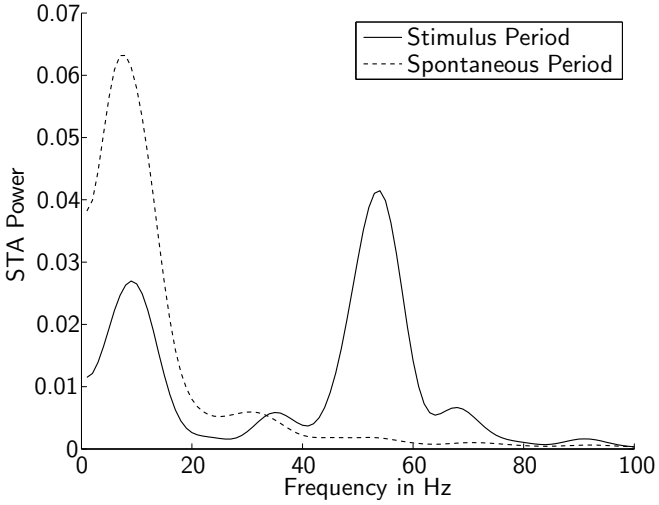

Figure 2.7: Example power spectrum of an STA comparing stimulus and delay (spontaneous) period. The power spectrum of an STA is plotted for the stimulus period (solid curve) and the delay period (dashed curve). (Averaged over five trials.)

spectrum increases with the bias. The gamma power shown is the average of the gamma power in the two selective pools (S1, S2).

Inhibition

Another parameter modifying attentional modulation is the inhibition in the network(w_I). To study its influence, we modify the connection weights of the inhibitory pool to the selective pools. Again we observe that both the rate and the gamma frequency modulation correlate positively with the inhibitory weights (see Fig. 2.8b). But contrary to the bias, the total power in the gamma frequency band decreases with more inhibition and therefore shows a negative correlation with the attentional modulation.

Altogether, we observe that with increasing competition (either higher bias or stronger inhibition) the attentional modulation in the network also increases. However, synchronization increases as a function of bias and decreases as a function of inhibition.

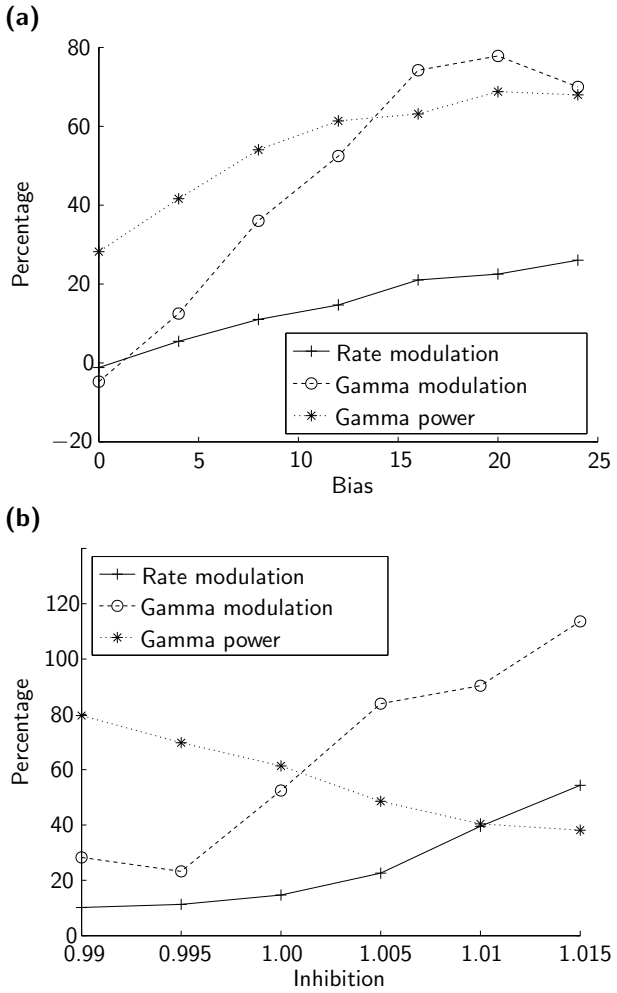

Figure 2.8: Dependences of attentional modulation on inhibition and bias. Gamma power (dotted curve) shows how much of the power of the spectrum is in the gamma band. Rate modulation (solid curve) and gamma modulation (dashed curve) show the difference between attended and unattended pools in percents. (Averaged over 200 trials.) **(a)** Gamma power, rate modulation and gamma modulation as a function of bias. For increasing bias, synchronization, rate modulation and gamma modulation increase. **(b)** Gamma power, rate modulation and gamma modulation as a function of inhibition. For increasing inhibition, synchronization decreases while both rate modulation and gamma modulation increase.

Level of Synchronization in the Network

Next we studied how the attentional modulations were affected by directly modifying the level of gamma frequency oscillation in the network. In order to do so, we adjusted the $g_{\text{AMPA}}/g_{\text{NMDA}}$ modification ratio. The power in the gamma frequency band increases monotonically with this ratio until reaching a level of more than 0.9, meaning that more than 90% of the power is concentrated in the gamma frequency band (see Fig. 2.9). The rate modulation as a function of $g_{\text{AMPA}}/g_{\text{NMDA}}$ modification ratio shows a constant decrease. The gamma frequency modulation increases until a $g_{\text{AMPA}}/g_{\text{NMDA}}$ modification ratio of about 0.12 is reached and then decreases. In summary, rate and gamma frequency modulation do *not* covary. The fact that rate modulation and gamma modulation can vary independently of each other should be considered as one of our main results. A comparison with the experimental findings by Fries et al. (2001) shows that for a $g_{\text{AMPA}}/g_{\text{NMDA}}$ modification ratio between 0.10 and 0.13, our model reveals similar attentional modulations.

If a stimulus is presented to the network, the rates in the selective pools (S1, S2) rise. The time from stimulus onset it takes a pool to reach its mean frequency is here referred to as reaction time (RT). RTs are shortest for a $g_{\text{AMPA}}/g_{\text{NMDA}}$ modification ratio of 0.12 (Fig. 2.10a). Furthermore, we observe that these RTs are different for the attended and the unattended pool, the ones of the attended pool being shorter. The difference in RT is shown in Fig. 2.10b. The biggest difference in RT we find for a $g_{\text{AMPA}}/g_{\text{NMDA}}$ modification ratio of about 0.12, which is also the range where attentional gamma modulations are strongest. A crucial observation is the fact that the inversely RTs correlate with the attentional modulation in the gamma band, i.e., the higher the attentional modulation, the shorter the RTs. Thus, our results show that gamma modulations make the system more efficient in terms of RTs, which suggests that gamma modulation has behavioral relevance.

2.3.3 Comparison of two different layers

One of the goals of this work was to study the variation of attentional modulation along the visual pathway. To address this question we compare the attentional modulation in two connected layers (V1, V4). The comparison shows that the modulatory effects in both layers are quite similar, though more pronounced in the upper layer (V4). The gamma modulation in the upper layer (V4) is up to 50% stronger than in the lower layer (V1). The rate modulation in V4 is about 28% stronger than in V1. See Fig. 2.11a.

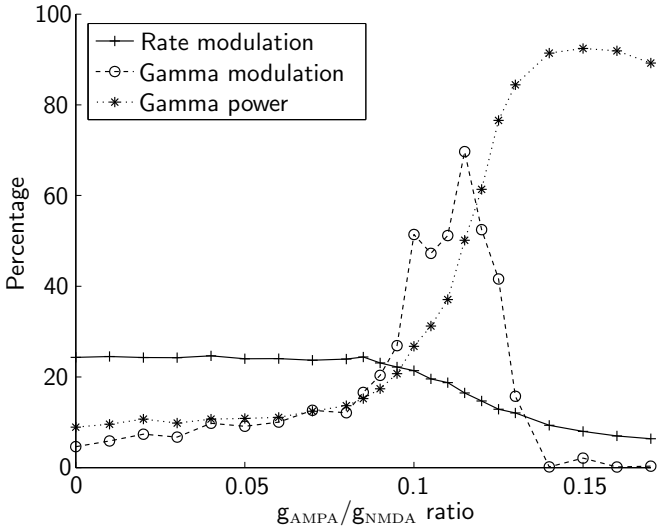

Figure 2.9: Rate modulation (solid) and gamma modulation (dashed) as a function of the $g_{\mathrm{AMPA}}/g_{\mathrm{NMDA}}$ modification ratio. The main effect of increasing the $g_{\mathrm{AMPA}}/g_{\mathrm{NMDA}}$ modification ratio is an increase in the network synchronization in the gamma band (dotted). The rate modulation decreases monotonically with the $g_{\mathrm{AMPA}}/g_{\mathrm{NMDA}}$ modification ratio. The gamma modulation increases until a $g_{\mathrm{AMPA}}/g_{\mathrm{NMDA}}$ modification ratio of about 0.12 and then decreases to almost zero. The figure shows that either of the two types of attentional modulation can be predominant. (Averaged over 200 trials.)

In summary, we find that the attentional modulation is stronger in the upper layer than in the lower one. These modeling results are thus consistent with an increase of the gamma frequency modulation along the visual pathway.

In sum, we show that there is an increase in the gamma modulation from the lower layer to the upper layer even if the $g_{\mathrm{AMPA}}/g_{\mathrm{NMDA}}$ modification ratio is the same in both layers. If we now modify this ratio independently in the different layers, we observe that whichever layer has its $g_{\mathrm{AMPA}}/g_{\mathrm{NMDA}}$ modification ratio closer to 0.12 (which is the optimal ratio to evoke gamma oscillations) has the higher gamma synchronization and the higher gamma modulation. This means that the upper layer can oscillate at gamma frequency even though the lower layer shows no or very little synchronization in the gamma band. See Fig. 2.11b.

In our model, we make the assumption that the $g_{\mathrm{AMPA}}/g_{\mathrm{NMDA}}$ modifi-

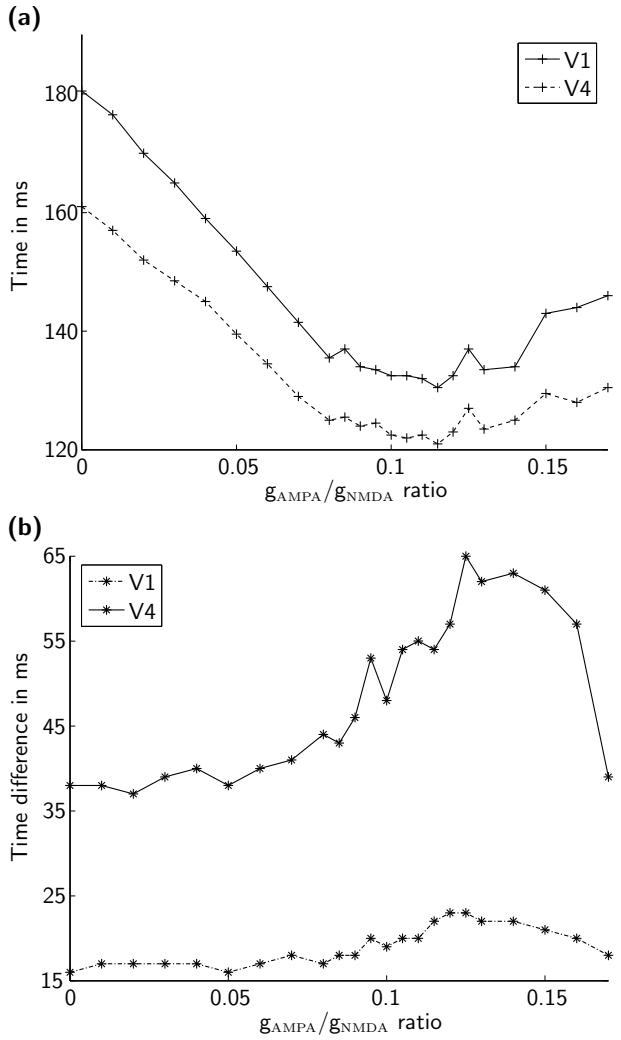

Figure 2.10: Reaction times. **(a)** Average time to reach the mean activity level after stimulus presentation in the selective pools. A higher $g_{\text{AMPA}}/g_{\text{NMDA}}$ modification ratio makes the rates rise faster. The mean activity level is reached fastest for a $g_{\text{AMPA}}/g_{\text{NMDA}}$ modification ratio between 0.10 and 0.13. In this range also the attentional gamma modulation is maximal. **(b)** Time difference in reaching the mean activity level after stimulus presentation between the pools encoding the attended and the unattended stimulus. This difference is biggest for a $g_{\text{AMPA}}/g_{\text{NMDA}}$ modification ratio around 0.12, which is also the range where attentional gamma modulation is maximal.

cation ratio increases in the posterior ventral cortex. On the other hand, it is often claimed that the $g_{\text{AMPA}}/g_{\text{NMDA}}$ modification ratio decreases towards prefrontal cortex, in order to stabilize memory. We assume here that the $g_{\text{AMPA}}/g_{\text{NMDA}}$ modification ratio increases only along the posterior ventral cortex (where memory is of less importance) and then decreases again towards prefrontal cortex.

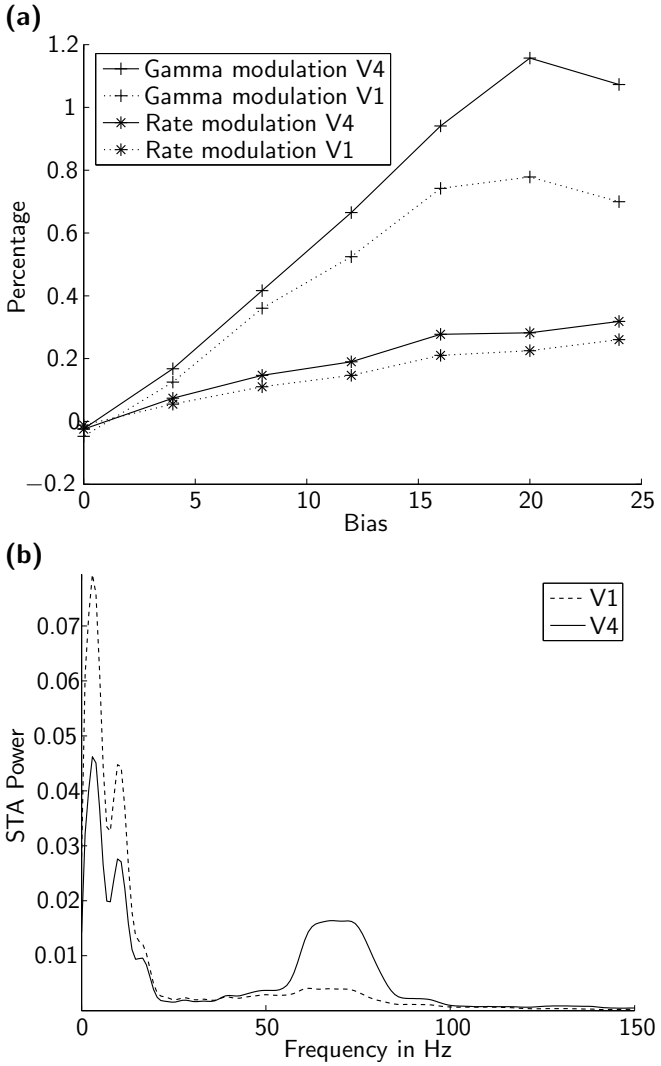

Figure 2.11: Comparison of attentional modulation in two layers. **(a)** Differences in attentional modulation between the two layers V1 and V4. The gamma modulation in the upper layer is up to 50% stronger than in the lower layer. The rate modulation in V4 is up to 28% stronger than in V1. In general, modulations in V4 are stronger than modulations in V1. **(b)** Different $g_{\text{AMPA}}/g_{\text{NMDA}}$ modification ratio in the two layers. The $g_{\text{AMPA}}/g_{\text{NMDA}}$ in layer V1 is 0.0 and in layer V4 0.15. Layer V4 clearly synchronizes in the gamma frequency band while V1 does not.

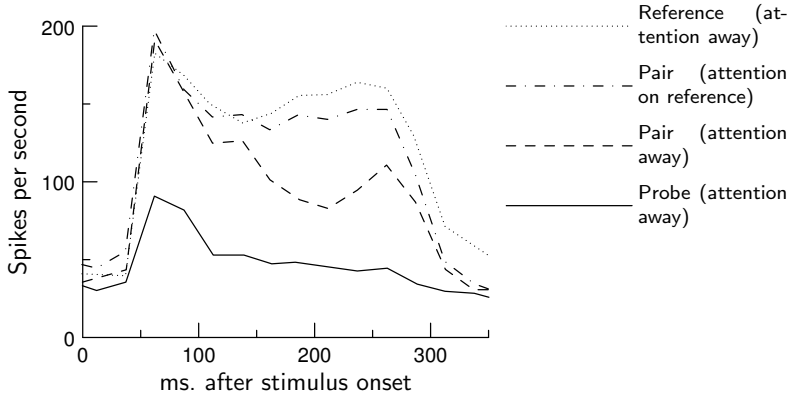

Supplementary Figure 2.1: Experimental Results. Attention filtering out the effect of a suppressive probe in V2. Dotted line: Response to reference stimulus. Solid line: Response to probe stimulus. Dashed line: Response to pair (suppressed by addition of probe). Dash dotted line: Pair response when attention is directed to reference stimulus. The response is almost equal as when only the reference stimulus is present. Figure adapted from Reynolds et al. (1999).

2.A Chapter appendix

2.A.1 Biased competition in experiment and model

Experiment

Reynolds et al. (1999) measured cell responses in V2 and V4 from monkeys performing an attentional task. In this task, stimuli could appear at four positions: Two within the receptive field (RF), and two outside. On each trial, the reference, the probe or the pair appeared within the RF. The monkey was cued to attend to one of the locations and had to respond when a diamond shaped target appeared at the attended location while ignoring distractor targets. They found that the presentation of the two stimuli together caused a response that lay in-between the responses to either of the single stimuli, when the monkey was attending to a location outside the RF. Then the monkey had to attend one of the two stimuli inside the RF. This caused a cell response similar to when the attended stimulus was presented alone. Their results are depicted in Suppl. Fig. 2.1. Their findings are consistent with the biased competition hypothesis for attention that states that attention biases the competition among neurons in the direction of the attended stimulus.

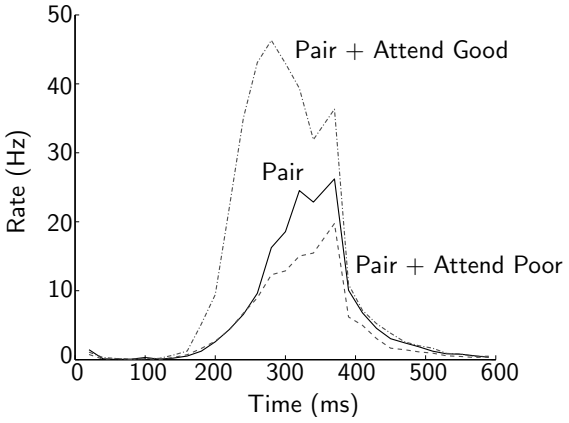

Supplementary Figure 2.2: Simulation corresponding to the experiment from Reynolds et al. (1999). Development of the firing rate under simultaneous presentation of a good and a poor stimulus inside the RF. Solid line: response when attention is outside the RF. Dashed line: Response when attention is directed to the poor stimulus (attentional suppression). Dash dotted line: Response when attention is directed to the good stimulus (attentional enhancement). Figure adapted from Deco & Rolls (2005).

Model

Using the model described above, we showed that top-down attentional effects can be explained by external attentional inputs biasing neurons (Deco & Rolls, 2005). This bias moves the activity of neurons towards different parts of their nonlinear activation functions. It is important to note that we are not assuming any kind of multiplicative effects but only additive synaptic effects. Therefore, attention seems to be a network phenomenon. The results from Reynolds et al. (1999) can be successfully reproduced, as shown in Suppl. Fig. 2.2. The middle line (solid) is the neural response when both stimuli are present in the RF, but the attended location is outside the RF. The top line (dash-dotted) shows the enhanced neural response when attention is directed to the reference (good) stimulus. The bottom line (dashed) shows the suppressed response, when attention is directed to the probe (bad stimulus).

3 Optimal information transfer in the cortex through synchronization

The work presented in this chapter is submitted. Abstract is published[1].

3.1 Introduction

In this chapter, we focus on the role of oscillations in information transmission.

Several authors have proposed that the interactions among neuronal groups depend on neuronal synchronization (Varela et al., 2001; Salinas & Sejnowski, 2001). Fries (2005) has referred to this hypothesis as communication through coherence (CTC). Several experimental studies have presented results supporting the CTC hypothesis (Buschman & Miller, 2007; Saalmann et al., 2007; Womelsdorf et al., 2007; Pesaran et al., 2008; Gregoriou et al., 2009).

We concentrate on the results shown by Womelsdorf et al. (2007). These authors conclude that the effective connectivity in a network can be maximized or minimized through synchronization of a specific phase relation, resulting in an effective interaction pattern.

While the results presented by Womelsdorf et al. (2007) clearly support the CTC hypothesis, they leave some open questions. Is it only the 60 Hz power that depends on the 60 Hz phase? Do phase and power only correlate or is there a causal dependence between the two? Is this effect restricted to the gamma band or can it be generalized to other frequency bands? What is the influence of the total gamma power in the signal?

[1] Buehlmann, A. & Deco, G. (2010). Optimal information transfer in the cortex through synchronisation. *Conference Abstract: Computational and systems neuroscience 2010. doi: 10.3389/conf.fnins.2010.03.00104.*

Here, to address these questions, we use a detailed biophysical, conductance based model network with realistic spiking properties. Many different interdependence measures such as mutual information, transfer information, nonlinear regression, phase synchronization and generalized synchronization have recently been proposed (see Ishiguro et al., 2008 and Wendling et al., 2009 for comparisons of the different methods). It has become evident that the appropriateness of each measure is determined by the data it is applied to. Thus, given our current data set, we opted to use transfer entropy (TE), introduced by Schreiber (2000). We measure the TE between the MUA of the two neuronal clusters, which allows us to study the interdependence of the spiking activity in each of them and not just the correlation of the spectral power in a specific frequency band, as was done in the experimental work. A further crucial advantage of the model is that we can change network parameters systematically and explore the dynamical range of the network. In all simulations, firing rates were normalized to rule out the possible influence of rate changes.

Our main results are:

- Correlation as measured by the Spearman rank correlation coefficient depends on the phase relation in the gamma band, confirming the experimental finding of Womelsdorf et al. (2007).
- TE depends very similarly on the phase shift, i.e., there is an optimal phase relation where the TE is maximal.
- TE increases as a function of the power in the gamma band.
- Information exchange gets faster if the gamma band synchronization increases.

3.2 Methods

3.2.1 Experimental analysis

Womelsdorf et al. (2007) analyzed four different data sets. The first data set consisted of measures from awake cats in area 17 (Fries et al., 1997), the second from awake cats in areas 18 and 21a (Fries et al., 2002), the third from awake monkeys in area V1 and the fourth from awake monkeys in area V4 (Fries et al., 2001; Womelsdorf et al., 2006). In all four data sets they recorded multi unit activity simultaneously from 4 to 8 electrodes. For each pair of neuronal groups, they quantified the synchronization by MUA-MUA phase coherence spectrum, which showed a peak in the gamma

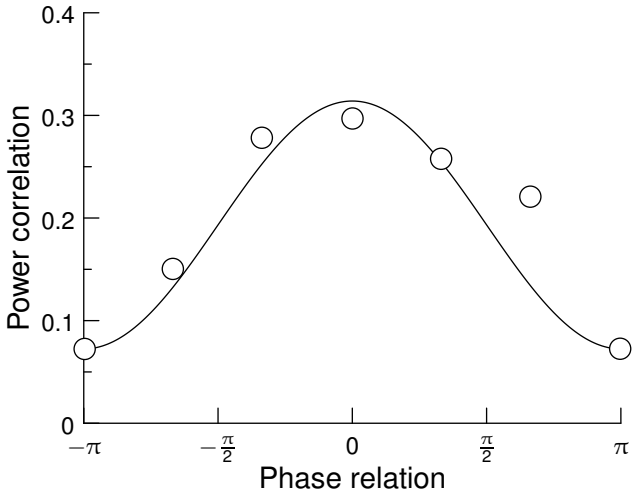

Figure 3.1: Spearman rank correlation coefficient. The rank correlation coefficient between the two MUAs' 60 Hz power is plotted as a function of their phase relation. The solid line indicates a cosine fit. Adapted from Womelsdorf et al. (2007).

frequency band. These authors then calculated the Spearman rank correlation coefficient between the two MUAs' 60 Hz power. They found that the fluctuations of the 60 Hz power were most strongly correlated when the 60 Hz phase relation was close to its mean, as illustrated in Fig. 3.1. From this they concluded that effective connectivity can be maximized or minimized through synchronization at a favorable or unfavorable phase relation.

3.2.2 Theoretical framework

We use a model with leaky integrate-and-fire (IF) dynamics, following Brunel & Wang (2001). Synaptic currents are mediated by excitatory (AMPA and NMDA) and inhibitory (GABA) receptors. AMPA has a very short decay time (2 ms) while NMDA has a long one (100 ms) and the GABA decay time lies in-between (10 ms). The rise times of AMPA and GABA currents are neglected, as they are typically very short (< 1 ms). The network is organized in pools. Neurons within a specific pool have stronger recurrent connections than neurons between the pools. The intention of this work is to study cortical neural interactions not limited to a specific brain area. However, as our simulations needed to be directly

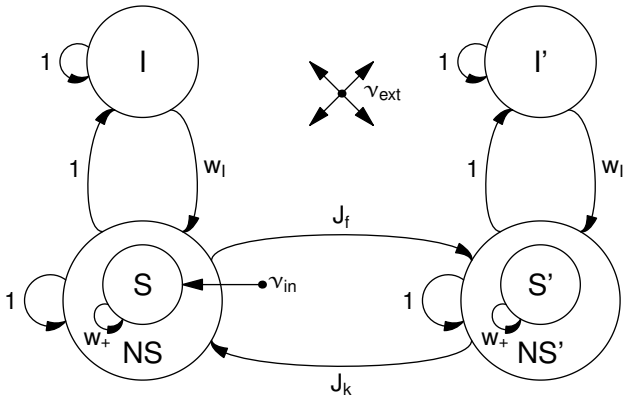

Figure 3.2: Schematic representation of the network. The network consists of two parts. In each part, there are excitatory (S, NS) and inhibitory (I) neurons. The excitatory neurons are divided into two pools. The selective pool (S) receives the external input (ν_{in}) and has strong recurrent connections (w_+). The non-selective pool (NS) simulates the surrounding cerebral cortex. In each part of the network, the excitatory neurons are connected to a pool of inhibitory neurons (I) via connection weights w_I. The two parts of the network are connected via the selective pools. There are both feedforward (J_f) and feedback (J_k) connections. The network is exposed to an external current ν_{ext}, modeling the spontaneous activity observed in the cerebral cortex.

comparable to Womelsdorf et al. (2007), and have specific parameter sets, our network models two clusters of cortical neurons in visual cortex V4.

The network model consists of two parts (Fig. 3.2). In each part there are pools of excitatory and inhibitory neurons, with a total of 800 excitatory and 200 inhibitory neurons. The excitatory neurons are subdivided into a selective pool and a non-selective pool. The neurons in the selective pools (S,S') are the ones that receive input either from outside or from the connected selective pool. The non-selective neurons (NS, NS') simulate the surrounding brain areas. Each population of excitatory neurons is connected to a pool of inhibitory neurons (I, I'). This allows for generating oscillations in each population separately. The two parts of the network are connected via feedforward and feedback connections that project onto the selective pools. The external input is a Poisson spike train that projects to the selective pool (S) of the first part of the network. In addition to the recurrent connections, the network is exposed to an external current,

modeling the spontaneous activity observed in the cerebral cortex. The network is fully connected.

Gamma oscillations in a network with excitatory and inhibitory neurons are generated through a pyramidal-interneuron feedback loop (Traub et al., 1997; Brunel & Wang, 2003). Pyramidal neurons excite interneurons and interneurons in turn send inhibition back on pyramidal cells. In our network we can therefore generate and control the oscillations in the gamma frequency band by adjusting the AMPA and NMDA conductances. By adjusting the synaptic decay constants, the oscillation frequency can be shifted into the beta band. The crucial parameter is τ_{GABA}. An increase of τ_{GABA} slows down the rhythm of the pyramidal-interneuronal loop and will therefore yield an oscillation at a lower frequency. To generate phase shifts in the gamma oscillations between the two parts of the network, we introduce a delay. The delay is set bidirectionally in the feedforward and feedback connections of the selective pools. Each spike emitted in S arrives at S' after Δt and vice versa. This lag in spike transmission generates a phase lag in the oscillations. Full details of the network and a table with the default values for all the parameters can be found in appendices A.4 and A.5, respectively, on p. 83 and following.

3.2.3 Analysis

Multi unit activity

From our spiking simulations we calculate the multi unit activity (MUA) to analyze our simulations, in order to be able to compare our results directly with the experiments. The MUA in the simulations is defined as the spikes of 10 randomly chosen neurons in each of the selective pools. This point process data is converted to a time series by binning the spikes in windows of 5 ms. The binning window is shifted in steps of 1 ms. The time series is then normalized by subtracting the mean and dividing by the standard deviation. We use the normalized time series to estimate power spectrum and TE. Normalization is applied to rule out the possible influence of rate changes.

Power spectrum and phase estimation

We use the multitaper method (Percival & Walden, 1993; Mitra & Pesaran, 1999) to calculate the spectral power of our data. The signal in each time window (1000 ms) is multiplied with a set of Slepian data tapers. The

tapered signal is then Fourier transformed, according to:

$$\tilde{x}_k(\nu) = \sum_{t=1}^{N} w_k(t) x(t) e^{-2\pi i \nu t} \tag{3.1}$$

where $w_k(t)$ are K orthogonal taper functions, $x(t)$ is the time series of our signal, and N is the number of elements in each time window. The power spectrum is then the squared amplitude of $\tilde{x}_k(\nu)$, averaged over the K tapers. We used $K = 4$ tapers in our study. The cross spectrum (S_{yx}) between two signals $\tilde{x}_k(\nu)$ and $\tilde{y}_k(\nu)$ (averaged over K tapers) is given by

$$S_{yx} = \frac{1}{K} \sum_{k=1}^{K} \tilde{y}_k(\nu) \tilde{x}_k^*(\nu). \tag{3.2}$$

The phase relation between two signals $\tilde{x}_k(\nu)$ and $\tilde{y}_k(\nu)$ is defined as the angle of the cross spectrum. We use this method for phase estimation to be able to compare directly to the experimental results.

Transfer entropy

Womelsdorf et al. (2007) quantify the mutual influence between two neuronal groups as the Spearman rank correlation coefficient of spectral power. The Spearman rank correlation is a non-parametric measure of correlation, which makes no assumptions about normality or linearity of the data. However, it is a symmetric measure and therefore fails to measure directionality of the flow of information. Thus, to overcome this limitation, here we use TE (Schreiber, 2000), which enables us to distinguish between shared and transported information. TE measures the deviation from the following generalized Markov property:

$$p(x_{t+1}|x_t^k) = p(x_{t+1}|x_t^k, y_t^l), \tag{3.3}$$

where p is the transition probability and k and l are the dimensions of the delay vectors. x_t and y_t are the time series of the signal. We write x_t and y_t instead of $x(t)$ and $y(t)$, respectively, for better readability. If the deviation is small, then Y has no relevance for the transmission probability of X. The incorrectness of this assumption can be quantified by the Kullback entropy

$$T_{y \to x} = \sum_t p(x_{t+1}, x_t^k, y_t^l) \log \frac{p(x_{t+1}|x_t^k, y_t^l)}{p(x_{t+1}|x_t^k)}. \tag{3.4}$$

In other words, TE represents the information about a future observation of variable x_t obtained from the simultaneous observation of past values

of both x_t and y_t, after discarding the information about the future of x_t obtained from the past of x_t alone (Ishiguro et al., 2008). In this study we use $k = l = 1$. Conditional probabilities required in equation 3.4 are calculated from the joint probabilities. We approximate the joint probabilities by using the histograms of the embedding vector (naive histogram technique; Lungarella et al., 2007). When the available data is limited (number of samples $N < 1000$) and the coupling between the time series is small, TE suffers from a finite sample effect, in particular for small resolution ($r < 0.05$), which makes the assessment of the significance of the obtained values difficult (Lungarella et al., 2007). However, for all our simulations $N > 1000$ and $r > 0.05$, so we can assume that the finite sample issue affects our results to a negligible extent. We calculate the TE between the MUA in the two neuronal pools.

3.3 Results

We test the hypothesis that neuronal synchronization modulates neuronal interactions. First we describe how the mean phase shift between pools of neurons is set by the delay in the feedforward and feedback connections. In accordance with the experimental results of Womelsdorf et al. (2007), we show that the correlation between the gamma power in the two pools, measured by the Spearman rank coefficient, depends on the phase relation in the gamma band. Then we measure the information exchange between the rates of the two pools with TE, an information theoretical measurement. We demonstrate that TE has a very similar dependence on the phase shift. By varying the amount of power in the gamma band in our model, we then show how TE increases as a function of gamma power. Furthermore, we reveal that if gamma power is high, information flow as measured by TE commences earlier.

3.3.1 Delay–Phase relation

Raster plots for 20 neurons from each neuronal pool are shown in (Fig. 3.3). The power spectrum of the MUA in our network shows a clear peak in the gamma band (Fig. 3.4), in accordance with the experimental results. Therefore, the introduced delay sets the phase shift for oscillations in the gamma band. The delay, however, sets only the mean phase shift, but the phase shifts fluctuate over time. Thus, even for a fixed delay they show a broad distribution around this mean phase shift. This distribution is shown in Fig. 3.5a. The mean phase in this specific simulation is 91.4°. This, however, is just an example, as the mean phase shift in the simu-

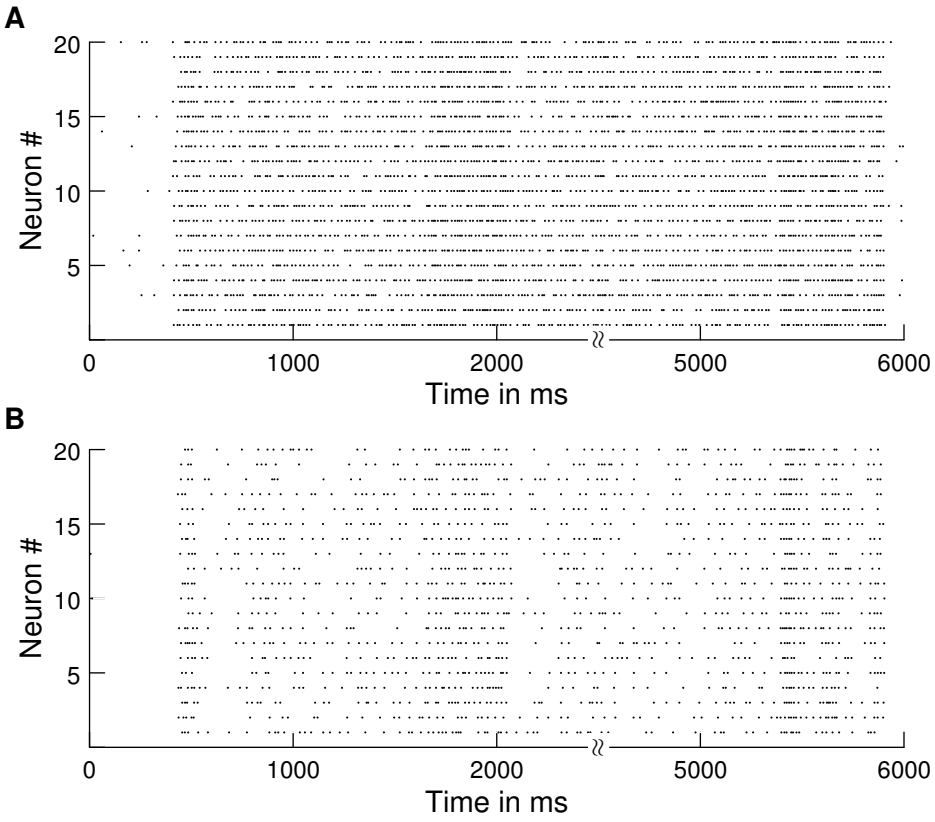

Figure 3.3: Raster plots. Raster plot of spikes of 20 neurons from the default simulations ($g_{\mathrm{AMPA}}/g_{\mathrm{NMDA}}$ modification ratio = 0.12). **(a)** Neurons from selective pool 1. **(b)** Neurons from selective pool 2.

lations can be set to any value by adjusting the delays accordingly. The phases are similarly widely distributed as in the experimental results by Womelsdorf et al. (2007), shown in Fig. 3.5b.

3.3.2 Dependence of correlations on phase

The phase shifts at 60 Hz between the two pools show a broad range of phases. We determine the phase shift in each time window of 500 ms. Then we calculate the correlation between the two pools for this time window by calculating the Spearman rank coefficient for the 60 Hz power in the two pools. The obtained correlation can now be sorted into different bins for the different phase shifts. We find that the correlation of the gamma

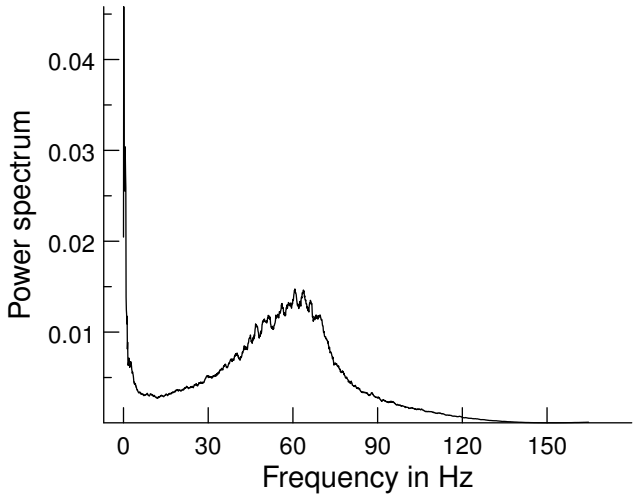

Figure 3.4: Power spectrum. The power spectrum of the MUA signal from a simulation with default parameters is shown. $g_{\mathrm{AMPA}}/g_{\mathrm{NMDA}}$ modification ratio = 0.12, averaged over 100 trials.

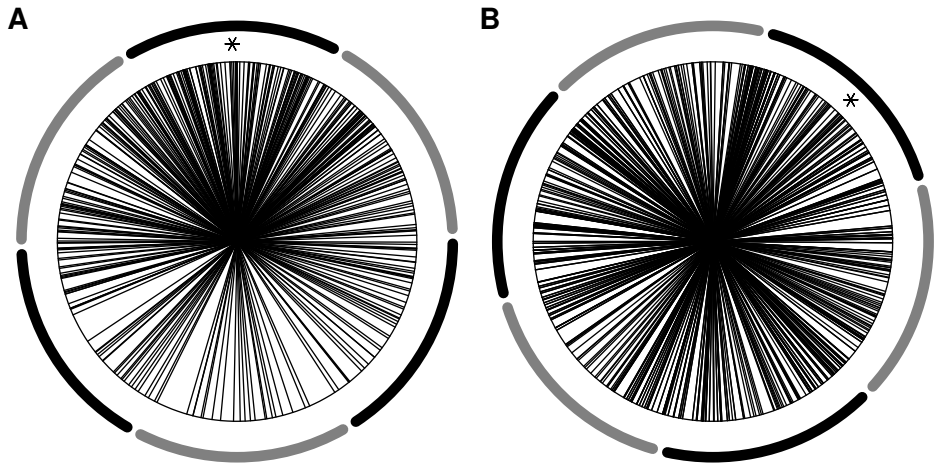

Figure 3.5: Phase distribution. The phases are widely distributed around the mean (marked with an asterix). The dark and light segments around the figures represent the phase bins into which trials were sorted. **(a)** Simulation: Phase distribution with an exemplary mean of 91.4° from the default simulations ($g_{\mathrm{AMPA}}/g_{\mathrm{NMDA}}$ modification ratio = 0.12). **(b)** Experiment: Phase distribution with a mean of 45.8°. Adapted from Womelsdorf et al. (2007).

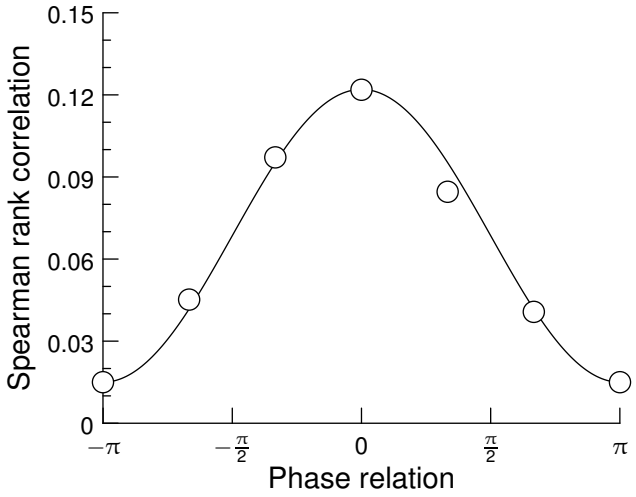

Figure 3.6: Spearman rank correlation coefficient. The rank correlation between the 60 Hz power in two neuronal pools is plotted as a function of the phase shift in the gamma band. A phase shift of zero represents the mean phase shift which is the point where the rank correlation is highest. The solid line indicates a cosine fit.

band power between the two pools depends on the mean phase shift in the gamma band. We emphasize that a change in firing rates could not account for this result, as they have been normalized. Fig. 3.6 shows the rank correlation plotted against the phase shifts. The correlation is highest for the bin containing the mean phase shift and drops as it moves away from the mean. This confirms the experimental results of Womelsdorf et al. (2007).

3.3.3 Dependence of TE on phase

The Spearman rank coefficient as used in the previous section gives only an estimate of the correlation between the two connected pools. It contains no information about which the driving and which the responding pool is. Therefore, we use an information theoretical measure, the so called transfer entropy (TE). The TE is able to quantify the directionality of the exchanged information between the pools (see Methods). We apply this measure now to the same data as in the previous section. However, we measure the TE between the MUA in the two pools and not only the 60 Hz power. We find that the TE depends strongly on the phase relation

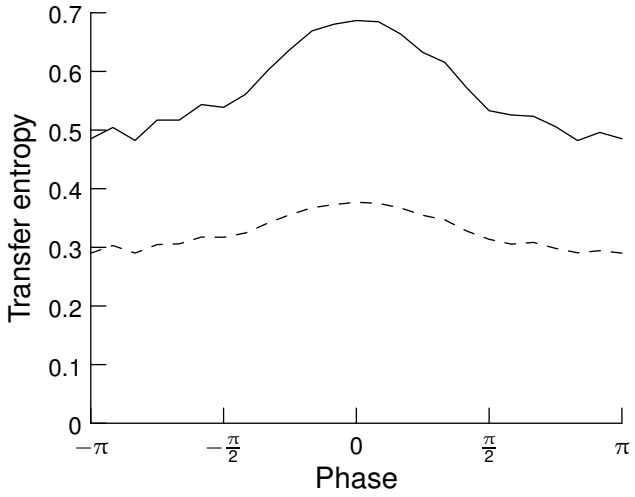

Figure 3.7: TE as a function of phase shifts and directionality. The phases are aligned relative to the mean phase, i.e., a phase shift of zero represents mean phase shift. TE is highest for the mean phase shift and gets lower the more it differs from it. The solid line represents TE from neuronal pool 1 to pool 2 (forward), the dashed line from pool 2 to pool 1 (backward). Forward TE is clearly stronger than backward TE. $g_{\text{AMPA}}/g_{\text{NMDA}}$ modification ratio = 0.12, averaged over 100 trials.

in the gamma band between the spiking activities of the two groups of neurons. It is highest for the mean phase between the two signals and drops as it moves away from the mean. This is consistent with our results for correlation. The phase dependence is illustrated in Fig. 3.7. TE is plotted as a function of the mean phase shift. The solid line represents TE from the first to the second pool (forward) and the dashed line TE from the second to the first one (backward). Forward TE is stronger than backward TE, implying that TE correctly detects the causal dependence of the second neuronal pool on the first one. Forward TE is stronger than backward TE even if the feedforward and feedback connections are symmetrical (not shown). The stronger the feedforward and the weaker the feedback connections, the bigger the difference in the TE for the two directions, as shown in Fig. 3.8. We plot the relative difference in the TE, calculated as $(\text{TE}_f - \text{TE}_k)/\text{TE}_k$. The feedback/feedforward ratio is defined as J_k/J_f. We use a feedback/feedforward ratio of 1/3 in the baseline simulations.

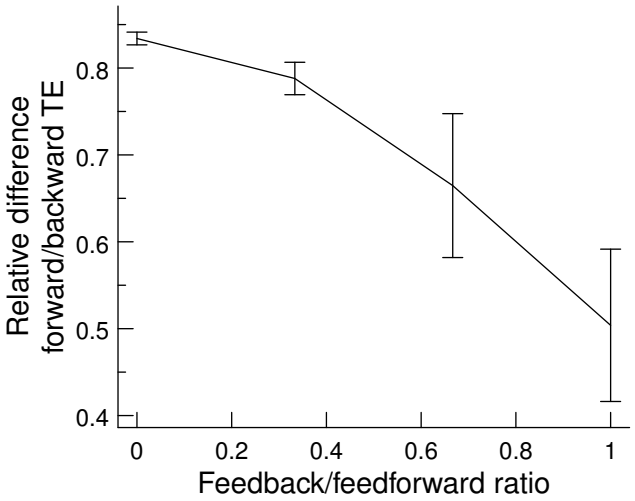

Figure 3.8: Relative differences in forward and backward TE. Differences in forward and backward TE are shown as a function of feedback/feedforward connection ratio, which is defined as J_k/J_f. The difference between forward and backward TE becomes smaller as the feedforward and feedback connections become more similar. Error bars indicate 95% confidence intervals, $g_{\text{AMPA}}/g_{\text{NMDA}}$ modification ratio = 0.12, averaged over 100 trials.

3.3.4 Different frequency bands

Another result we obtain is that an optimal phase relation for information transport is not restricted to the gamma band. We find that even in simulations with a network oscillating strongly in the beta band (around 20 Hz), the TE is again highest for the mean phase shift. In Fig. 3.9, we compare the results for networks oscillating in the beta and gamma frequency band. Fig. 3.9a shows the TE for a network oscillating in the gamma band. The trials are sorted according to their phase relation in the gamma band. Fig. 3.9b shows the same network but with the trials now sorted according to their phase relation in the beta band. The phase dependence curve becomes a lot flatter and the optimal phase for maximal TE is much less pronounced. Fig. 3.9c shows the TE for a network oscillating in the beta band with trials sorted according to the phase relation in the gamma band. And Fig. 3.9d shows the TE for a network oscillating in the beta band with trials sorted according to the phase relation in the beta band. It becomes clear that it is the phase of the dominating fre-

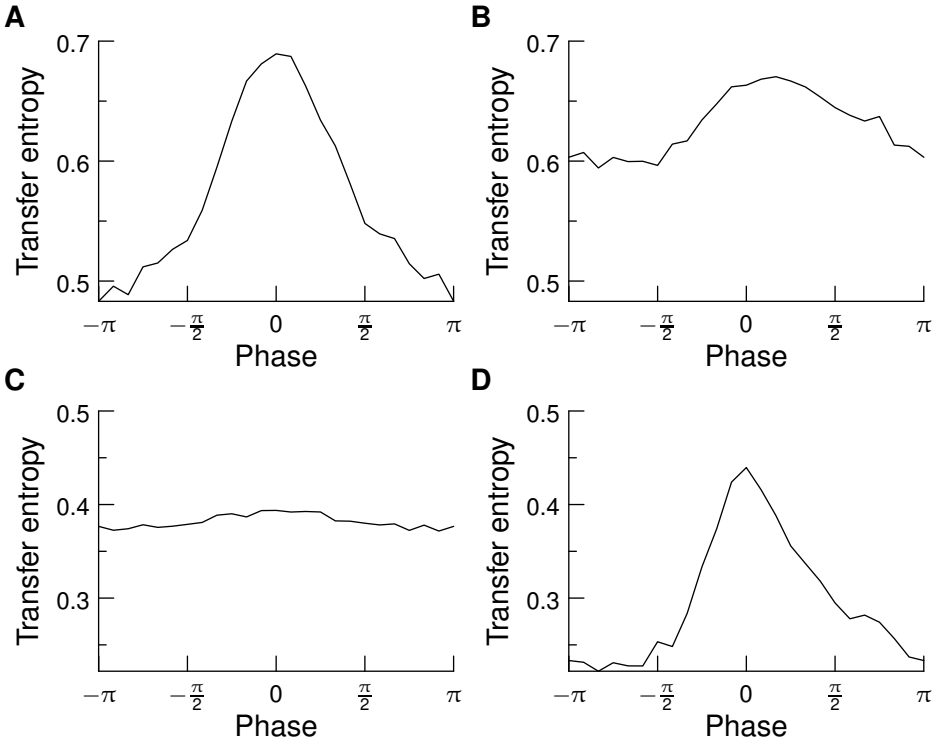

Figure 3.9: TE as a function of the mean phase shift in the gamma and beta band. The network oscillates strongly in one frequency band (either beta or gamma). The trials are sorted according to their phase shift either in the beta or gamma band. **(a)** Network oscillating in the gamma band. The trials are sorted according to their phase shift in the gamma band. **(b)** Network oscillating in the gamma band. The trials are sorted according to their phase shift in the beta band. **(c)** Network oscillating in the beta band. The trials are sorted according to their phase shift in the gamma band. **(d)** Network oscillating in the beta band. The trials are sorted according to their phase shift in the beta band. In all four graphics, $g_{\mathrm{AMPA}}/g_{\mathrm{NMDA}}$ modification ratio $= 0.12$, averaged over 100 trials.

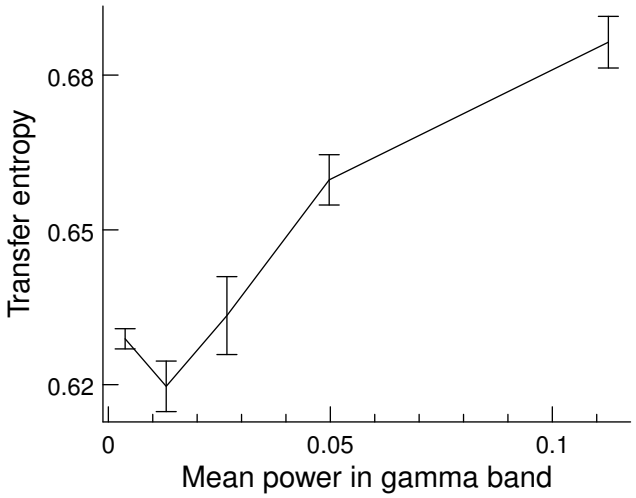

Figure 3.10: TE of trials sorted by power in the gamma band. Network parameters are kept fixed. The TE increases as a function of gamma power. $g_{\mathrm{AMPA}}/g_{\mathrm{NMDA}}$ modification ratio = 0.12, averaged over 100 trials. Error bars indicate 95% confidence intervals.

quency band that is responsible for high of low TE. We therefore conclude that it is not only the gamma band that has the ability to shape effective network connections via the phase, but that it is a general mechanism, observable in different frequency bands.

3.3.5 Dependence of TE on gamma band power (without parameter modification)

We further find that TE depends on the spectral power in the gamma band (30-85 Hz). For a fixed parameter set, we first sort all the trials according to their power in the gamma band into bins. In each of these bins, we measure the TE for the mean phase relation. The TE as a function of the power in the gamma band is plotted in Fig. 3.10. We find that the TE increases as a function of power. Note, however, that instead of sorting the trials according to their gamma band power for a fixed parameter set, we can also vary the parameters in the network. This allows us to vary the power over a wider range and the effect becomes clearer (see the next section).

3.3.6 Dependence of TE on gamma band power (with parameter modification)

In the previous section we have shown how TE depends on power in the gamma band for a fixed parameter set. Now we explicitly vary the amount of gamma power and study the TE dependence. Gamma band oscillations in a network of excitatory and inhibitory integrate-and-fire neurons appear when excitation is faster then inhibition (Brunel & Wang, 2003). Thus, we made the network oscillate by increasing AMPA conductance and decrease NMDA conductance. This change was applied to both excitatory and inhibitory neurons. In our simulations, we vary the $g_{\mathrm{AMPA}}/g_{\mathrm{NMDA}}$ modification ratio from 0 to 0.12, which results in a gamma band that contains from 10 to 65% of power. If we sort the data according to its shift as in the previous section, we find that, for the different $g_{\mathrm{AMPA}}/g_{\mathrm{NMDA}}$ modification ratios, the TE shows a similar dependence on the phases. However, if the $g_{\mathrm{AMPA}}/g_{\mathrm{NMDA}}$ modification ratio is too low, the phase measurement is not reliable any more and the curve gets flat, consistent with the case of random phase distribution. Fig. 3.11 shows the TE as a function of phase shift for several different $g_{\mathrm{AMPA}}/g_{\mathrm{NMDA}}$ modification ratios. To summarize this result, we take the TE at the mean phase shift and plot it against the $g_{\mathrm{AMPA}}/g_{\mathrm{NMDA}}$ modification ratio. As the spectral power in the gamma band increases from 10 to 65%, the TE increases from 0.38 to 0.65 and thus shows strong positive correlation with the level of gamma band power (Fig. 3.12). In other words, the higher the gamma band synchronization between the two pools, the higher the information throughput. Again, this cannot be an effect of firing rate changes, as all trials have been normalized for firing rate. This result suggests that gamma band oscillations improve the signal processing in a network of IF neurons, as they increase the amount of transmitted information. This in turn confirms the idea that gamma band synchronization can shape effective networks, especially as it can influence the information transmission in a given direction, as shown above.

3.3.7 Timing

Finally, we are interested in whether the gamma band oscillations also have an influence on the speed of information exchange, on top of the increased amount of information exchange. To do this, we measure the time required until the stimulus presentation to the first pool leads to an increase in TE towards the second pool. We find that the onset of TE increase is significantly earlier when there is a lot of power in the gamma

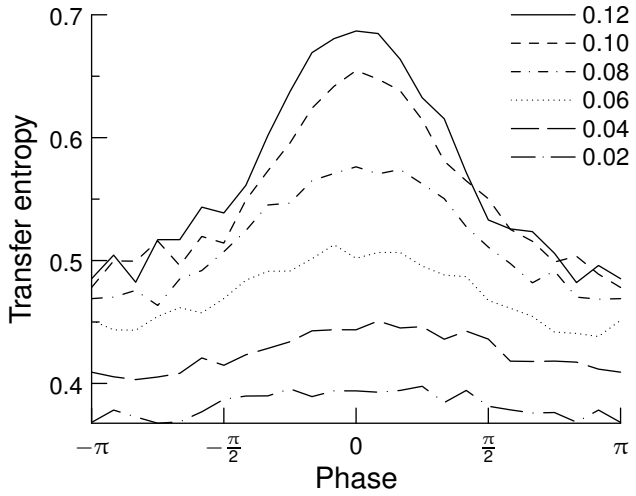

Figure 3.11: TE as a function of phase shifts and gamma oscillations. If the oscillations are strong in the gamma band ($g_{\text{AMPA}}/g_{\text{NMDA}}$ modification ratio = 0.12), there is a clear phase shift between the two groups of neurons and the phase dependence curve is clearly bell shaped. If the oscillations are too low, there is no meaningful phase shift and the curve becomes flat ($g_{\text{AMPA}}/g_{\text{NMDA}}$ modification ratio = 0.02). Averaged over 100 trials.

band. While for a $g_{\text{AMPA}}/g_{\text{NMDA}}$ modification ratio of 0.02 it requires 28 ms to reach 50% of the average TE, for a $g_{\text{AMPA}}/g_{\text{NMDA}}$ modification ratio of 0.12 it takes only 17 ms. The onset of information flow is clearly faster for higher levels of gamma band power (Fig. 3.13). This increase in speed is a further demonstration of how gamma oscillations increase network performance and shows how a network can be made more competitive.

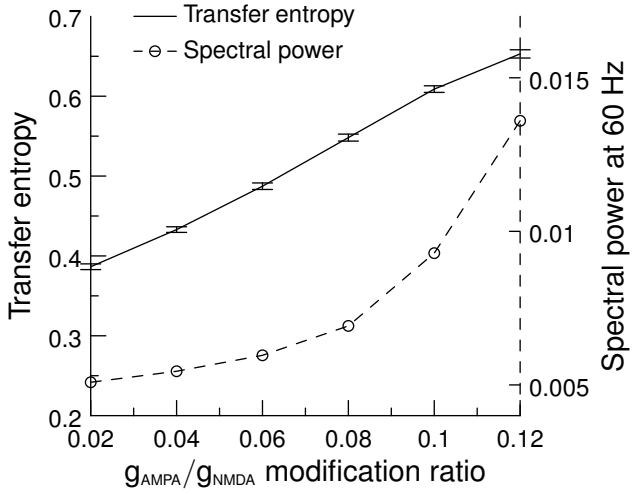

Figure 3.12: Mean TE as a function of gamma frequency band power. We plot the TE for six different $g_{\mathrm{AMPA}}/g_{\mathrm{NMDA}}$ modification ratios (solid line). A higher $g_{\mathrm{AMPA}}/g_{\mathrm{NMDA}}$ modification ratio causes the network to oscillate in the gamma frequency range and thus increases the power in the gamma frequency band (dashed line). Error bars indicate 95% confidence intervals; averaged over 100 trials.

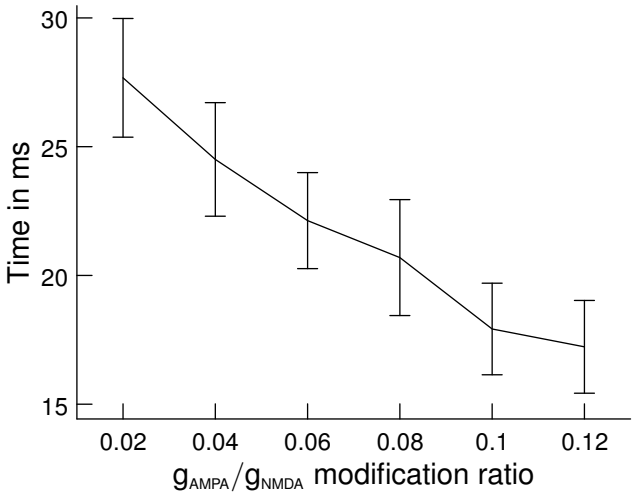

Figure 3.13: Rise times of TE as a function of gamma band power. Information starts flowing after stimulus onset when, consequently, TE starts rising. The plot shows the time required to reach 50% of the average TE. TE clearly rises faster for higher power in the gamma band (high $g_{\mathrm{AMPA}}/g_{\mathrm{NMDA}}$ modification ratio). Error bars indicate 95% confidence intervals; averaged over 100 trials.

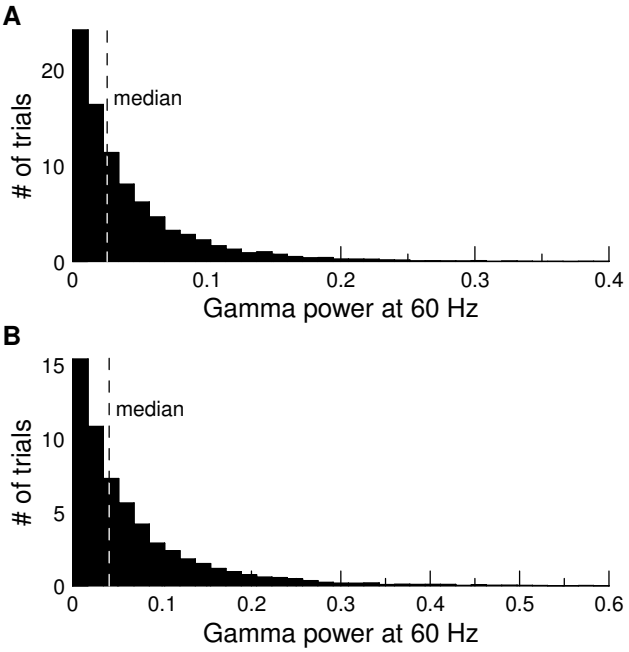

Supplementary Figure 3.1: Histogram of the power in the gamma band over trials. **(a)** lower layer, **(b)** upper layer.

3.A Chapter appendix

3.A.1 Is phase distribution an artifact of measuring phase?

Not all the trials have the same power at 60 Hz. Suppl. Fig. 3.1 shows a histogram with the distribution of power of all the trials.

One concern was that the peak in the phase dependence stems from this distribution, i.e., that trials with high gamma would lead to high coherence and trials with low gamma to low coherence and that therefore only trials with high gamma would contribute to the phase dependency as shown in Fig. 3.7. This seems not to be the case. Suppl. Fig. 3.2a and Suppl. Fig. 3.2b show the phase dependency for all trials with gamma power below median and above median, respectively. In both cases, the phase dependency is very similar to the original one.

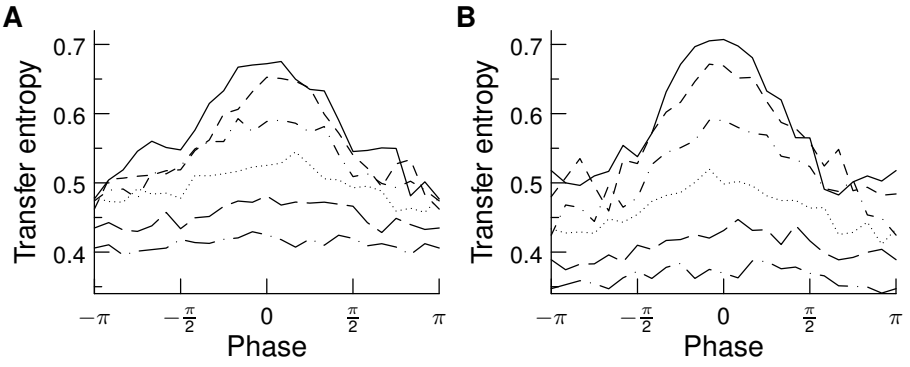

Supplementary Figure 3.2: TE as a function of the phase shift for high and low gamma power. **(a)** Trials with gamma power below the median. **(b)** Trials with gamma power above the median.

3.A.2 Transfer entropy dependence on connection weights

To check whether the measure of TE would give meaningful results in the context of our network model, we measured the TE as a function of the feedforward connection (J_f). If there is no connection between the two pools, there is no flow of information and TE should be zero. If we increase the connection strength, the signal can pass through to the second pool and the TE should increase. In Suppl. Fig. 3.3 we plot TE against the feedforward connection weights. As expected, for a zero feedforward connection weight, the TE is zero and then increases as a function of the feedforward connection weights.

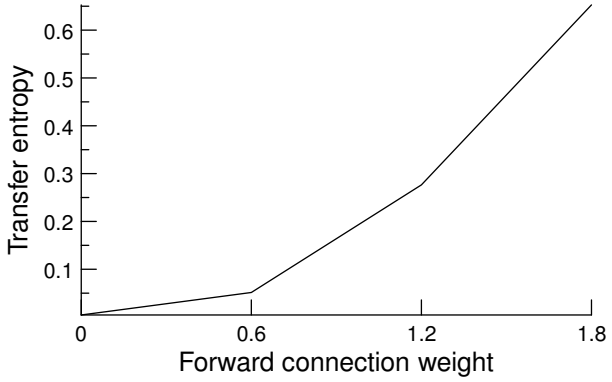

Supplementary Figure 3.3: Transfer entropy as a function of the feed-forward connection weights. We plot the TE for four different weights J_f. The data shown is for a simulation with a $g_{\text{AMPA}}/g_{\text{NMDA}}$ modification ratio of 0.12.

4 Discussion

4.1 Neuronal correlates of attention

In the first part of this thesis, we study the underlying mechanisms of neuronal correlates of visual attention by means of a computational framework. We implement a minimal model of leaky integrate-and-fire neurons that has global inhibition and is fully connected. Our network shows oscillations in the gamma frequency range. Whether there are oscillations or not depends on the relative contributions of AMPA and NMDA mediated currents ($g_{\mathrm{AMPA}}/g_{\mathrm{NMDA}}$ modification ratio). As Brunel & Wang (2003) state, the properties of the firing rhythm are determined essentially by the ratio of time scales of excitatory and inhibitory currents and by the balance between the mean recurrent excitation and inhibition. Faster excitation than inhibition, or a higher excitation/inhibition ratio, favors the feedback loop and oscillations in the gamma range.

These oscillations appear only when the stimulus is present. If one of the two types of input to the network is enhanced by an attentional bias, the synchronization between spikes and the local field potential in the gamma frequency band is enhanced. The increase in gamma frequency oscillations is stable over a wide range of input. We find that, depending on the $g_{\mathrm{AMPA}}/g_{\mathrm{NMDA}}$ modification ratio, there is a range where the attentional bias leads either to an increase in the firing rate or to an increase in the gamma frequency band synchronization. About a possible origin of this ratio in the brain we can only speculate. The $g_{\mathrm{AMPA}}/g_{\mathrm{NMDA}}$ modification ratio could be changed through slow synaptic plasticity or short-term synaptic plasticity induced by the attentional input.

Rate modulation can occur without gamma modulation, but gamma modulation never appears without rate modulation. However, the strength of gamma modulation can vary independently of rate modulation, which leads to the main finding of this study, namely that the two proposed neural correlates of selective attention (increase in firing rate and increase in gamma frequency synchronization) are not concomitant. Both seem to

have a role of their own in the attentional process.

We also show that, after stimulus presentation, rates rise the quickest when the gamma modulations are the strongest. This rise time can be interpreted as a reaction time (RT) of the system to a stimulus under attention. The RTs get shorter in the presence of gamma synchronization. The main reason is that the probability to generate a postsynaptic spike is higher if the presynaptic spikes arrive synchronously and therefore in a more concentrated way in time (Salinas & Sejnowski, 2001). A more theoretical explanation for this behavior can be found in the work of Deco & Schürmann (1999). They study a dynamical neural system that has to discriminate different stimuli. They show that, if the discrimination is tuned to maximal reliability in minimal time, the network responds for different stimuli with different clusters of synchronized neurons. These synchronizations can be tuned to 40 Hz. In other words, if the information in spikes has to be maximal in minimal time, synchronization appears, which is consistent with the energy-based arguments of Abeles (1982). Synchronous firing generates spatiotemporal patterns in minimal time, because its energy is concentrated in time.

Furthermore, the difference in the RT between the attended and the unattended pool correlates with gamma modulation. This suggests that the presence of gamma modulation is advantageous for the processing of the attended stimulus. Altogether, we show that rate and gamma modulation can vary independently, but to obtain an optimal information flow, gamma synchronization is necessary and the $g_{\mathrm{AMPA}}/g_{\mathrm{NMDA}}$ modification ratio has to stay within a certain range. This sensibility has its origin in the nature of the network and only experiments can show how sensitive the real brain is to this ratio. Gamma modulation therefore seems to have an essential behavioral relevance. This corresponds well with experimental findings. Pesaran et al. (2002) have shown that pre-stimulus fluctuations in visual gamma band synchronization predict the efficiency of detecting a subsequent change in a visual stimulus. Womelsdorf et al. (2006) analyze how RTs are related to gamma band synchronization in visual areas. They show that the behavioral response time to a stimulus change can be predicted specifically by the degree of gamma band synchronization among those neurons in monkeys' V4 visual area that are activated by the behaviorally relevant stimulus. In other words, trials leading to fast RTs contain more gamma band power. Their results also indicate that this increase in gamma band power is indeed an effect of selective attention and not just a general increase in arousal. Our findings about the RTs confirm this experimental result.

Extending our model to two layers, our results show that gamma fre-

quency synchronization is higher in the upper layer (V4) than in the lower layer (V1). We think that this is due to the fact that input to V1 is Poissonian, but input to V4 comes from V1. As a one-layer network already shows oscillations in the gamma range, the input to V4 is not Poissonian any more but oscillating in the gamma range. This facilitates the synchronization in V4. Moreover, we show that attentional modulations are stronger in V4 than in V1. Our findings are thus consistent with an increase of the gamma frequency modulation along the visual pathway. Furthermore, if the $g_{\mathrm{AMPA}}/g_{\mathrm{NMDA}}$ modification ratio is different in the different layers and is high enough in the upper layer, the neurons in this layer start to synchronize even when there is no or very little synchronization in the lower layer. Together, this might explain why in experimental work these modulations have been found in V4 (Fries et al., 2001), but not in V1 (Roelfsema et al., 2004).

4.2 Communication through coherence

In the second part of this thesis, we study the hypothesis that interactions among neuronal groups depend on neuronal synchronization. Recent results show that gamma band oscillations and especially the phase relation in the gamma band can modify the strength of correlations in a network and therefore influence the effective connections in it (Womelsdorf et al., 2007). These effects could be used as a mechanism to connect and disconnect areas in a network without altering the physical connections. Here, using a model network of IF neurons, we intend to test this hypothesis. We demonstrate that also in a model network, the correlation between two areas depends on the phase shift in the gamma band between these two areas. Our modeling approach enables us to generate more data than in an experiment and, therefore, to use a better statistical measure. Thus, we use transfer entropy (TE), which has the advantage of being able to distinguish driving and responding elements in a network. We show that also for TE there is an optimal phase shift between two neuronal groups, where TE is highest. We study this phase dependence in different bands (beta and gamma). Our results demonstrate that, in a network with strong beta oscillations, TE depends on the phase shift in the beta band similarly to the way TE depends on the phase shift in the gamma band in a network with strong gamma oscillations. The ability to shape network connections seems therefore not to depend on the frequency range and seems to be a general mechanism. We also study how TE depends on power in a specific frequency band. We do this here for the gamma band. For a fixed set

of parameters, we sort the trials in a simulation according to their power in the gamma band. We find that, within a simulation, the trials with high gamma power have a high TE. Then we modify the parameters and vary the gamma power over a wider range. Again, we find that TE increases as a function of gamma power. Finally, we reveal that it is not only the amount of exchanged information that increases but also the speed: The higher the power in the gamma band, the earlier the onset of the information flow.

Our results support the CTC hypothesis. If the effective connections in a network are to be influenced by the phase lock in a specific frequency band between two areas, it is important that it not only affects the coherence between them, but also the throughput of information in a specific direction. We achieve this by measuring TE, which is capable of detecting directionality. This is an extension of the work by Womelsdorf et al. (2007) who used the Spearman rank correlation, which is a symmetric measure and therefore not capable of distinguishing between driving and responding elements in a network. Our result is also more general, as we use the rates to measure TE and not only the 60 Hz power. Our study of different frequency bands is a further extension. We provide evidence that the CTC mechanism is not restricted to the gamma band, but also functions in different frequency bands. In addition, our modeling approach also enables us to study how the information transport depends on the total power in a specific frequency band. Our finding that TE increases as a function of power suggests that both the phase and the power in a specific frequency band are important to shape effective connections in a network. Based on our modeling work, we make the prediction that the increase of TE as a function of the power can also be found in experimental data. This could easily be verified by sorting trials according to their power in the gamma band. Furthermore, we demonstrate that the onset of information exchange depends on the power, which contributes to effectively shaping the connections in a network. In the previous section on attention (4.1), we have already shown that gamma power increases the network effect of an attentional bias and that it makes the network more efficient. Here, we can confirm this finding and put it in a more general context, independent of attention.

4.3 Implications for visual information transmission

As we are modeling results from visual cortical areas, we can assume that the neuronal clusters in the model transmit largely visual information. Our results indicate that gamma oscillations improve information transmission in the visual system. These results are complemented by several recent studies. Henrie & Shapley (2005) found that LFP power gradually increases as a function of stimulus contrast and gamma band LFP power increases differentially, that is, to a higher extent with respect to the baseline than relative to either higher or lower bands. For the highest stimulus contrast, these authors report a clear peak in the gamma frequency band. In other words, the contrast dependence of the LFP is different in different frequency bands and the LFP power spectrum changes shape depending on contrast, with a peak in the gamma band emerging at high contrast. Belitski et al. (2008) studied the encoding of naturalistic sensory stimuli in LFPs and spikes. They found that the most informative LFP frequency ranges were 1–8 Hz and 60–100 Hz. They showed that the LFP in the 60–100 Hz high gamma band showed little noise correlation during visual stimulation but showed the highest observed signal correlation across all LFP frequencies. The high gamma band also had the highest proportional power increase during visual stimulation. These experimental results are supported by the modeling work of Mazzoni et al. (2008). These authors showed that their modeling network encoded static input spike rates into gamma-range oscillations generated by inhibitory-excitatory neural interactions. In sum, these reports indicate that the gamma frequency range is the one used most frequently to encode visual information in the visual cortex and that visual information is encoded by the power of gamma range oscillations. These observations, together with our result that gamma oscillations increase both the overall amount and the speed of information indicate that information about preferred stimuli is treated preferentially and, in consequence, that cortical modules mostly exchange information about their preferred stimuli.

4.4 Link to behavior

As described earlier, gamma oscillations appear in a multitude of species, brain areas and during very different tasks. But it has been and still is very difficult to link these gamma oscillations to behavior. Our work shows that gamma synchronization improves both the speed and amount

of information transmission. The processing of sensory stimuli could then be improved by these oscillations, by making it faster and more efficient and enabling it to process weak stimuli. Altogether, on a very speculative side, we argue that this does establish a link between neuronal oscillations and behavior.

4.5 Outlook

4.5.1 Influence of input characteristics

Most experimental work showing oscillations in the visual system discussed in this thesis use some form of moving gratings as input. It has been argued that these oscillations are in part a consequence of the specific stimuli used, and that with more naturalistic input these oscillations would not appear. It is therefore important to understand the relation between the input and its neuronal encoding. In recent experimental (Belitski et al., 2008) and theoretical (Mazzoni et al., 2008) studies, it has been shown that static input spike rates are encoded into gamma range oscillations generated by inhibitory-excitatory neural interactions and slow dynamic features of the input into slow LFP fluctuations.

In a future project, we plan to extend this work by studying how the information transmission between two neuronal clusters depends on stimulus features. One can for example study how the TE between phase in a specific frequency band in one cluster and rates in the other cluster depend on the different types of input, like constant input, oscillating input or naturalistic input. We plan to use the LFP measured in the lateral geniculate nucleus of macaque monkeys while they are exposed to naturalistic movies. It is planned to study which frequency band will control the effectiveness of information transmission, whether it is still the gamma band (as with the artificial stimuli) or shifts to different frequency bands.

4.5.2 Synaptic facilitation

The current theoretical framework of working memory holds that the delay activity emerges either from intrinsic cell properties (Loewenstein & Sompolinsky, 2003; Fransen et al., 2006) or as persistent reverberations in selective neural populations, coding for different memories (Wang, 2001; Brunel, 2003; Goldman et al., 2003; Machens et al., 2005). However, delay activity can be very modest (Naya et al., 1996; Shafi et al., 2007) or nonexistent. Working memory might therefore not reside entirely in the

spiking activity. Furthermore, holding information in a spiking form is energetically expensive because of high metabolic cost. Mongillo et al. (2008) propose an alternative account, based on properties of excitatory synaptic transmission in the prefrontal cortex. They propose that working memory is sustained by calcium-mediated synaptic facilitation. Accumulation of residual calcium in the presynaptic terminals could carry the information about the recalled memory in a working form, reducing the need for metabolically costly action potentials. However, not all encountered stimuli enter working memory, and which stimuli enter and which not is probably mediated by attention. Given the relation between attention and oscillations, this opens intriguing perspectives for studying the relation between synaptic facilitation and neuronal oscillations. In particular, it would be interesting to study how synaptic facilitation affects neuronal oscillations and how speed and amount of transferred information depend on synaptic facilitation.

4.5.3 What controls the oscillations?

One fundamental question that remains to be answered is how oscillations are actually controlled. One could argue that identifying oscillations as being responsible for controlling communication between cortical areas is effectively only pushing the problem of cortical communication one level back, as there is still a mechanism required for controlling the oscillations. In particular, it would be interesting to study what controls and establishes the correlations. Thus, this is another issue which future research needs to approach.

4.6 Summary

We have presented results that suggest that attention can modify firing rates and neuronal oscillations independently, that information is processed advantageously under attention if both rate and synchronization modulation is present, and that both the amount and speed of information transmission increases as a function of neuronal oscillations. Therefore, oscillations are a plausible mechanism to effectively shape the flow of information in a network. Our results thus support the CTC hypothesis.

A Appendix

A.1 Theoretical framework (The neuronal basis of attention)

As a description at the neural level, we use models of neurons with leaky integrate-and-fire (IF) dynamics. We follow the model of Brunel & Wang (2001). A leaky IF unit consists of a single membrane capacitance C_m for integrating the charge delivered by synaptic input, a membrane resistance R_m, accounting for leakage currents through the membrane and a fixed voltage threshold V_{thr} for spike initiation. The membrane charges up to its stationary value as long as the membrane potential stays below V_{thr}. If it reaches the threshold potential, an action potential is fired. All connected neurons receive an input, the circuit is shunted for a refractory time period τ_{refr} and the membrane potential is reset to V_{reset}.

Synaptic currents are mediated by the excitatory receptors AMPA and NMDA (activated by glutamate) and the inhibitory receptor GABA_A (activated by GABA). There are two types of excitatory synapses. AMPA and NMDA receptors have different time constants, AMPA decays very fast (2 ms) while NMDA decays slowly (100 ms). The decay constant of GABA (10 ms) lies in between the two. These decay constants determine the oscillation frequency of the network (see below).

The network is organized in pools. Pools are created because different parts of the network get different exposure to stimuli. Neurons in one pool are defined by increased mutual connection strength and by the input they receive. The synaptic efficacies are kept fixed through the simulation. They are set consistent with a Hebbian rule: the synapse between two cells is strong if they were active in a correlated manner in the past. Therefore, cells within one pool have strong recurrent connections (w_+) while the connections between pools are weak (w_-). Details for all the weights in the network (w_+, w_-, w_I, w_n) are given below.

Our model, shown in Fig. 2.2 on p. 32, consists of two layers (corre-

sponding to V1 and V4). Each layer consists of 800 pyramidal neurons and 200 interneurons. These proportions are the ones observed in the cerebral cortex. The network is fully connected. Sparse connectivity has been shown to increase mainly the noise in the network due to finite size effects (Mattia & Giudice, 2002, 2004). As noise was not an explicit point of this study, we used the simplification of all-to-all connectivity. Each layer is subdivided into four pools. There are three pools of excitatory neurons (the two selective pools and the nonspecific neurons) that are all connected to one pool of inhibitory neurons. The selective pools are the ones that receive the input, either externally (as in V1) or from the lower layer (as in V4). They have strong recurrent connections (w_+). The nonspecific pool emulates the spontaneous activity in surrounding brain areas. Neurons in the nonspecific pool are connected to the selective excitatory pools by a feed forward connection of $w_n = (-fJ_k - fK_k)/(1-2f) + w_-$ in layer V4 and $w'_n = (-fJ_f - fK_f)/(1-2f) + w_-$ in layer V1. (f is the fraction of excitatory neurons in each selective pool, i.e., each selective pool contains $f \cdot N_E$ neurons, N_E being the total number of excitatory neurons in the network.) These connections normalize each layer so that the overall recurrent excitatory synaptic drive in the spontaneous state remains constant as the external connections J_f, J_k, K_f and K_k are varied. The selective pools (S1, S2, S1', S2') of the two layers are connected to each other. Within one layer, this connection is given by $w_- = 1 - f(w_+ - 1)/(1-f)$, so that the overall recurrent excitatory drive in the spontaneous state remains constant as w_+ is varied. Between the layers, we take into account that a stimulus that is a preferred one for S1 (S2) also provokes a strong stimulation of S1' (S2'). Therefore, the J connections are stronger than the K connections ($K_x = cJ_x$, with $c = 0.1$). The two selective pools in layer V1 (S1, S2) encode two non-overlapping RF. The RFs in layer V4 are larger, each covering the two selective pools in V1. By having overlapping RFs, the competition in V4 is stronger than in V1. This is taken into account by setting the inhibitions to $w_I = 1$ in V1 and $w'_I = 1.35$ in V4.

By having only one inhibitory pool per layer, each layer has global inhibition. Deco & Rolls (2004) showed that in a model with biased competition, inhibition has gradually increasing global character along the visual pathway. As we implement only a minimal model in this study, we use global inhibition directly. The more active the excitatory pools are, the more active the inhibitory pool will be and consequently, excitatory pools will compete. By introducing an external top-down bias, i.e., an increase of excitatory input to the pool representing the attended stimulus, the competition can be shifted in favor of a specific pool. This computational model implements therefore the biased competition hypothesis. Deco and

colleagues have shown that local competition of neurons between pools combined with top-down biasing of this competition gives rise to a process which can be identified with attentional filtering (Deco et al., 2002; Szabo et al., 2004). This is in line with the biased-competition model of attention by Chelazzi et al. (1993).

In our model of attention, we assume that the stimulus (ν_{in}) is passed on to the modeled brain area V1 as a Poisson spike train of typically 250 Hz. The attentional bias (ν_{bias}) was modeled as a Poisson spike train of typically 4 to 8 Hz, received only by the attended pool S1. In addition to the recurrent connection, the network is exposed to an external current (ν_{ext}), modeled as a Poisson spike train of 800 neurons, firing at 3 Hz. This is consistent with the spontaneous activity observed in the cerebral cortex.

In a network consisting of excitatory and inhibitory neurons with recurrent connections, oscillations are generated by a pyramidal-to-interneuron loop (Brunel & Wang, 2003). This oscillation frequency depends on the relative time scales of the decay constants. Faster excitation than inhibition, or a higher excitation/inhibition ratio favors the feedback loop and gives rise to oscillations in the gamma range (Brunel & Wang, 2003). In our network, oscillations are therefore generated by adjusting the conductances g_{AMPA} and g_{NMDA}. An increase of g_{AMPA} and a decrease of g_{NMDA} is equivalent to an increase in the excitation/inhibition ratio and would increase oscillations. The conductances in our network are varied according to the following rule: $g_{\text{NMDA}} = g_{\text{NMDA}}(1-\delta)$ and $g_{\text{AMPA}} = g_{\text{AMPA}}(1+10\delta)$. Throughout the chapter, we will refer to the parameter δ as the $g_{\text{AMPA}}/g_{\text{NMDA}}$ modification ratio. The factor 10 stems from the fact that near the firing threshold, the ratio of NMDA:AMPA components becomes 10 in terms of charge entry, as stated in Brunel & Wang (2001). Therefore, in order not to change the spontaneous state, a decrease in g_{NMDA} is compensated by a tenfold increase in g_{AMPA}. All recurrent conductances (both inhibitory and excitatory) are changed according to these rules. The excitation/inhibition ratio is adjusted so that the network only shows oscillations during the stimulus presentation.

All simulations were initiated with a period of 1000 ms where no stimulus was presented, followed by a period of 1000 ms composed of the presentation of the stimuli and the attentional bias, followed by another 200 ms where no stimulus was presented. The evolution of spiking activity was averaged over all the neurons in the pool and over 200 trials initialized with different random seeds.

The mathematical details of the network and a table with the default values for all the parameters can be found in appendices A.2 and A.3,

respectively.

A.2 Mathematical description (The neuronal basis of attention)

The membrane potentials of a neuron in the subthreshold regime is given by:

$$C_m \frac{\mathrm{d}V(t)}{\mathrm{d}t} + \frac{V(t) - V_L}{R_m} = I_{\mathrm{syn}}(t) \tag{A.1}$$

C_m is the membrane capacitance, R_m is the membrane resistance, I_{syn} are the synaptic currents and V_L is the resting potential. The synaptic currents are the sum of the external current $I_{\mathrm{AMPA,ext}}$ driven by the background noise ν_{ext}, the stimulus ν_{in} and the attentional bias ν_{bias}, the recurrent excitatory currents $I_{\mathrm{AMPA,rec}}$ and I_{NMDA} and the inhibitory recurrent current I_{GABA}:

$$I_{\mathrm{syn}}(t) = I_{\mathrm{AMPA,ext}}(t) + I_{\mathrm{AMPA,rec}}(t) + I_{\mathrm{NMDA}}(t) + I_{\mathrm{GABA}}(t) \tag{A.2}$$

Every current is of the form $I = \frac{V}{R}$ and thus $I = gV$. They are defined by:

$$I_{\mathrm{AMPA,ext}}(t) = g_{\mathrm{AMPA,ext}} \left(V(t) - V_E\right) \sum_{j=1}^{N_{\mathrm{ext}}} s_j^{\mathrm{AMPA,ext}}(t) \tag{A.3}$$

$$I_{\mathrm{AMPA,rec}}(t) = g_{\mathrm{AMPA,rec}} \left(V(t) - V_E\right) \sum_{j=1}^{N_E} w_j s_j^{\mathrm{AMPA,rec}}(t) \tag{A.4}$$

$$I_{\mathrm{NMDA}}(t) = \frac{g_{\mathrm{NMDA}} \left(V(t) - V_E\right)}{1 + \left[\mathrm{Mg}^{2+}\right] \exp\left(-0.062V(t)\right)/3.57} \times \sum_{j=1}^{N_E} w_j s_j^{\mathrm{NMDA}}(t) \tag{A.5}$$

$$I_{\mathrm{GABA}}(t) = g_{\mathrm{GABA}} \left(V(t) - V_I\right) \sum_{j=1}^{N_I} w_j s_j^{\mathrm{GABA}}(t) \tag{A.6}$$

The g's are the synaptic conductances, the s_j's the fractions of open channels and the w_j's the synaptic weights. V_E and V_I are the reverse potentials of the excitatory and inhibitory neurons, respectively, N_{ext} is the number of neurons encoding the spontaneous activity in the cortex, N_E and N_I are the numbers of excitatory and inhibitory neurons in the network. The sum in each expression runs over all neurons, summing their open channels, weighted by the w_j's that implement the connection strengths between neurons, organizing them into pools. The NMDA synaptic current

is dependent on the membrane potential and controlled by the extracellular concentration of $\left[Mg^{2+}\right]$. $g_{\mathrm{AMPA,ext}}$, $g_{\mathrm{AMPA,rec}}$, g_{NMDA} and g_{GABA} are the receptor-specific conductances.

The fractions of open channels are given by:

$$\frac{\mathrm{d}s_j^{\mathrm{AMPA,ext}}(t)}{\mathrm{d}t} = -\frac{s_j^{\mathrm{AMPA,ext}}(t)}{\tau_{\mathrm{AMPA}}} + \sum_k \delta\left(t - t_j^k\right) \tag{A.7}$$

$$\frac{\mathrm{d}s_j^{\mathrm{AMPA,rec}}(t)}{\mathrm{d}t} = -\frac{s_j^{\mathrm{AMPA,rec}}(t)}{\tau_{\mathrm{AMPA}}} + \sum_k \delta\left(t - t_j^k\right) \tag{A.8}$$

$$\frac{\mathrm{d}s_j^{\mathrm{NMDA}}(t)}{\mathrm{d}t} = -\frac{s_j^{\mathrm{NMDA}}(t)}{\tau_{\mathrm{NMDA,decay}}} + \alpha x_j(t)\left(1 - s_j^{\mathrm{NMDA}}(t)\right) \tag{A.9}$$

$$\frac{\mathrm{d}x_j(t)}{\mathrm{d}t} = -\frac{x_j(t)}{\tau_{\mathrm{NMDA,rise}}} + \sum_k \delta\left(t - t_j^k\right) \tag{A.10}$$

$$\frac{\mathrm{d}s_j^{\mathrm{GABA}}(t)}{\mathrm{d}t} = -\frac{s_j^{\mathrm{GABA}}(t)}{\tau_{\mathrm{GABA}}} + \sum_k \delta\left(t - t_j^k\right) \tag{A.11}$$

τ_{AMPA}, $\tau_{\mathrm{NMDA,decay}}$ and τ_{GABA} are the decay times and $\tau_{\mathrm{NMDA,rise}}$ is the rise time for the corresponding synapses. The rise times of AMPA and GABA currents are neglected, as they are typically very short (< 1 ms). The sums over k represent a sum over spikes formulated as δ-peaks ($\delta(t)$) emitted by presynaptic neuron k at time t_j^k.

A.3 Default parameter set (The neuronal basis of attention)

The default parameter set for the numerical simulations presented in chapter 2 is listed in Table A.1.

A.4 Theoretical framework (Optimal information transfer)

We use a model with leaky integrate-and-fire (IF) dynamics, following Brunel & Wang (2001). Each IF unit charges up to its stationary value as long as its membrane potential stays below a threshold. The membrane potential $V(t)$ is given by:

$$C_m \frac{dV(t)}{dt} = -g_m(V(t) - V_L) - I_{\mathrm{syn}}(t). \tag{A.12}$$

Table A.1: The default parameter set used in the integrate-and-fire simulations.

Parameter	Value	Parameter	Value
C_m (excitatory)	0.5 nF	V_E	0 mV
C_m (inhibitory)	0.2 nF	V_I	-70 mV
f	0.10	V_L	-70 mV
$g_{\mathrm{AMPA,ext}}$ (excitatory)	2.08 nS	V_{reset}	-55 mV
$g_{\mathrm{AMPA,ext}}$ (inhibitory)	1.62 nS	V_{thr}	-50 mV
$g_{\mathrm{AMPA,rec}}$ (excitatory)	0.104 nS	w_+	1.5
$g_{\mathrm{AMPA,rec}}$ (inhibitory)	0.081 nS	w_I	1.0
g_{GABA} (excitatory)	1.287 nS	w'_I	1.35
g_{GABA} (inhibitory)	1.002 nS	α	0.5 ms^{-1}
g_{NMDA} (excitatory)	0.327 nS	ν_{in}	250 Hz
g_{NMDA} (inhibitory)	0.258 nS	ν_{bias}	8 Hz
g_m (excitatory)	25 nS	ν_{ext}	2.4 kHz
g_m (inhibitory)	20 nS	τ_{AMPA}	2 ms
J_f	1.8	τ_{GABA}	10 ms
J_k	0.6	$\tau_{\mathrm{NMDA,decay}}$	100 ms
N_E	800	$\tau_{\mathrm{NMDA,rise}}$	2 ms
N_{ext}	800	τ_{refr} (excitatory)	2 ms
N_I	200	τ_{refr} (inhibitory)	1 ms

C_m is a membrane capacitance, g_m a membrane leak conductance, V_L a resting potential and I_{syn} is the total synaptic current flowing into the cell. When the membrane potential reaches the threshold potential, it sends out a spike to all connected neurons and resets its membrane potential to the reset potential. The circuit remains shunted for a refractory period. Synaptic currents are mediated by excitatory (AMPA and NMDA) and inhibitory (GABA) receptors. The total synaptic current is given by

$$I_{\mathrm{syn}}(t) = I_{\mathrm{AMPA,ext}} + I_{\mathrm{AMPA,rec}} + I_{\mathrm{NMDA}} + I_{\mathrm{GABA}}. \tag{A.13}$$

The currents are defined as follows:

$$I_{\mathrm{AMPA,ext}}(t)=g_{\mathrm{AMPA,ext}}\left(V(t)-V_E\right)\sum_{j=1}^{N_{\mathrm{ext}}}s_j^{\mathrm{AMPA,ext}}(t) \tag{A.14}$$

$$I_{\mathrm{AMPA,rec}}(t)=g_{\mathrm{AMPA,rec}}\left(V(t)-V_E\right)\sum_{j=1}^{N_E}w_j s_j^{\mathrm{AMPA,rec}}(t) \tag{A.15}$$

$$I_{\mathrm{NMDA}}(t)=\frac{g_{\mathrm{NMDA}}\left(V(t)-V_E\right)}{1+\left[\mathrm{Mg}^{2+}\right]\exp\left(-0.062V(t)\right)/3.57}\times\sum_{j=1}^{N_E}w_j s_j^{\mathrm{NMDA}}(t) \tag{A.16}$$

$$I_{\mathrm{GABA}}(t)=g_{\mathrm{GABA}}\left(V(t)-V_I\right)\sum_{j=1}^{N_I}w_j s_j^{\mathrm{GABA}}(t) \tag{A.17}$$

g denotes the receptor specific synaptic conductances, s_j the fractions of open channels and the w_j the synaptic weights. V_E and V_I are the reversal potentials of the excitatory and inhibitory neurons, respectively, N_{ext} is the number of neurons encoding the spontaneous activity in the cortex, and N_E and N_I are the numbers of excitatory and inhibitory neurons in the network. The sum in each expression runs over all neurons, summing their open channels, weighted by the synaptic weights that implement the connection strengths between neurons. The NMDA synaptic current is dependent on the membrane potential and controlled by the extracellular concentration of $\left[\mathrm{Mg}^{2+}\right]$.

The fractions of open channels are given by:

$$\frac{\mathrm{d}s_j^{\mathrm{AMPA,ext}}(t)}{\mathrm{d}t} = -\frac{s_j^{\mathrm{AMPA,ext}}(t)}{\tau_{\mathrm{AMPA}}}+\sum_k\delta\left(t-t_j^k\right) \tag{A.18}$$

$$\frac{\mathrm{d}s_j^{\mathrm{AMPA,rec}}(t)}{\mathrm{d}t} = -\frac{s_j^{\mathrm{AMPA,rec}}(t)}{\tau_{\mathrm{AMPA}}}+\sum_k\delta\left(t-t_j^k\right) \tag{A.19}$$

$$\frac{\mathrm{d}s_j^{\mathrm{NMDA}}(t)}{\mathrm{d}t} = -\frac{s_j^{\mathrm{NMDA}}(t)}{\tau_{\mathrm{NMDA,decay}}}+\alpha x_j(t)\left(1-s_j^{\mathrm{NMDA}}(t)\right) \tag{A.20}$$

$$\frac{\mathrm{d}x_j(t)}{\mathrm{d}t} = -\frac{x_j(t)}{\tau_{\mathrm{NMDA,rise}}}+\sum_k\delta\left(t-t_j^k\right) \tag{A.21}$$

$$\frac{\mathrm{d}s_j^{\mathrm{GABA}}(t)}{\mathrm{d}t} = -\frac{s_j^{\mathrm{GABA}}(t)}{\tau_{\mathrm{GABA}}}+\sum_k\delta\left(t-t_j^k\right) \tag{A.22}$$

τ_{AMPA}, $\tau_{\mathrm{NMDA,decay}}$ and τ_{GABA} are the decay times and $\tau_{\mathrm{NMDA,rise}}$ is the rise time for the corresponding synapses. AMPA has a very short decay time

(2 ms) while NMDA has a long one (100 ms) and the GABA decay time lies in-between (10 ms). The rise times of AMPA and GABA currents are neglected, as they are typically very short (< 1 ms). The sums over k represent a sum over spikes formulated as δ-peaks ($\delta(t)$) emitted by presynaptic neuron k at time t_j^k.

The equations are integrated using a fourth order Runge-Kutta method with a time step of 0.02 ms. The network is organized in pools. Neurons within a specific pool have stronger recurrent connections than neurons between the pools. The intention of this work is to study cortical neural interactions not limited to a specific brain area. However, as our simulations needed to be directly comparable to Womelsdorf et al. (2007), and have specific parameter sets, our network models two clusters of cortical neurons in visual cortex V4.

The network model consists of two parts (Fig. 3.2 on p. 52). In each part there are pools of excitatory and inhibitory neurons, with a total of 800 excitatory and 200 inhibitory neurons. The excitatory neurons are subdivided into a selective pool and a non-selective pool. The neurons in the selective pools (S,S') are the ones that receive input either from outside or from the connected selective pool. The non-selective neurons (NS, NS') simulate the surrounding brain areas. Each population of excitatory neurons is connected to a pool of inhibitory neurons (I, I'). This allows for generating oscillations in each population separately. The two parts of the network are connected via feedforward (J_f) and feedback (J_k) connections that project onto the selective pools. The external input (ν_{in}) is a Poisson spike train that projects to the selective pool (S) of the first part of the network. In addition to the recurrent connections, the network is exposed to an external current (ν_{ext}), modeled as a Poisson spike train of 800 neurons, firing at 3 Hz. This models the spontaneous activity observed in the cerebral cortex. The network is fully connected.

Gamma oscillations in a network with excitatory and inhibitory neurons are generated through a pyramidal-interneuron feedback loop (Traub et al., 1997; Brunel & Wang, 2003). Pyramidal neurons excite interneurons and interneurons in turn send inhibition back on pyramidal cells. The population frequency is determined by the sum of excitatory and inhibitory lags. The recurrent excitatory connections tend to decrease the oscillation frequency (as compared to only excitatory-inhibitory and inhibitory-excitatory connections) as they tend to prolong the positive phase in each cycle. In our network we can therefore generate and control the oscillations in the gamma frequency band by adjusting the AMPA and NMDA conductances. For example, increasing the g_{AMPA} and decreasing g_{NMDA} shifts the balance in the network towards fast excitation (AMPA) and slow inhibi-

tion (GABA) and thus increases the gamma frequency band oscillations. The conductances in our network are varied according to the following rule: $g_{\mathrm{NMDA}} = g_{\mathrm{NMDA}}(1-\delta)$ and $g_{\mathrm{AMPA}} = g_{\mathrm{AMPA}}(1+10\delta)$. Throughout the chapter, we will refer to the parameter δ as the $g_{\mathrm{AMPA}}/g_{\mathrm{NMDA}}$ modification ratio. The factor 10 stems from the fact that near the firing threshold, the ratio of NMDA:AMPA components becomes 10 in terms of charge entry, as stated in Brunel & Wang (2001). Therefore, in order not to change the spontaneous state, a decrease in g_{NMDA} is compensated by a tenfold increase in g_{AMPA}. All recurrent conductances (both inhibitory and excitatory) are changed according to these rules. By adjusting the synaptic decay constants, the oscillation frequency can be shifted into the beta band. The crucial parameter is τ_{GABA}. An increase of τ_{GABA} slows down the rhythm of the pyramidal-interneuronal loop and will therefore yield an oscillation at a lower frequency. To generate oscillations in the beta range (around 20 Hz), we use $\tau_{\mathrm{AMPA}} = 1.5$ ms and $\tau_{\mathrm{GABA}} = 38$ ms. To generate phase shifts in the gamma oscillations between the two parts of the network, we introduce a delay. The delay is set bidirectionally in the feedforward and feedback connections of the selective pools. Each spike emitted in S arrives at S' after Δt and vice versa. This lag in spike transmission generates a phase lag in the oscillations. A delay of, e.g., 4 ms yields a phase shift of about 90° in a 60 Hz oscillation. All trials are initiated with a period of 400 ms in which no stimulus is presented, followed by a period of 5500 ms composed of the presentation of the stimulus, followed by 100 ms in which no stimulus is present. Each simulation consists of 100 trials. All parameter values are listed in Table A.2.

A.5 Default parameter set (Optimal information transfer)

The default parameter set for the numerical simulations presented in chapter 3 is listed in Table A.2.

Table A.2: The default parameter set used in the integrate-and-fire simulations.

Parameter	Value	Parameter	Value
C_m (excitatory)	0.5 nF	V_L	-70 mV
C_m (inhibitory)	0.2 nF	V_{reset}	-55 mV
$g_{\text{AMPA,ext}}$ (excitatory)	2.08 nS	V_{thr}	-50 mV
$g_{\text{AMPA,ext}}$ (inhibitory)	1.62 nS	w_+	1.5
$g_{\text{AMPA,rec}}$ (excitatory)	0.104 nS	w_I	1.0
$g_{\text{AMPA,rec}}$ (inhibitory)	0.081 nS	α	0.5 ms^{-1}
g_{GABA} (excitatory)	1.287 nS	ν_{in}	250 Hz
g_{GABA} (inhibitory)	1.002 nS	ν_{ext}	2.4 kHz
g_{NMDA} (excitatory)	0.327 nS	τ_{AMPA}	2 ms
g_{NMDA} (inhibitory)	0.258 nS	τ_{AMPA} (beta osc.)	1.5 ms
g_m (excitatory)	25 nS	τ_{GABA}	10 ms
g_m (inhibitory)	20 nS	τ_{GABA} (beta osc.)	38 ms
J_f	1.8	$\tau_{\text{NMDA,decay}}$	100 ms
J_k	0.6	$\tau_{\text{NMDA,rise}}$	2 ms
N_E	800	τ_{refr} (excitatory)	2 ms
N_{ext}	800	τ_{refr} (inhibitory)	1 ms
N_I	200	Δt (delay)	4 ms
V_E	0 mV	feedback/feedforward ratio	1/3
V_I	-70 mV		

List of Abbreviations

AMPA	α-amino-3-hydroxy-5-methyl-4-isoazoleproprionic acid
CTC	communication through coherence
GABA	γ-aminobutyric acid
EPSP	excitatory postsynaptic potential
IF	integrate-and-fire
IPSP	inhibitory postsynaptic potential
LFP	local field potential
MUA	multi unit activity
NMDA	N-methyl-D-aspartate acid
RF	receptive field
RT	reaction time
STA	spike triggered average
SFC	spike field coherence
TE	transfer entropy

Bibliography

Abeles, M. (1982). Role of the cortical neuron - integrator or coincidence detector. *Israel J. Med. Sci.*, 18:83–92.

Bartos, M., Vida, I., Frotscher, M., Geiger, J. R., & Jonas, P. (2001). Rapid signaling at inhibitory synapses in a dentate gyrus interneuron network. *J. Neurosci.*, 21:2687–2698.

Bartos, M., Vida, I., Frotscher, M., Meyer, A., Monyer, H., Geiger, J. R., & Jonas, P. (2002). Fast synaptic inhibition promotes synchronized gamma oscillations in hippocampal interneuron networks. *Proc. Natl. Acad. Sci. U.S.A.*, 99:13222–13227.

Bartos, M., Vida, I., & Jonas, P. (2007). Synaptic mechanisms of synchronized gamma oscillations in inhibitory interneuron networks. *Nat. Rev. Neurosci.*, 8:45–56.

Belitski, A., Gretton, A., Magri, C., Murayama, Y., Montemurro, M. A., Logothetis, N. K., & Panzeri, S. (2008). Low-frequency local field potentials and spikes in primary visual cortex convey independent visual information. *J. Neurosci.*, 28(22):5696.

Bichot, N. P., Rossi, A. F., & Desimone, R. (2005). Parallel and serial neural mechanisms for visual search in macaque area V4. *Science*, 308:529–534.

Bragin, A., Jando, G., Nadasdy, Z., Hetke, J., Wise, K., & Buzsaki, G. (1995). Gamma (40-100 Hz) oscillation in the hippocampus of the behaving rat. *J. Neurosci.*, 15:47–60.

Bressler, S. L., Coppola, R., & Nakamura, R. (1993). Episodic multiregional cortical coherence at multiple frequencies during visual task performance. *Nature*, 366:153–156.

Broadbent, D. E. (1971). *Decision and stress.* Academic Press, New York.

Brosch, M., Budinger, E., & Scheich, H. (2002). Stimulus-related gamma oscillations in primate auditory cortex. *J. Neurophysiol.*, 87:2715–2725.

Brunel, N. (2003). Dynamics and plasticity of stimulus-selective persistent activity in cortical network models. *Cereb. Cortex*, 13:1151–1161.

Brunel, N. & Wang, X. J. (2001). Effects of neuromodulation in a cortical network model of object working memory dominated by recurrent inhibition. *J. Comput. Neurosci*, 11:63–85.

Brunel, N. & Wang, X. J. (2003). What determines the frequency of fast network oscillations with irregular neural discharges? I. Synaptic dynamics and excitation-inhibition balance. *J. Neurophysiol.*, 90:415–430.

Buehlmann, A. & Deco, G. (2008). The neuronal basis of attention: Rate versus synchronization modulation. *J. Neurosci.*, 28:7679–7686.

Buehlmann, A. & Deco, G. (2009). Rate and gamma modulation in attentional tasks. *New Math. Nat. Comput.*, 5(1).

Buehlmann, A. & Deco, G. (2010). Optimal information transfer in the cortex through synchronisation. *Conference Abstract: Computational and systems neuroscience 2010. doi: 10.3389/conf.fnins.2010.03.00104.*

Buhl, D. L., Harris, K. D., Hormuzdi, S. G., Monyer, H., & Buzsaki, G. (2003). Selective impairment of hippocampal gamma oscillations in connexin-36 knock-out mouse in vivo. *J. Neurosci.*, 23:1013–1018.

Buschman, T. J. & Miller, E. K. (2007). Top-down versus bottom-up control of attention in the prefrontal and posterior parietal cortices. *Science*, 315:1860–1862.

Chelazzi, L. (1999). Serial attention mechanisms in visual search: A critical look at the evidence. *Psychol. Res.-Psych. Fo.*, 62:195–219.

Chelazzi, L., Miller, E. K., Duncan, J., & Desimone, R. (1993). A neural basis for visual-search in inferior temporal cortex. *Nature*, 363:345–347.

Coull, J. (1998). Neural correlates of attention and arousal: insights from electrophysiology, functional neuroimaging and psychopharmacology. *Prog. Neurobiol.*, 55(4):343–361.

Csicsvari, J., Hirase, H., Czurko, A., & Buzsaki, G. (1998). Reliability and state dependence of pyramidal cell-interneuron synapses in the hippocampus: an ensemble approach in the behaving rat. *Neuron*, 21:179–189.

Csicsvari, J., Hirase, H., Czurko, A., Mamiya, A., & Buzsaki, G. (1999). Oscillatory coupling of hippocampal pyramidal cells and interneurons in the behaving Rat. *J. Neurosci.*, 19:274–287.

Csicsvari, J., Jamieson, B., Wise, K. D., & Buzsaki, G. (2003). Mechanisms of gamma oscillations in the hippocampus of the behaving rat. *Neuron*, 37:311–322.

deCharms, R. C. & Merzenich, M. M. (1996). Primary cortical representation of sounds by the coordination of action-potential timing. *Nature*, 381:610–613.

Deco, G., Pollatos, O., & Zihl, J. (2002). The time course of selective visual attention: Theory and experiments. *Vision Res.*, 42:2925–2945.

Deco, G. & Rolls, E. T. (2004). A neurodynamical cortical model of visual attention and invariant object recognition. *Vision Res.*, 44:621–642.

Deco, G. & Rolls, E. T. (2005). Neurodynamics of biased competition and cooperation for attention: A model with spiking neurons. *J. Neurophysiol.*, 94:295–313.

Deco, G. & Schürmann, B. (1999). Spatiotemporal coding in the cortex: Information flow-based learning in spiking neural networks. *Neural. Comput.*, 11:919–934.

Desimone, R. (1998). Visual attention mediated by biased competition in extrastriate visual cortex. *Philos. T. Roy. Soc. B.*, 353(1373):1245.

Desimone, R. & Duncan, J. (1995). Neural mechanisms of selective visual-attention. *Annu. Rev. Neurosci.*, 18:193–222.

Destexhe, A., Contreras, D., & Steriade, M. (1999). Spatiotemporal analysis of local field potentials and unit discharges in cat cerebral cortex during natural wake and sleep states. *J. Neurosci.*, 19:4595–4608.

Eckhorn, R., Bauer, R., Jordan, W., Brosch, M., Kruse, W., Munk, M., & Reitboeck, H. J. (1988). Coherent oscillations: a mechanism of feature linking in the visual cortex? Multiple electrode and correlation analyses in the cat. *Biol. Cybern.*, 60:121–130.

Eeckman, F. H. & Freeman, W. J. (1990). Correlations between unit firing and EEG in the rat olfactory system. *Brain Res.*, 528:238–244.

Engel, A. K., König, P., Kreiter, A. K., & Singer, W. (1991a). Interhemispheric synchronization of oscillatory neuronal responses in cat visual cortex. *Science*, 252:1177–1179.

Engel, A. K., König, P., & Singer, W. (1991b). Direct physiological evidence for scene segmentation by temporal coding. *Proc. Natl. Acad. Sci. U.S.A.*, 88:9136–9140.

Engel, A. K., Kreiter, A. K., König, P., & Singer, W. (1991c). Synchronization of oscillatory neuronal responses between striate and extrastriate visual cortical areas of the cat. *Proc. Natl. Acad. Sci. U.S.A.*, 88:6048–6052.

Fisahn, A., Contractor, A., Traub, R. D., Buhl, E. H., Heinemann, S. F., & McBain, C. J. (2004). Distinct roles for the kainate receptor subunits GluR5 and GluR6 in kainate-induced hippocampal gamma oscillations. *J. Neurosci.*, 24:9658–9668.

Fransen, E., Tahvildari, B., Egorov, A. V., Hasselmo, M. E., & Alonso, A. A. (2006). Mechanism of graded persistent cellular activity of entorhinal cortex layer v neurons. *Neuron*, 49:735–746.

Freeman, W. J. (1968). Relations between unit activity and evoked potentials in prepyriform cortex of cats. *J. Neurophysiol.*, 31:337–348.

Friedman-Hill, S., Maldonado, P. E., & Gray, C. M. (2000). Dynamics of striate cortical activity in the alert macaque: I. Incidence and stimulus-dependence of gamma-band neuronal oscillations. *Cereb. Cortex*, 10:1105–1116.

Frien, A., Eckhorn, R., Bauer, R., Woelbern, T., & Kehr, H. (1994). Stimulus-specific fast oscillations at zero phase between visual areas V1 and V2 of awake monkey. *Neuroreport*, 5:2273–2277.

Fries, P. (2005). A mechanism for cognitive dynamics: neuronal communication through neuronal coherence. *Trends Cogn. Sci.*, 9:474–480.

Fries, P., Reynolds, J. H., Rorie, A. E., & Desimone, R. (2001). Modulation of oscillatory neuronal synchronization by selective visual attention. *Science*, 291:1560–1563.

Fries, P., Roelfsema, P. R., Engel, A. K., König, P., & Singer, W. (1997). Synchronization of oscillatory responses in visual cortex correlates with perception in interocular rivalry. *Proc. Natl. Acad. Sci. U.S.A.*, 94:12699–12704.

Fries, P., Schröder, J. H., Roelfsema, P. R., Singer, W., & Engel, A. K. (2002). Oscillatory neuronal synchronization in primary visual cortex as a correlate of stimulus selection. *J. Neurosci.*, 22:3739–3754.

Fries, P., Womelsdorf, T., Oostenveld, R., & Desimone, R. (2008). The effects of visual stimulation and selective visual attention on rhythmic neuronal synchronization in macaque area V4. *J. Neurosci.*, 28:4823–4835.

Girard, P., Hupe, J. M., & Bullier, J. (2001). Feedforward and feedback connections between areas V1 and V2 of the monkey have similar rapid conduction velocities. *J. Neurophysiol.*, 85:1328–1331.

Goldman, M. S., Levine, J. H., Major, G., Tank, D. W., & Seung, H. S. (2003). Robust persistent neural activity in a model integrator with multiple hysteretic dendrites per neuron. *Cereb. Cortex*, 13:1185–1195.

Gray, C. M. (1999). The temporal correlation hypothesis of visual feature integration: still alive and well. *Neuron*, 24:31–47.

Gray, C. M., König, P., Engel, A. K., & Singer, W. (1989). Oscillatory responses in cat visual cortex exhibit inter-columnar synchronization which reflects global stimulus properties. *Nature*, 338:334–337.

Gray, C. M. & Prisco, G. V. D. (1997). Stimulus-dependent neuronal oscillations and local synchronization in striate cortex of the alert cat. *J. Neurosci.*, 17:3239–3253.

Gray, C. M. & Singer, W. (1989). Stimulus-specific neuronal oscillations in orientation columns of cat visual cortex. *Proc. Natl. Acad. Sci. U.S.A.*, 86:1698–1702.

Gregoriou, G. G., Gotts, S. J., Zhou, H., & Desimone, R. (2009). High-frequency, long-range coupling between prefrontal and visual cortex during attention. *Science*, 324:1207–1210.

Gruber, T., Müller, M. M., Keil, A., & Elbert, T. (1999). Selective visual-spatial attention alters induced gamma band responses in the human EEG. *Clin. Neurophysiol.*, 110:2074–2085.

Hajos, N., Palhalmi, J., Mann, E. O., Nemeth, B., Paulsen, O., & Freund, T. F. (2004). Spike timing of distinct types of GABAergic interneuron during hippocampal gamma oscillations in vitro. *J. Neurosci.*, 24:9127–9137.

Henrie, J. A. & Shapley, R. (2005). LFP power spectra in V1 cortex: the graded effect of stimulus contrast. *J. Neurophysiol.*, 94(1):479.

Ishiguro, K., Otsu, N., Lungarella, M., & Kuniyoshi, Y. (2008). Comparison of nonlinear Granger causality extensions for low-dimensional systems. *Phys. Rev. E Stat. Nonlin. Soft Matter Phys.*, 77:036217.

James, W. (1998). *Principles of Psychology (1890)*. University of Chicago Press.

Jefferys, J. G., Traub, R. D., & Whittington, M. A. (1996). Neuronal networks for induced '40 Hz' rhythms. *Trends Neurosci.*, 19:202–208.

Kreiter, A. K. & Singer, W. (1996). Stimulus-dependent synchronization of neuronal responses in the visual cortex of the awake macaque monkey. *J. Neurosci.*, 16:2381–2396.

Laurent, G. (2002). Olfactory network dynamics and the coding of multidimensional signals. *Nat. Rev. Neurosci.*, 3:884–895.

Loewenstein, Y. & Sompolinsky, H. (2003). Temporal integration by calcium dynamics in a model neuron. *Nat. Neurosci.*, 6:961–967.

Logothetis, N. K. (2003). The underpinnings of the BOLD functional magnetic resonance imaging signal. *J. Neurosci.*, 23:3963–3971.

Lungarella, M., Ishiguro, K., Kuniyoshi, Y., & Otsu, N. (2007). Methods for quantifying the causal structure of bivariate time series. *Int. J. Bifurcat. Chaos*, 17(3):903.

Machens, C. K., Romo, R., & Brody, C. D. (2005). Flexible control of mutual inhibition: a neural model of two-interval discrimination. *Science*, 307:1121–1124.

Maldonado, P. E., Friedman-Hill, S., & Gray, C. M. (2000). Dynamics of striate cortical activity in the alert macaque: II. Fast time scale synchronization. *Cereb. Cortex*, 10:1117–1131.

Mann, E. O., Suckling, J. M., Hajos, N., Greenfield, S. A., & Paulsen, O. (2005). Perisomatic feedback inhibition underlies cholinergically induced fast network oscillations in the rat hippocampus in vitro. *Neuron*, 45:105–117.

Mattia, M. & Giudice, P. D. (2002). Population dynamics of interacting spiking neurons. *Phys. Rev. E*, 66(5):051917. doi:10.1103/PhysRevE.66.051917.

Mattia, M. & Giudice, P. D. (2004). Finite-size dynamics of inhibitory and excitatory interacting spiking neurons. *Phys. Rev. E*, 70(5):052903. doi:10.1103/PhysRevE.70.052903.

Mazzoni, A., Panzeri, S., Logothetis, N. K., & Brunel, N. (2008). Encoding of naturalistic stimuli by local field potential spectra in networks of excitatory and inhibitory neurons. *PLoS Comput. Biol.*, 4(12):e1000239. doi:10.1371/journal.pcbi.1000239.

McAdams, C. J. & Maunsell, J. H. R. (1999). Effects of attention on orientation-tuning functions of single neurons in macaque cortical area V4. *J. Neurosci.*, 19(1):431.

Mitra, P. P. & Pesaran, B. (1999). Analysis of dynamic brain imaging data. *Biophys. J.*, 76:691–708.

Mongillo, G., Barak, O., & Tsodyks, M. (2008). Synaptic theory of working memory. *Science*, 319:1543–1546.

Montgomery, S. M. & Buzsaki, G. (2007). Gamma oscillations dynamically couple hippocampal CA3 and CA1 regions during memory task performance. *Proc. Natl. Acad. Sci. U.S.A.*, 104:14495–14500.

Montgomery, S. M., Sirota, A., & Buzsaki, G. (2008). Theta and gamma coordination of hippocampal networks during waking and rapid eye movement sleep. *J. Neurosci.*, 28:6731–6741.

Moran, J. & Desimone, R. (1985). Selective attention gates visual processing in the extrastriate cortex. *Science*, 229:782–784.

Naya, Y., Sakai, K., & Miyashita, Y. (1996). Activity of primate inferotemporal neurons related to a sought target in pair-association task. *Proc. Natl. Acad. Sci. U.S.A.*, 93:2664–2669.

Neltner, L., Hansel, D., Mato, G., & Meunier, C. (2000). Synchrony in heterogeneous networks of spiking neurons. *Neural. Comput.*, 12:1607–1641.

Percival, D. B. & Walden, A. T. (1993). *Spectral Analysis for Physical Applications: Multitaper and Conventional Univariate Techniques.* Cambridge University Press.

Pesaran, B., Nelson, M. J., & Andersen, R. A. (2008). Free choice activates a decision circuit between frontal and parietal cortex. *Nature*, 453:406–409.

Pesaran, B., Pezaris, J. S., Sahani, M., Mitra, P. P., & Andersen, R. A. (2002). Temporal structure in neuronal activity during working memory in macaque parietal cortex. *Nat. Neurosci.*, 5:805–811.

Phillips, W. A. & Singer, W. (1997). In search of common foundations for cortical computation. *Behav Brain Sci*, 20:657–683.

Reynolds, J. H., Chelazzi, L., & Desimone, R. (1999). Competitive mechanisms subserve attention in macaque areas V2 and V4. *J. Neurosci.*, 19(5):1736–53.

Riehle, A., Grun, S., Diesmann, M., & Aertsen, A. (1997). Spike synchronization and rate modulation differentially involved in motor cortical function. *Science*, 278:1950–1953.

Robbins, T. (1984). Cortical noradrenaline, attention and arousal. *Psychol. Med.*, 14(1):13.

Roelfsema, P. R., Engel, A. K., König, P., & Singer, W. (1997). Visuomotor integration is associated with zero time-lag synchronization among cortical areas. *Nature*, 385:157–161.

Roelfsema, P. R., Lamme, V. A. F., & Spekreijse, H. (2004). Synchrony and covariation of firing rates in the primary visual cortex during contour grouping. *Nat. Neurosci.*, 7:982–991.

Rols, G., Tallon-Baudry, C., Girard, P., Bertrand, O., & Bullier, J. (2001). Cortical mapping of gamma oscillations in areas V1 and V4 of the macaque monkey. *Vis. Neurosci.*, 18:527–540.

Roskies, A. L. (1999). The binding problem. *Neuron*, 24:7–9.

Saalmann, Y. B., Pigarev, I. N., & Vidyasagar, T. R. (2007). Neural mechanisms of visual attention: how top-down feedback highlights relevant locations. *Science*, 316:1612–1615.

Salinas, E. & Sejnowski, T. J. (2000). Impact of correlated synaptic input on output firing rate and variability in simple neuronal models. *J. Neurosci.*, 20:6193–6209.

Salinas, E. & Sejnowski, T. J. (2001). Correlated neuronal activity and the flow of neural information. *Nat. Rev. Neurosci.*, 2:539–550.

Schreiber, T. (2000). Measuring information transfer. *Phys. Rev. Lett.*, 85:461–464.

Shafi, M., Zhou, Y., Quintana, J., Chow, C., Fuster, J., & Bodner, M. (2007). Variability in neuronal activity in primate cortex during working memory tasks. *Neuroscience*, 146:1082–1108.

Steinmetz, P. N., Roy, A., Fitzgerald, P. J., Hsiao, S. S., Johnson, K. O., & Niebur, E. (2000). Attention modulates synchronized neuronal firing in primate somatosensory cortex. *Nature*, 404:187–190.

Stopfer, M., Bhagavan, S., Smith, B. H., & Laurent, G. (1997). Impaired odour discrimination on desynchronization of odour-encoding neural assemblies. *Nature*, 390:70–74.

Szabo, M., Almeida, R., Deco, G., & Stetter, M. (2004). Cooperation and biased competition model can explain attentional filtering in the prefrontal cortex. *Eur. J. Neurosci.*, 19:1969–1977.

Taylor, K., Mandon, S., Freiwald, W. A., & Kreiter, A. K. (2005). Coherent oscillatory activity in monkey area V4 predicts successful allocation of attention. *Cereb. Cortex*, 15:1424–1437.

Tiesinga, P. & Sejnowski, T. J. (2009). Cortical enlightenment: are attentional gamma oscillations driven by ING or PING? *Neuron*, 63:727–732.

Traub, R., Whittington, M., & Jeffreys, J. (1999). *Fast Oscillations in Cortical Networks*. MIT Press, Cambridge.

Traub, R. D., Jefferys, J. G., & Whittington, M. A. (1997). Simulation of gamma rhythms in networks of interneurons and pyramidal cells. *J. Comput. Neurosci.*, 4:141–150.

Treue, S. & Martínez Trujillo, J. C. (1999). Feature-based attention influences motion processing gain in macaque visual cortex. *Nature*, 399(6736):575–579.

Vaadia, E., Haalman, I., Abeles, M., Bergman, H., Prut, Y., Slovin, H., & Aertsen, A. (1995). Dynamics of neuronal interactions in monkey cortex in relation to behavioural events. *Nature*, 373:515–518.

van Hooft, J. A., Giuffrida, R., Blatow, M., & Monyer, H. (2000). Differential expression of group I metabotropic glutamate receptors in functionally distinct hippocampal interneurons. *J. Neurosci.*, 20:3544–3551.

Varela, F., Lachaux, J. P., Rodriguez, E., & Martinerie, J. (2001). The brainweb: phase synchronization and large-scale integration. *Nat. Rev. Neurosci.*, 2:229–239.

Wang, X. J. (2001). Synaptic reverberation underlying mnemonic persistent activity. *Trends Neurosci.*, 24:455–463.

Wang, X. J. & Buzsaki, G. (1996). Gamma oscillation by synaptic inhibition in a hippocampal interneuronal network model. *J. Neurosci.*, 16:6402–6413.

Wehr, M. & Laurent, G. (1996). Odour encoding by temporal sequences of firing in oscillating neural assemblies. *Nature*, 384:162–166.

Wendling, F., Ansari-Asl, K., Bartolomei, F., & Senhadji, L. (2009). From EEG signals to brain connectivity: a model-based evaluation of interdependence measures. *J. Neurosci. Methods*, 183:9–18.

Whittington, M. A., Traub, R. D., & Jefferys, J. G. (1995). Synchronized oscillations in interneuron networks driven by metabotropic glutamate receptor activation. *Nature*, 373:612–615.

Wilson, M. & Bower, J. M. (1992). Cortical oscillations and temporal interactions in a computer simulation of piriform cortex. *J. Neurophysiol.*, 67:981–995.

Wilson, M. A. & Bower, J. M. (1991). A computer simulation of oscillatory behavior in primary visual cortex. *Neural. Comput.*, 3(4):498–509.

Womelsdorf, T., Fries, P., Mitra, P. P., & Desimone, R. (2006). Gamma-band synchronization in visual cortex predicts speed of change detection. *Nature*, 439:733–736.

Womelsdorf, T., Schoffelen, J. M., Oostenveld, R., Singer, W., Desimone, R., Engel, A. K., & Fries, P. (2007). Modulation of neuronal interactions through neuronal synchronization. *Science*, 316:1609–1612.